INERTIAL OSCILLATIONS IN THE MEDITERRANEAN

by

HENRY T. PERKINS

S.B., Massachusetts Institute of Technology
(1960)

M.S., New York University
(1964)

SUBMITTED IN PARTIAL FULFILLMENT OF THE
REQUIREMENTS FOR THE DEGREE OF
DOCTOR OF PHILOSOPHY

at the

MASSACHUSETTS INSTITUTE OF TECHNOLOGY

and the

WOODS HOLE OCEANOGRAPHIC INSTITUTION

June, 1970

Signature of Author .....
Joint Program in Oceanography, Massachusetts Institute of Technology - Woods Hole Oceanographic Institution, and Department of Earth and Planetary Sciences, and Department of Meteorology, Massachusetts Institute of Technology, June 1970

Certified by .....
Thesis Supervisor

Accepted by .....
Chairman, Joint Oceanography Committee in the Earth Sciences, Massachusetts Institute of Technology - Woods Hole Oceanographic Institution

WITHDRAWN
Windgren
MASS. INST. TECH.
SEP 9 1970
MIT LIBRARIES

Inertial Oscillations in the Mediterranean

by

Henry T. Perkins

Submitted to the Joint Oceanographic Committee in the Earth Sciences, Massachusetts Institute of Technology and Woods Hole Oceanographic Institution, on June, 1970, in partial fulfillment of the requirements for the degree of Doctor of Philosophy.

ABSTRACT

Measurements of ocean currents were made by the author in the Western Mediterranean Sea at five depths for two months during early 1969. In terms of the dominant and persistent presence of inertial oscillations, circularly polarized currents having periods of a half pendulum day, the data are among the most striking ever collected.

Two contemporary theories have been adapted for interpretation of this data. On the basis of a ray or short-wave-length theory, energy arriving at the observing site is found to fall into two categories, that making direct arrival from the surface where it is assumed to have been generated, and that which undergoes one or more reflections. To the extent that the former dominates, it is found that the Algerian Coast about 130 km. to the south would cast a shadow to the north, the precise shape of which would be highly dependent on small variations in frequency. The nature of this frequency dependence implies a gradual increase in frequency with depth at the observing latitude. Although the data show a measurable shift (about 3%) towards higher frequencies, which is roughly the required amount, the lack of progressive frequency change with depth does not support the shadow hypothesis.

In addition, the data is interpreted in terms of normal mode theory, where the nearby coast is seen to force a discrete modal structure to the solutions. The observed variation of current phase with depth indicates that a single internal mode dominates over

a large portion of the data, while variations of both current amplitude and phase with depth are consistent this being the third internal vertical mode. Existence of a normal mode is also consistent with the long time, on the order of three weeks, for which the oscillations were observed to persist and with the dimensions of the Mediterranean Basin.

Thesis Supervisor.....Ferris Webster.....
Associate Scientist, Department of
Physical Oceanography, Woods Hole
Oceanographic Institution

To Valerie

Acknowledgements

The author is particularly grateful to Dr. Ferris Webster for his unfailing cooperation and encouragement throughout this study. A more patient and effective advisor is diffucult to imagine.

Thanks are expressed to Drs. N. P. Fofonoff and R. T. Pollard for numerous helpful discussions. Also, the author wishes to thank what is usually called the "buoy group" at the Woods Hole Oceanographic Institution for sharing their expertise in the difficult art of gathering and processing data from moored instruments.

This work was supported by the National Science Foundation under contract GA10208 and by the Office of Naval Research under contract NONR 241-11.

Table of Contents

	Page
Abstract	2
Acknowledgements	5
List of figures and tables	7
I. Introduction	10
II. Observations	18
III. A ray theory interpretation	70
IV. Normal mode analysis	98
V. Discussion	123
Appendix I The effect of neglecting the horizontal component of earth rotation on rays having near-inertial frequency.	133
Appendix II Airy-function structure of inertial oscillations as derived from a local beta-plane approximation.	140
Bibliography	150
Biographical note	154

List of Figures and Tables

Figure No.		Page
1	Bathymetric chart of the observing region after chart BC 3916 of the U. S. Oceanographic Office.	19
2	Schematic diagram of mooring configuration.	20
3	Speed and direction of currents as a function of time as measured at each of five depths.	26
4	East and north component of currents at the five observing depths.	30
5	Progressive vector diagram of currents at 200 meters.	32
6	Progressive vector diagram of currents at 700 meters.	33
7	Progressive vector diagram of currents at 1200 meters.	34
8	Progressive vector diagram of currents at 1700 meters.	35
9	Progressive vector diagram of currents at 2200 meters.	36
10	Power spectrum of currents at 200 meters.	38
11	Power spectrum of currents at 700 meters.	39
12	Power spectrum of currents at 1200 meters.	40
13	Power spectrum of currents at 1700 meters.	41
14	Power spectrum of currents at 2200 meters.	42
15	Energy spectra near inertial frequency at maximum frequency resolution for each of the data series.	45

List of Figures and Tables (cont.)

Figure No.		Page
16	Coherence vs. frequency for the east components of data series at 200 and 1700 meters. The lower dashed line shows the expected value for incoherent processes and the upper the 95% confidence level.	53
17	Complex demodulate of a synthetic signal plus noise as discussed in the text. The demodulation frequency was 3% lower than the signal frequency. Exact values of amplitude and phase for the signal alone are shown by dashed lines.	59
18	Complex demodulates of the five series of current measurements shown as amplitude and phase.	61
19	Temperature and salinity vs. depth.	64
20	Brunt-Väisälä or stability frequency vs. depth.	65
21	Geostrophic wind speed and direction at 12 hour intervals at the observing site.	68
22	Plan view of ray paths corresponding to inertial frequency at 38°N.	83
23	Reflection properties of waves near inertial frequency in wavenumber and geographic spaces.	87
24	Trajectories of north-bound rays (r = 0) originating near the Algerian coast for various frequencies.	93
25	Rays having turning latitudes at 38°N projected into a north-south plane.	95

List of Figures and Tables (cont.)

Figure No.		Page
26	Structure of the first five vertical modes at inertial frequency at the observing site.	103
27	Permissable values for east-west wavenumber k and vertical eigenvalue γ for each of the first five internal modes.	116
28	The three possible north-south modes corresponding to the third vertical mode.	117
29	Paths of rays having frequency corresponding to inertial frequency at 40°, both with and without the horizontal component of the earth's rotation.	138

Table

1	Clockwise and counterclockwise constituents of kinetic energy at inertial frequency for each data series.	49
2	Coherence at inertial frequency between various pairs of current records.	51
3	Separation constants for vertical modes 0 through 5.	102
4	Amplitudes and phases of the first few normal modes as inferred from complex demodulation.	111
5	Periods in hours for the first five internal modes in east-west, north-south, and up-down directions.	121

Chapter I Introduction

Inertial oscillations are defined for the purpose of this investigation as horizontal ocean currents in which the current vector rotates in a nearly circular, clockwise sense (counter-clockwise in the southern hemisphere) with period of about a half pendulum day. It is now generally believed that such oscillations are commonly, if not universally, found in the deep oceans of the world away from equatorial latitudes. They have been observed independently by lowered and moored current meters, by neutrally buoyant floats, and by electromagnetic current measurements. Webster (1968) recently has made an extensive survey of the published data which shows evidence of inertial oscillations, listing some 23 sites, all in the northern hemisphere, where observations have been made, several of them including more than one series of observations.

Most of the long duration, high-quality measurements which form the basis for much of what is now known about inertial oscillations in the open ocean have been collected intermittently from a single site near 39° 20'N 70° 00'W, usually called Site D. They have been partly summarized by Webster and Fofonoff (1965, 1966, 1967). Chief features

of these measurements are their relatively extensive coverage in the vertical, duration for typically two months per record and rapid sampling in time. Several of these are accompanied by surface wind data.

Other significant recent observations of inertial motion have been made in enclosed or semi-enclosed basins such as the Sea of Japan where Nan-niti, Akamatsu, and Yasuoka (1966) have reported observations made with neutrally buoyant floats. This technique was devised for a study of steady drifts and is not particularly well suited for periodic motions since it usually involves a small number of infrequent observations. Extensive current measurements in the Great Lakes have been made, primarily in connection with pollution studies, and these generally show strong inertial-period motion (Verber, 1966; Malone, 1968), especially during periods when a thermocline exists. Finally in the Mediterranean itself, a continuing French program has made numerous simultaneous measurements of winds and currents from their manned buoy, the Bouée Laboratoire (Gonella, Crépon, and Madelain, 1969), located about 100 km. south of Nice. Their current measurements have so far been limited to the upper 100 meters of the ocean due to operational difficulties (the buoy is

on a slack mooring, requiring large drift corrections).

From this body of data, a consistent pattern of properties of inertial motion has been established. By the nature of the observations, time variations are most easily resolved. One finds nearly circular, clockwise currents having periods within a few percent of the local inertial period or half pendulum day. These are superimposed on a broad spectrum of other processes but are usually quite noticeable in the data and often are the most energetic constituent present, dominating even the mean current. However, the motions are transient, persisting for a few days at most; indeed, the persistence is generally for only a few cycles. No systematic correlation between amplitude and duration of the bursts of inertial energy has been found nor is any asymmetry between the rise and decay apparent. Vertical persistence (that is, separation in the vertical across which inertial currents do not differ appreciably) is likewise limited. The author has recently examined most of the largely unpublished data collected at W.H.O.I. by computing coherencies between contemporaneous pairs of current meter records. No records separated by more than 100 meters showed significant coherence, a single pair of instruments separated by 80 meters showed moderate coherence (0.6)

at inertial period only, while a pair of instruments only 2 meters apart showed almost perfect coherence. Since suitably close instrument spacing is available only in the upper part of the ocean, the possibility of there being larger scales of vertical coherence in the deep water must be left open. Measurements suitable for estimating horizontal scales of inertial oscillations are sparse indeed owing to the difficulty and expense of maintaining two or more moorings at the same time. We know of only two such sets of measurements made in the deep sea which simultaneously take into account the demonstratedly important depth dependence; both were made by Fofonoff and Webster. In the first of these, two instruments at 620 meters depth, near 29°N 68° 30'W and separated by about 65 km. showed no coherence even though there was a strong inertial signal at one of the instruments. The second pair of measurements was made near Site D with a horizontal separation of 3 km. and with current meters at 88 and 98 meters. Appreciable coherence was found ($\sim$ 0.7) and part of the coherence loss may have been due to vertical separation instead of horizontal. The features of inertial oscillations which require explanation are thus persistence in time of a few days, in the vertical of several tens of meters and in the horizontal for a few tens of kilometers.

It has been understood for some time that any disturbance of the ocean with a broad spectrum of input energy will give rise to inertial oscillations; e.g. Cahn (1945). Since the group velocity of these motions becomes vanishingly small as frequencies approach inertial, this effect is easy to understand; all other constituents of the initially induced motion disperse relatively rapidly. Determination of the precise nature of the forcing has proved elusive however. Hendershott (1964) considered, in a statistical sense, forcing of the ocean induced by tidal interaction with the irregular ocean bottom. We now know that tidal forcing, which should be important only near latitude 30°, is not the only source of inertial period currents since they have often been found at other latitudes. Nevertheless, Hendershott's theoretical treatment of the problem anticipates much of what is now known.

Most recent studies involving forced motion have dealt with wind-induced motion. The Great Lakes measurements have been treated in this respect by Csanaday (1968) and by Birchfield (1969) and the Bouée Laboratoire data in a series of papers by Crépon (1969), the most recent of which is referenced here. These studies show that qualitatively inertial currents of the magnitude observed near the ocean surface can in fact be established by

fluctuations of the wind. With regard to the Site D data, Pollard and Millard (1970) have demonstrated how the wind, acting as a driving body force in simplified equations of motion, excites inertial period motion in the mixed surface layer which strongly resembles that observed.

A more complete treatment of how energy near inertial period propagates was given by Blandford (1966). This was summarized and extended in a major contribution by Munk and Phillips (1968) who worked out the structure of inertio-gravity waves in regions where the wave period nearly equals the local inertial period. After finding detailed solutions for the relevant equations, they were able to estimate coherence and persistence scales on the basis of a model involving assumptions about how energy is distributed among the various frequencies and wavenumbers. Doing this, Munk and Phillips found reasonable values for both horizontal and vertical coherence scales, but the corresponding persistence was about 100 days which is much too large. However, their calculations neglected the possibility of slowly propagating inertial waves being advected away by mean currents, thus reducing persistence. A second model which they considered assumes the energy arises from a single, discrete source. It is

argued that such a source would imply very large coherence scales, although it is not clear how this can be reconciled with the very slow propagation rate of the waves and the fact that this rate is different for various constituents of the waves. We will return to these important points later. For the moment we simply argue against excluding either model on the basis of existing data.

The general plan of this thesis is to present new evidence of a type which will bear more directly on the problems outlined above. A truly comprehensive experiment, which will probably be done someday, would involve a sufficiently large number of instruments to permit tracing the flow of energy within a suitably large region. Such an experiment is beyond the scope of a thesis experiment and, due to limited instrument reliability, may not even be technologically feasible at this time. Instead, it was decided to exploit the profound effect which a coastline can have on inertial oscillations and which can help explain their properties. It is clear at once that the effect must be considerable since the horizontal component of current velocity, which is by far the largest component in inertial motion, must vanish at the coastline. If the coastline is

chosen to run east-west and be southward (or more generally equatorward) of an observing site, its effect is particularly useful for interpretation of the resulting data. These effects can be viewed in two ways; in terms of ray theory, or in terms of normal modes, both of which will be explored in succeeding chapters.

In more detail, the thesis will proceed as follows. Chapter II will describe a series of current measurements made in the Mediterranean during January, February and March of 1969. The site was chosen so that effects of the Algerian coast, which is one of the few coasts in the world having the desired properties, could be interpreted most easily. Chapter III discusses the Mediterranean observations on the basis of a ray theory of propagation, the chief effect of which is to prohibit energy of exactly inertial frequency which originates in the surface layers from penetrating below a certain critical depth providing that certain conditions at the coast are satisfied. Normal modes are considered in Chapter IV. The presence of the coast is found to force a particular structure to the inertial motion; the wavenumber spectrum must be discrete instead of continuous. Finally, a general discussion of results and conclusions are given in Chapter V.

Chapter II Observations

Description of site and mooring

During the period from January 22 to March 12, 1969, current measurements were made in the Mediterranean Sea at 38° 01′N 5° 00′E, about 120 km. north of the Algerian coast. The mooring was set and recovered by the R/V Atlantis II during cruise number 49. Interest in this region was aroused by the properties which theory predicted should be imparted to oscillations of inertial period by the long east-west coastline south of the observing site. In particular, a ray theory for the propagation of such oscillations had raised the possibility of associating them with motions induced in the surface layers, perhaps by storms. A more complete description for the motivation for these measurements is deferred until the next chapter when, at the same time, the data can be interpreted in terms of ray theory.

Topography of the Western Mediterranean Basin is shown in figure 1. Note particularly the straightness of the Algerian coastline and flatness of the bottom near the observing site, where the water depth is generally within a few hundred meters of 2800 meters ($\sim$ 1500 fathoms). These features together combine to simplify greatly the calculations which will later be

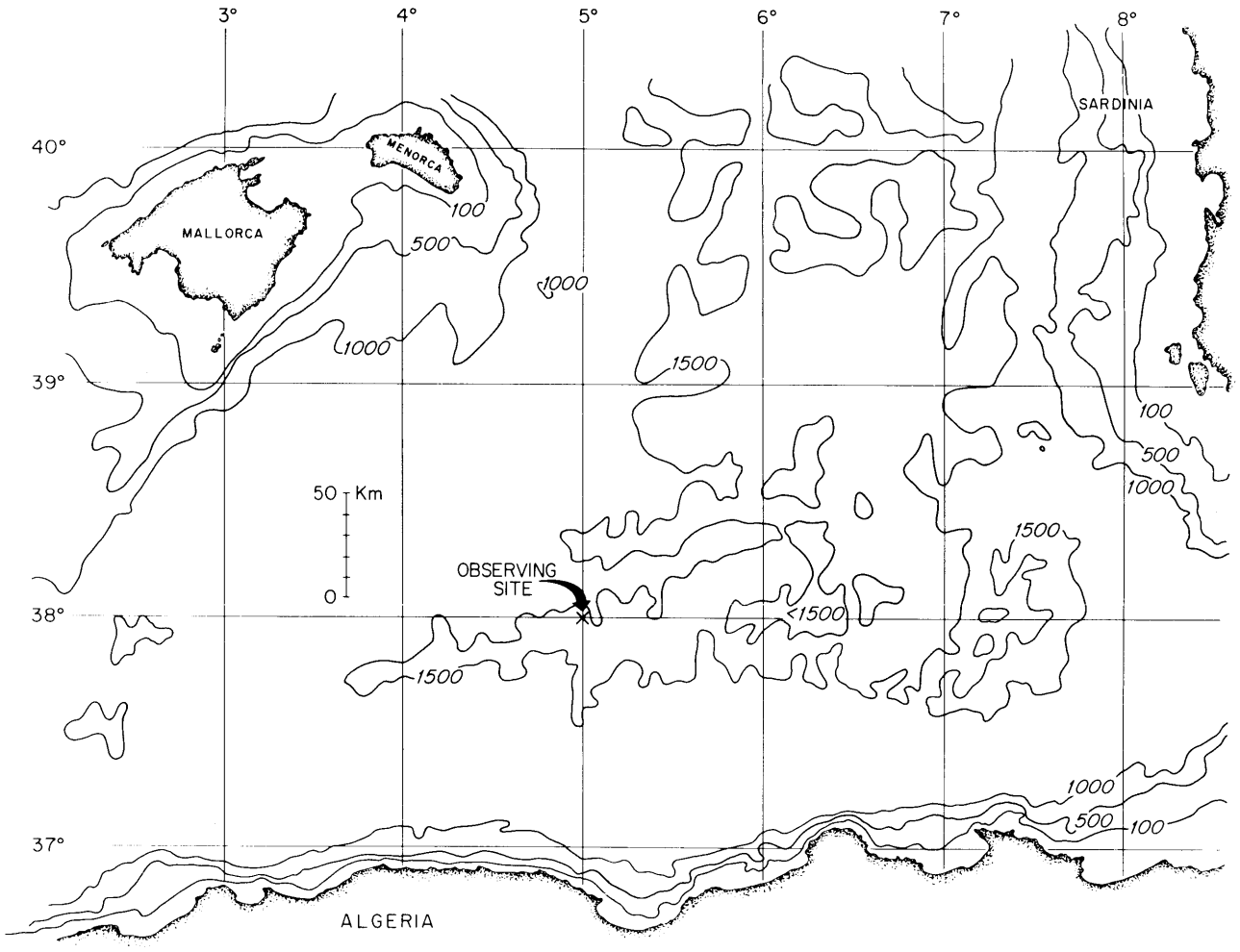


Figure 1 Bathymetric chart of the observing region after chart BC 3916 of the U. S. Oceanographic Office. Contours are in fathoms.

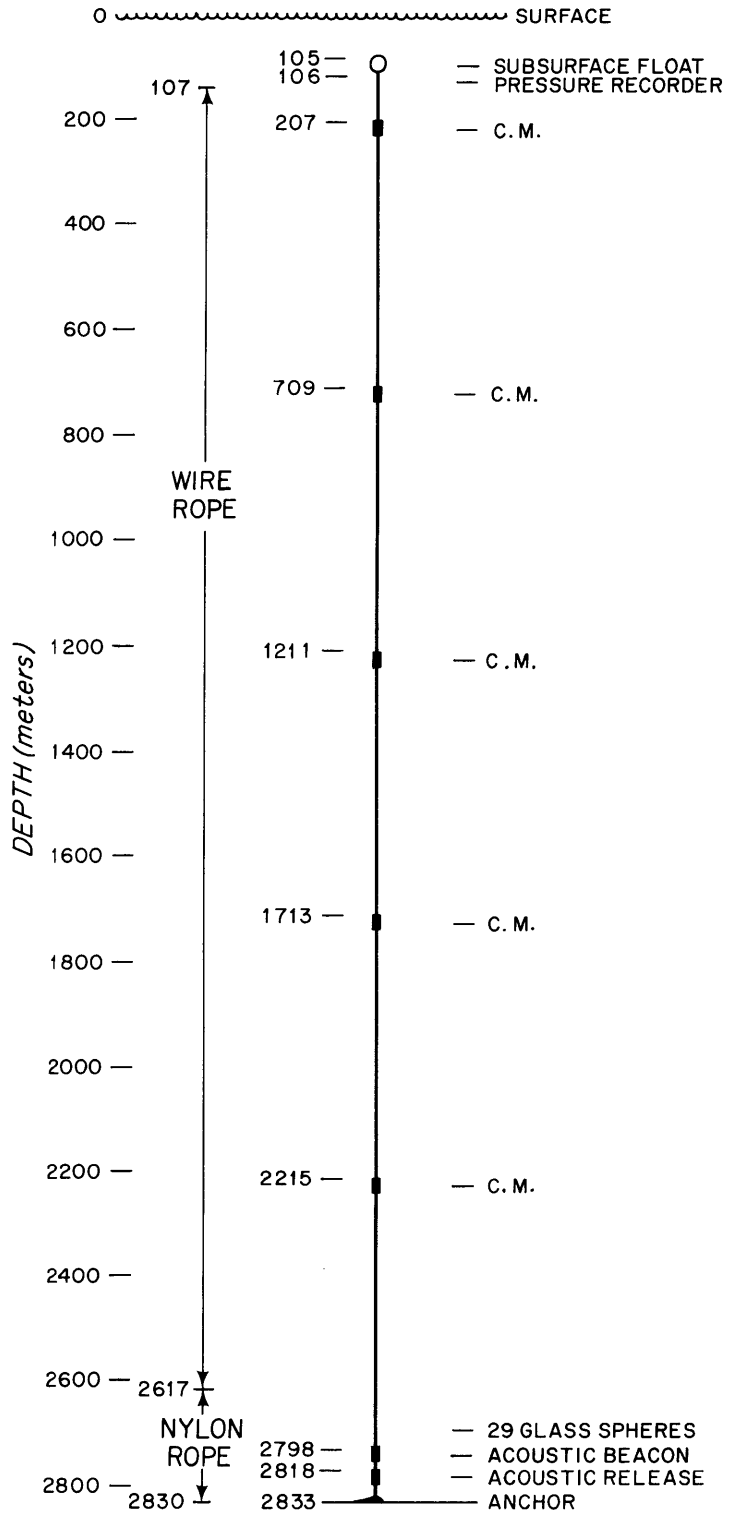


Figure 2 Schematic diagram of mooring configuration. The drawing is not done to scale.

made in connection with interpretation of the data.

Figure 2 shows schematically the mooring configuration and depths at which each of the five current meters were located. The design is basically an adaptation of that developed at the Woods Hole Oceanographic Institution for similar applications. A subsurface float, equipped with beacon light and radio transmitter which operate only when the float is at the surface, was used for reasons of reliability and security; there is a great deal of shipping through the area. Recovery of the mooring was achieved through the acoustic release, which released the anchor upon receiving a coded acoustic command. A number of glass spheres were located immediately above the release in order to float the instrument packages to the surface in the event that the mooring line parted, which did not occur. For the mooring line itself, wire cable was used except towards the bottom of the mooring where braided nylon rope was used so that it could be cut and terminated at sea to correspond to the depth of water measured at the time. The wire cable was chosen for protection against fish attack which has in the past severed a number of nylon mooring lines in the upper several hundred meters of the ocean. However, no fish bites were evident in the polyethelene jacket of the cable when it was recovered.

Depths of the instruments were determined by two methods. The first of these was to measure the water depth on location and cut the line to appropriate length, taking into account the anticipated stretch of the nylon line of about 18%. More directly, a pressure recorder was located immediately under the primary flotation sphere, giving a continuous record of pressure versus time for the whole duration of the mooring. The two depth determinations gave the same result to within experimental error, fixing depth of the subsurface float at 105 meters ± 5 meters. No significant variation in depth with time was found from the pressure record.

In keeping with conventions established at the Woods Hole Oceanographic Institution, where the data is kept in archive, the mooring is designated as number 289. Data series collected by each of the five current meters are designated as numbers 2892 through 2896 in order of increasing depth.

Instrument performance

The current meters used in this experiment were Geodyne model 850 instruments with minor modifications. In operation, the instruments record speed in terms of rotor rotations and direction in terms of orientation of a vane and of the instrument case with respect to an

internal compass. The data are recorded internally in digital form on magnetic tape. In the recording mode used, the instrument is turned on once every fifteen minutes. A burst of speed and direction samples are taken at five second intervals for about two and one-half minutes after which the instrument is shut down for the remainder of the fifteen minute cycle. During subsequent processing, the data are vector averaged over these 2.5 minute bursts to give a single value of speed and direction every 15 minutes. Consequences of this procedure in terms of spectral content of the data have been described in detail by Webster (1967). The principle advantage is that it effectively reduces the quantizing interval for the data and thus reduces the noise level introduced by quantizing. The effect is not important at the frequencies of interest here which have periods long compared with 15 minutes.

Timing of the instruments is critical for many of the inferences to be drawn from the data, making it essential to establish accuracy of the internal instrument clocks. Each instrument has two clocks, one to initiate sampling a burst of data every 15 minutes and another which only inserts a mark into the data every 12 hours. By comparing the two clocks in each instrument, it was determined that each pair was running at a common rate. Next, the absolute rate of each pair was found by

noting the number of 15 minute intervals between two precisely timed events inserted in the record, one immediately before deploying the instrument and one immediately after recovering it. This procedure was applied to each data series, except as noted below, showing the time base to have a long-term error of less than ± 0.1% in each case. Short term errors seem unlikely insofar as they would have been detected unless both clocks experienced the same rate anomaly at the same time. Also, past testing has shown that the clocks normally run at a very uniform rate in the constant thermal enviornment of the sea.

The single exception where the absolute time could not be double-checked occurred in the instrument at 1200 meters depth. During recovery of this instrument, the internal tape recorder failed so that it was not possible to detect the event inserted at the end of the data series as was done with the other instruments. On the other hand, the two internal clocks did run at the same rate and the total data length until recovery agreed well with the other instruments. It therefore seems reasonable to conclude that timing accuracy for this instrument was comparable with the others and that all clocks ran within ± 0.1% of the proper rate.

A variety of other instrument malfunctions occurred, most of the effects of which were edited out during subsequent data processing. A detailed description of these would involve discussing working of the instrument at greater length than is appropriate here even though the associated editing consumed a great deal of time. The two most important of these intermittent failures involved occasional failure of the instrument to turn on for a scheduled burst of observations and occasional bit failures in the binary output associated with the photodiodes and fiber optics of the direction sensors. Both problems were easily detected and corrected by suitable interpolation.

The final data, edited, vector averaged to give 15 minute samples, and plotted as speed and direction, are shown in figure 3. The figure is presented at this time since it shows two other problems with the data which were not removed by editing. The first of these is a design failure rather than a malfunction. Because the speeds at the observing site were so low, there are numerous instances in the data from the bottom four instruments where the rotor did not turn at all, particularly towards the middle of the observing period. This property of the rotor is well understood (Fofonoff and Ercan, 1967) and is due to the magnets imbedded in the rotor being

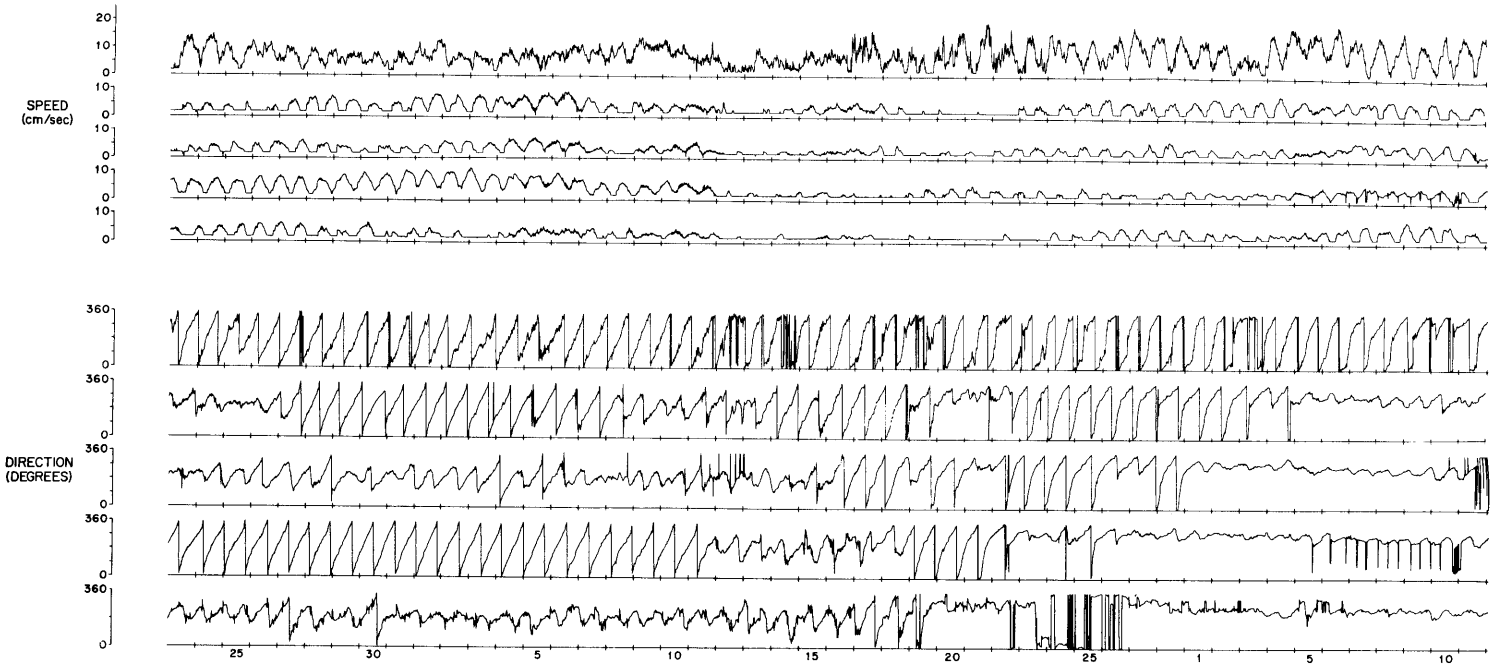


Figure 3 Speed and direction of currents as a function of time as measured at each of five depths.

attracted to the magnetically operated reed switch used for readout. Since the direction sensors did not stall, some information is available during these periods, and to make use of it, a speed of 1.8 cm/sec, corresponding to the stall speed of the rotor,was inserted when the rotor stalled. Then when computing Cartesian components, upon which all subsequent calculations were made, a smooth transition across the rotor-stall period resulted. Since the data are dominated by the sum of a mean current and an inertial period oscillation over much of its length, other interpolations are easy to devise. For the present purpose, however, the simple procedure outlined above proved satisfactory and allows the reader to view the rotor-stall problem in an undisguised form. No conclusion of this thesis would be altered by using a more complex interpolation scheme for the missing speeds.

The final instrument problem has to do with sticking of the direction sensors. As noted earlier, there are two of these, both resembling an ordinary compass card, measuring orientation of the case and of a vane, and having optical read-out attachments. These sensors have a history of sticking; that is, of requiring increasing torque for the sensing card to change its angular position within its frame. This is generally attributed to a combination of thermal contraction in cold water

and distortion of the instrument due to high pressure in deep water but the causes are not well understood. In the present instruments, the vane sensors of the three deepest instruments began to stick on March 1, February 25 and February 20 respectively, in order of increasing depth. There is also some evidence of a sticking vane during the last few days of the 700 meter record. In all cases except for the bottommost instrument there was only partial sticking so that a precise date of failure cannot be assigned. These failures are particularly troublesome to the extent that they destroy the characteristic circular polarization of inertial currents, but this failure was total only in the deepest instrument.

Fortunately, the only serious instrument malfunctions were confined to roughly the last third of the data so that several weeks of data are available from all five instruments and during this period the overall quality of the data is excellent. It should be noted especially that those malfunctions which occurred are not such as to affect estimates of frequency made from the data.

Summary of measurements

The basic data series have already been shown in polar form in figure 3 and discussed from the point of view of instrument performance. Of more interest for purposes of interpretation and analysis are the correspond-

ing Cartesian components which are shown in figure 4. The topmost five traces show the east-west component of current in order of increasing depth with the lower five traces giving a similar presentation for the north-south current component. Eastward and northward flows are considered positive with westward and southward flows considered negative. Time is shown as days originating at 0000 Greenwich mean time. As was claimed earlier, assignment of a non-zero speed to the intervals where the rotor has stalled permits data available in the direction sensors to produce smooth values for the Cartesian components.

A number of features of the data are apparent at once. Attention is directed in particular to the fourth or 1700 meter depth from the beginning of the record until about mid-February, where a series of inertial oscillations of extraordinary clarity and persistence can be seen.

Long term trends are more clearly seen from what are commonly called progressive vector diagrams, defined as the hodograph of

$$\int_{t_o}^{t} \vec{u}(\tau)\,d\tau$$

where t_o is the starting time of the series and $\vec{u}$ is the

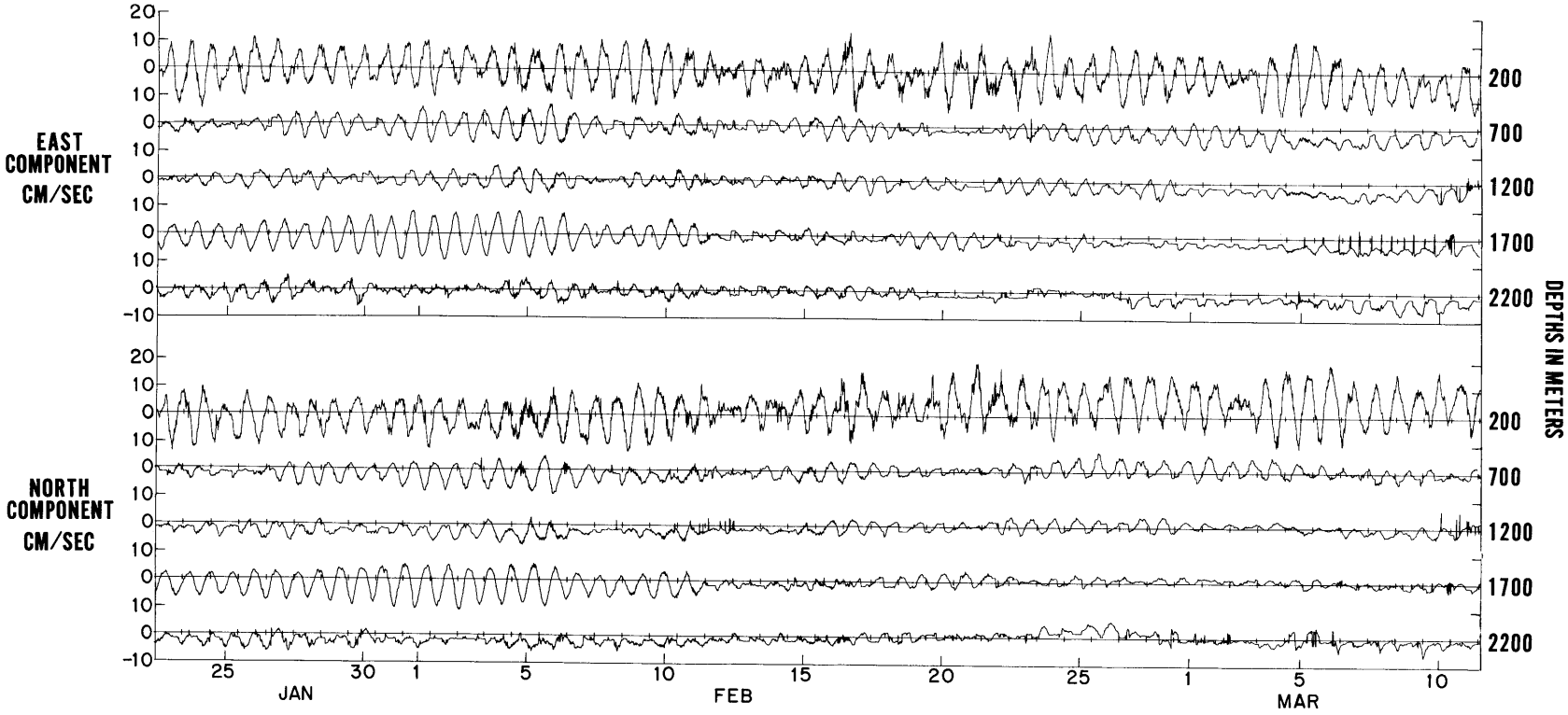


Figure 4 East and north component of currents at the five observing depths.

horizontal vector velocity. This quantity for each data series is shown in figures 5 through 9. Small tick marks along the curve correspond to 0000 GMT of the indicated date. At the 200 meter level there is a mean current towards the south until about February 10 after which it turned towards the north or northwest. In order to show more detail for that portion of the curve where it traces over itself, the second, smaller curve in figure 5 shows part of the curve expanded by a factor of two. Progressive vector diagrams for the remaining four data series are very similar in overall appearance, being directed towards the south-southwest until about February 17 and towards the west-northwest thereafter. Since the direction sensors of the deepest instrument were not functioning properly after February 20, the rough agreement of this series with that above it after that date may be fortuitous. The long term drifts are thus well correlated between the various pairs of records. All show a sudden shift in the mean flow on about February 16, except at the 200 meter level, where the change occurred some six days earlier.

It is clear at once from the basic data series that there is an enormous concentration of energy near the inertial frequency f in all the data series. This is

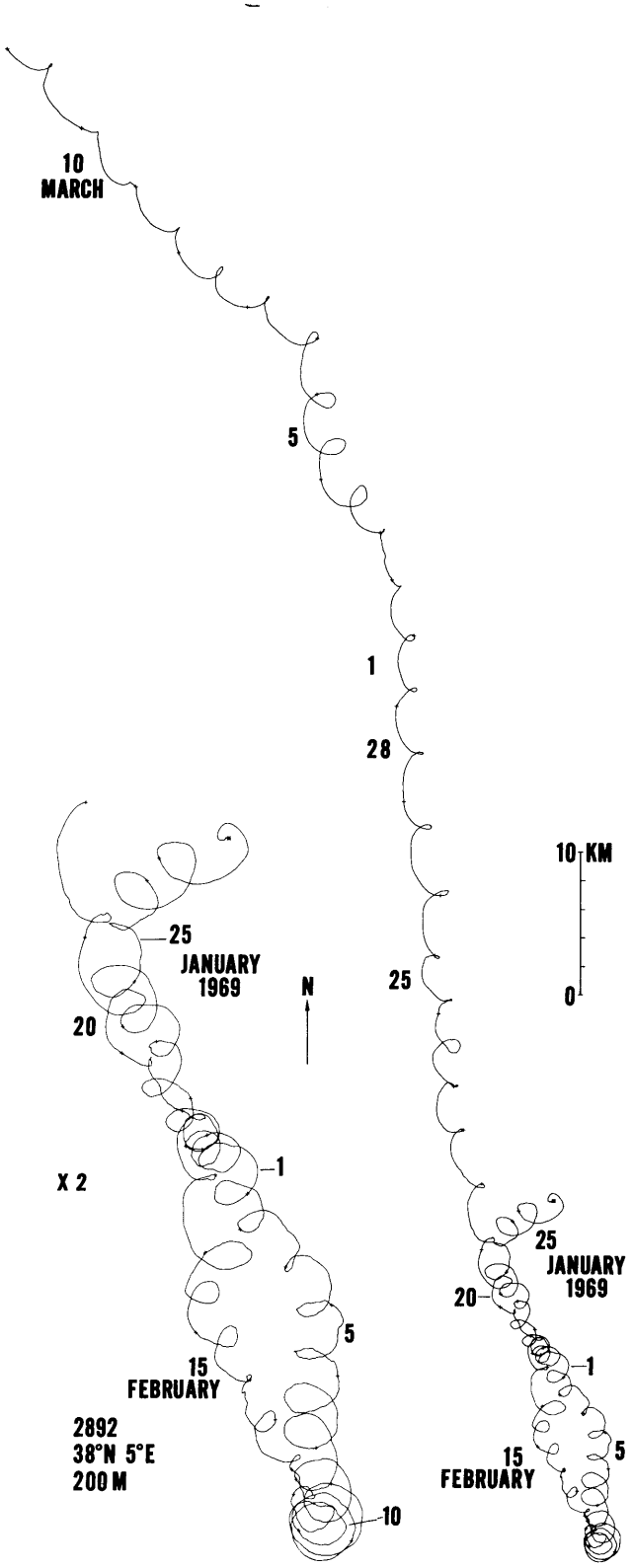


Figure 5 Progressive vector diagram of currents at 200 meters

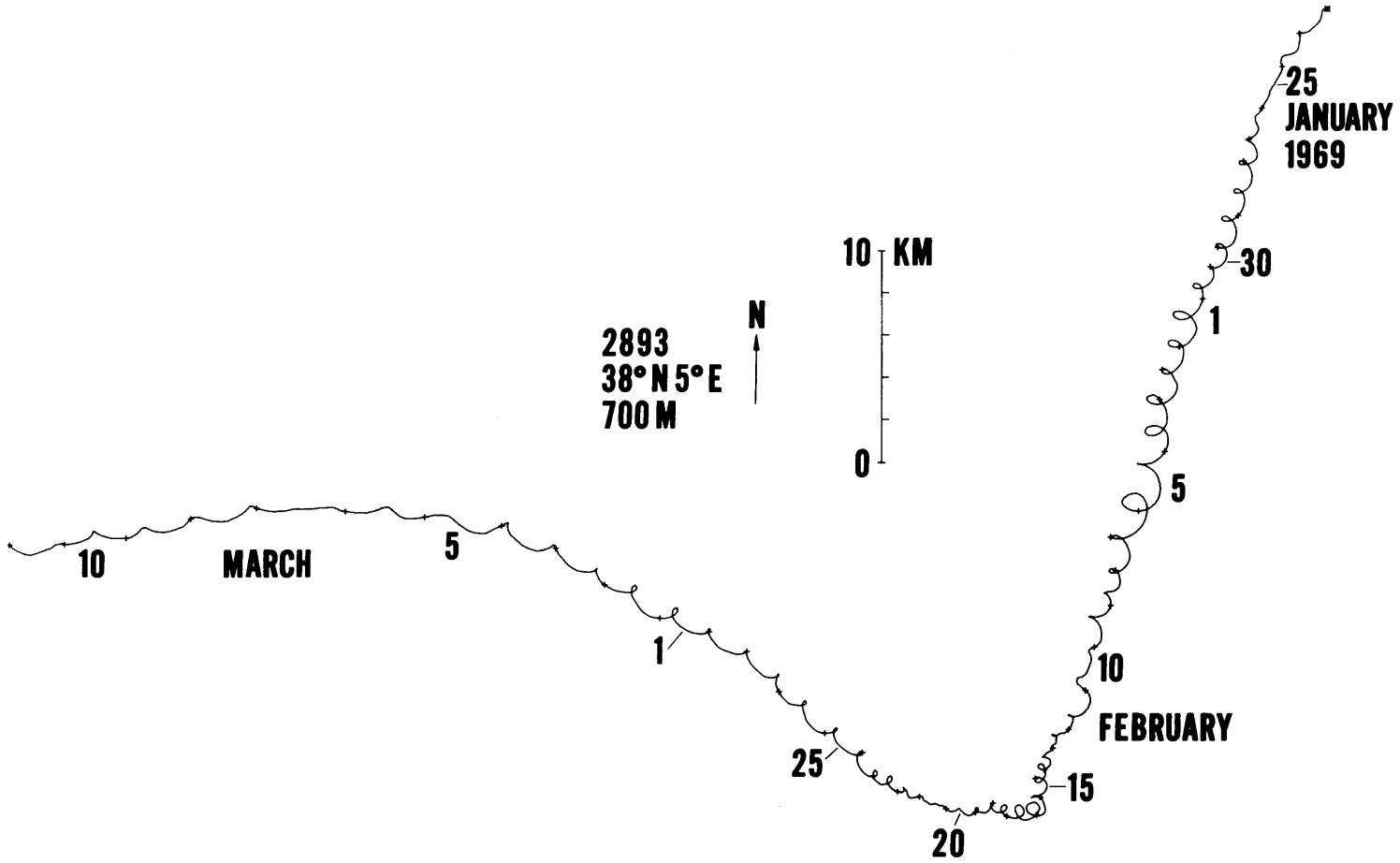


Figure 6 Progressive vector diagram of currents at 700 meters.

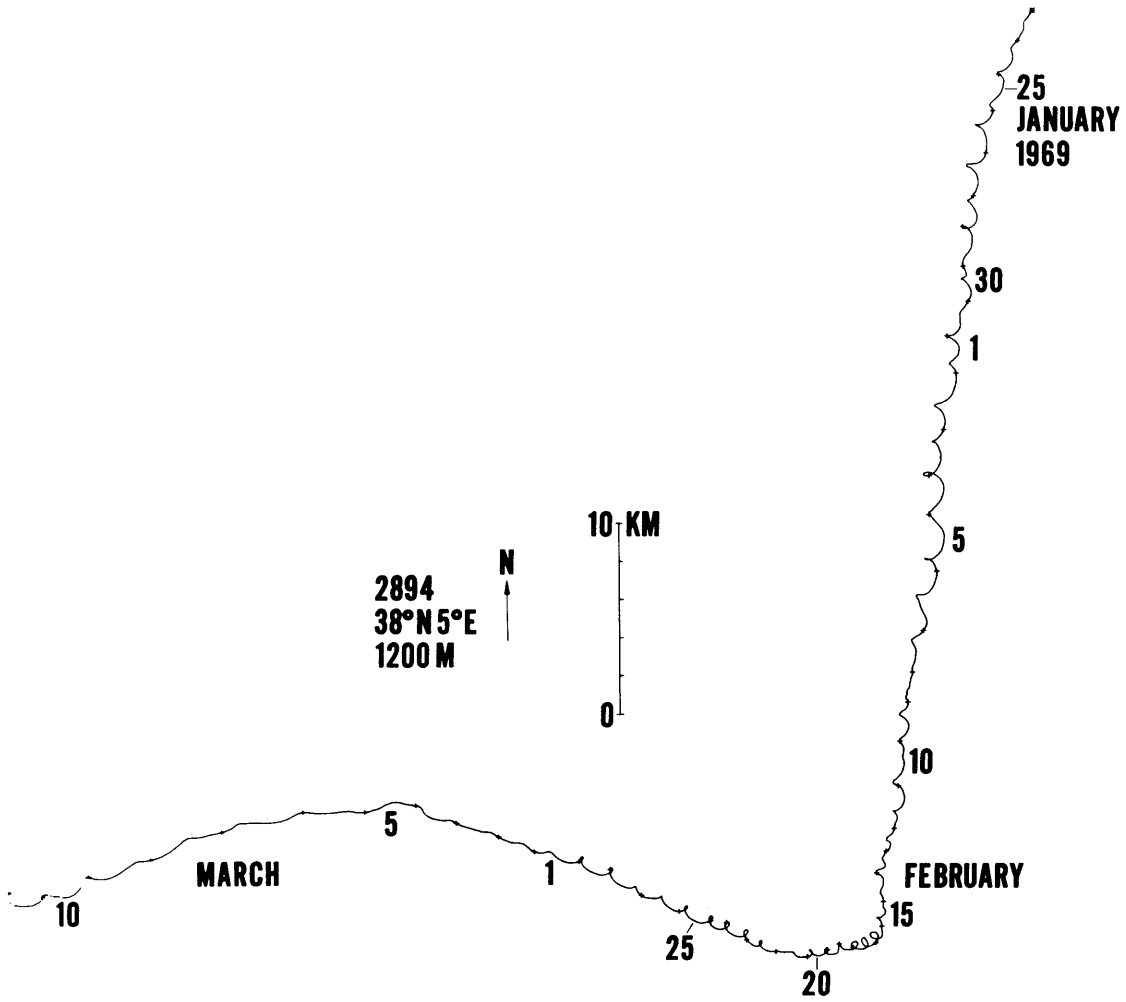


Figure 7 Progressive vector diagram of currents at 1200 meters.

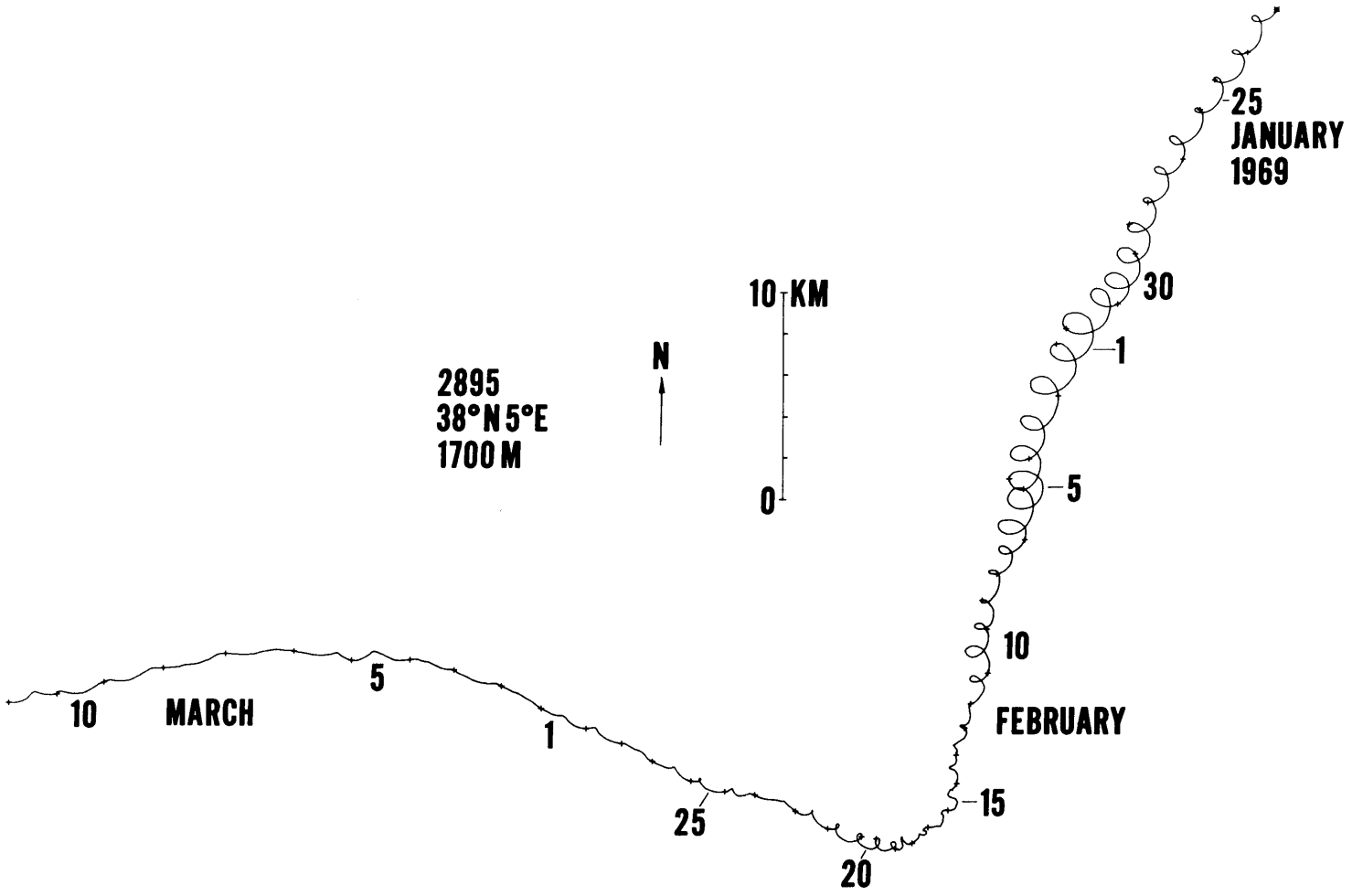


Figure 8 Progressive vector diagram of currents at 1700 meters.

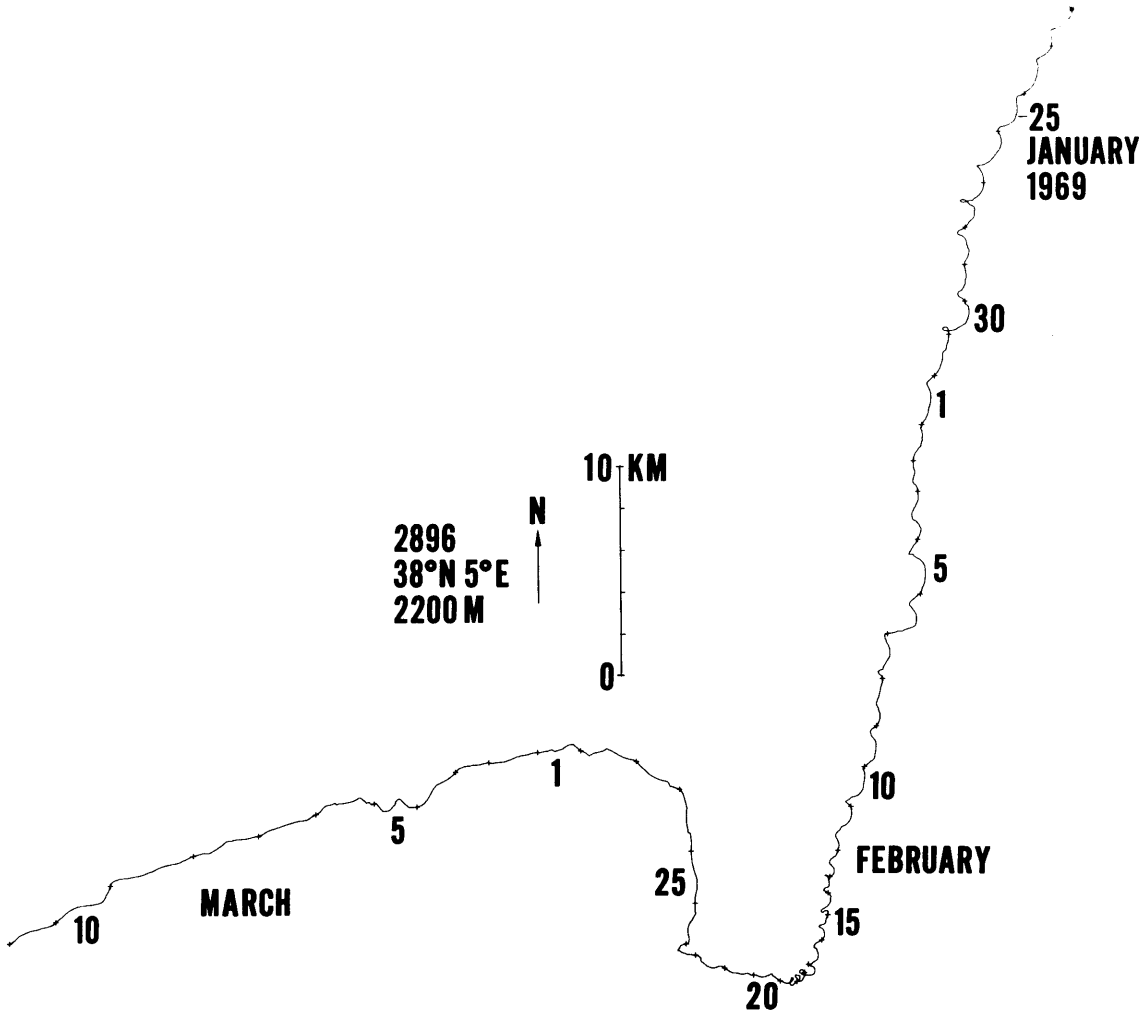


Figure 9 Progressive vector diagram of currents at 2200 meters.

shown quantitatively in figures 10 through 14 where spectra of each of the data series are plotted. The quantities plotted are the kinetic energy spectra, defined as the average of the autospectra of east and north current components. Spectral analysis techniques are well known so that the procedure used can be summarized briefly. The Cartesian component of each data series was broken into four sections, each of which contained 1024 samples. Each section was then Fourier analyzed and the resulting Fourier coefficients smoothed according to the usual procedure

$$a_n' = -\frac{1}{\sqrt{6}} a_{n-1} + \frac{2}{\sqrt{6}} a_n - \frac{1}{\sqrt{6}} a_{n+1}$$

with a similar formula for b_n, where a_n' is the smoothed estimate and the a_n the original estimates. Such smoothing provides a convolution window for the spectrum which behaves asymptotically as the inverse sixth power of frequency, which is sufficient to resolve most of the high-frequency spectrum except in the immediate vicinity of the inertial peak.

The procedure used yields frequency resolution of .004 cycles per hour (1/256 hours). According to the usual statistical argument, the resulting spectral

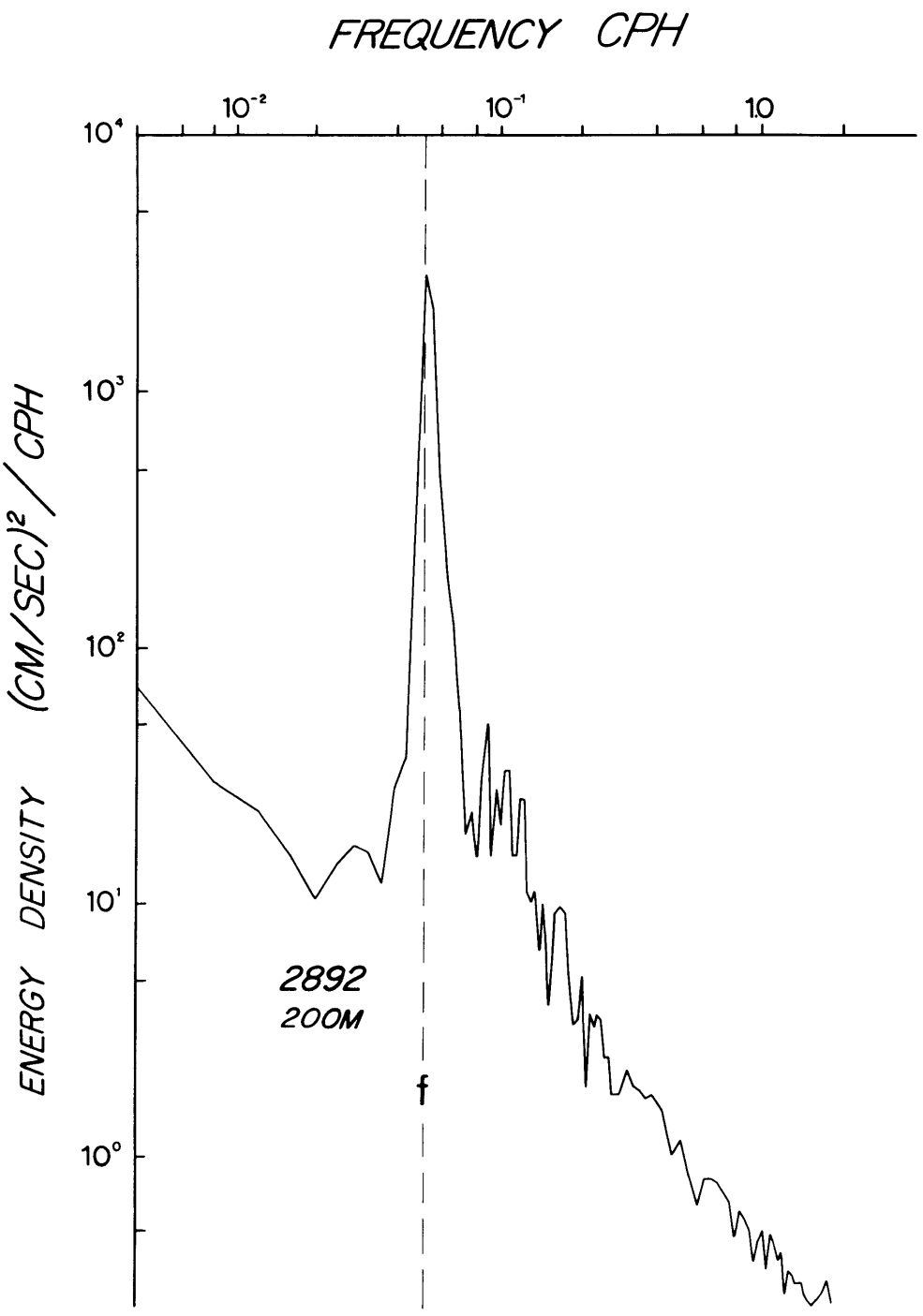


Figure 10 Power spectrum of currents at 200 meters.

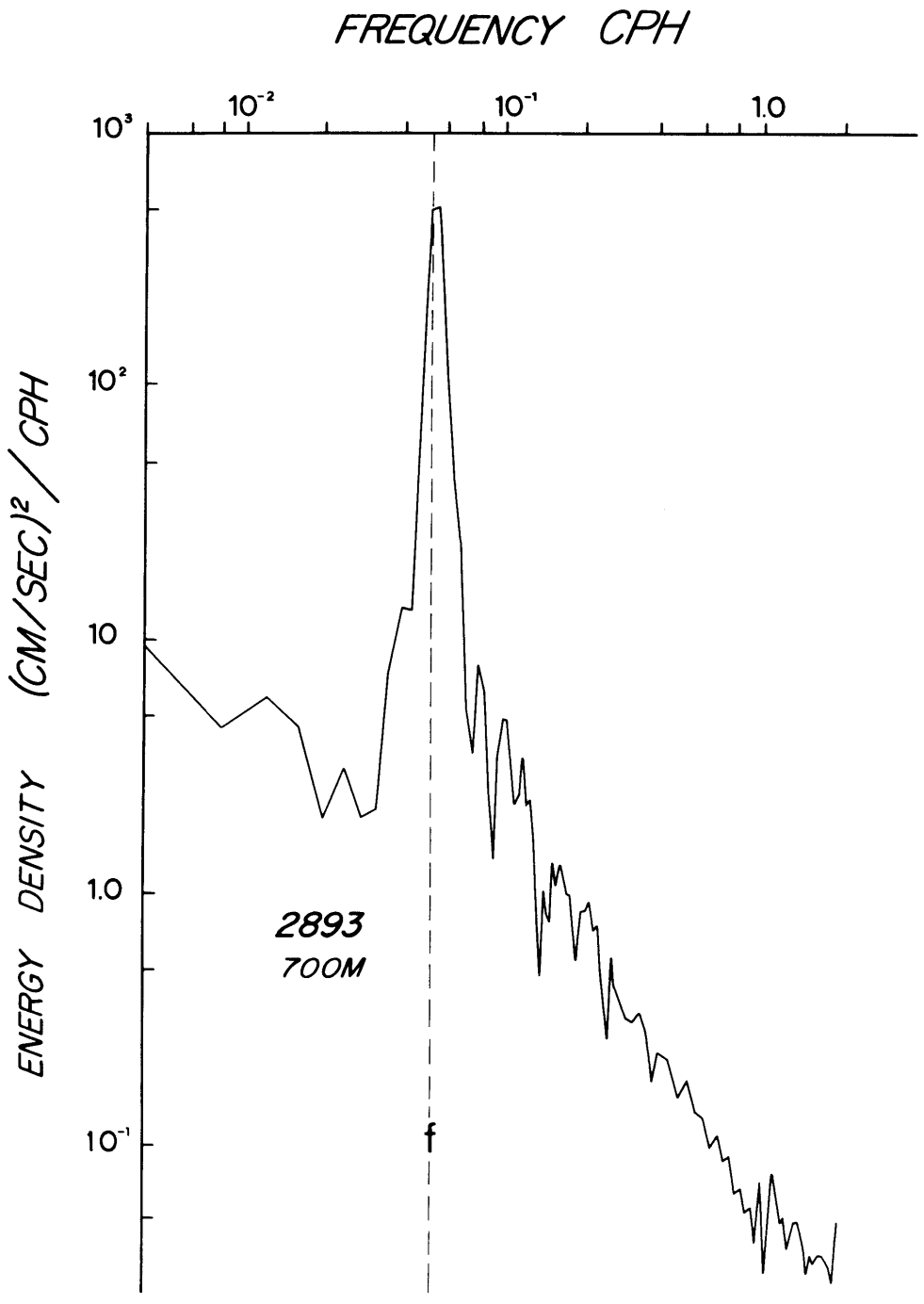


Figure 11 Power spectrum of currents at 700 meters.

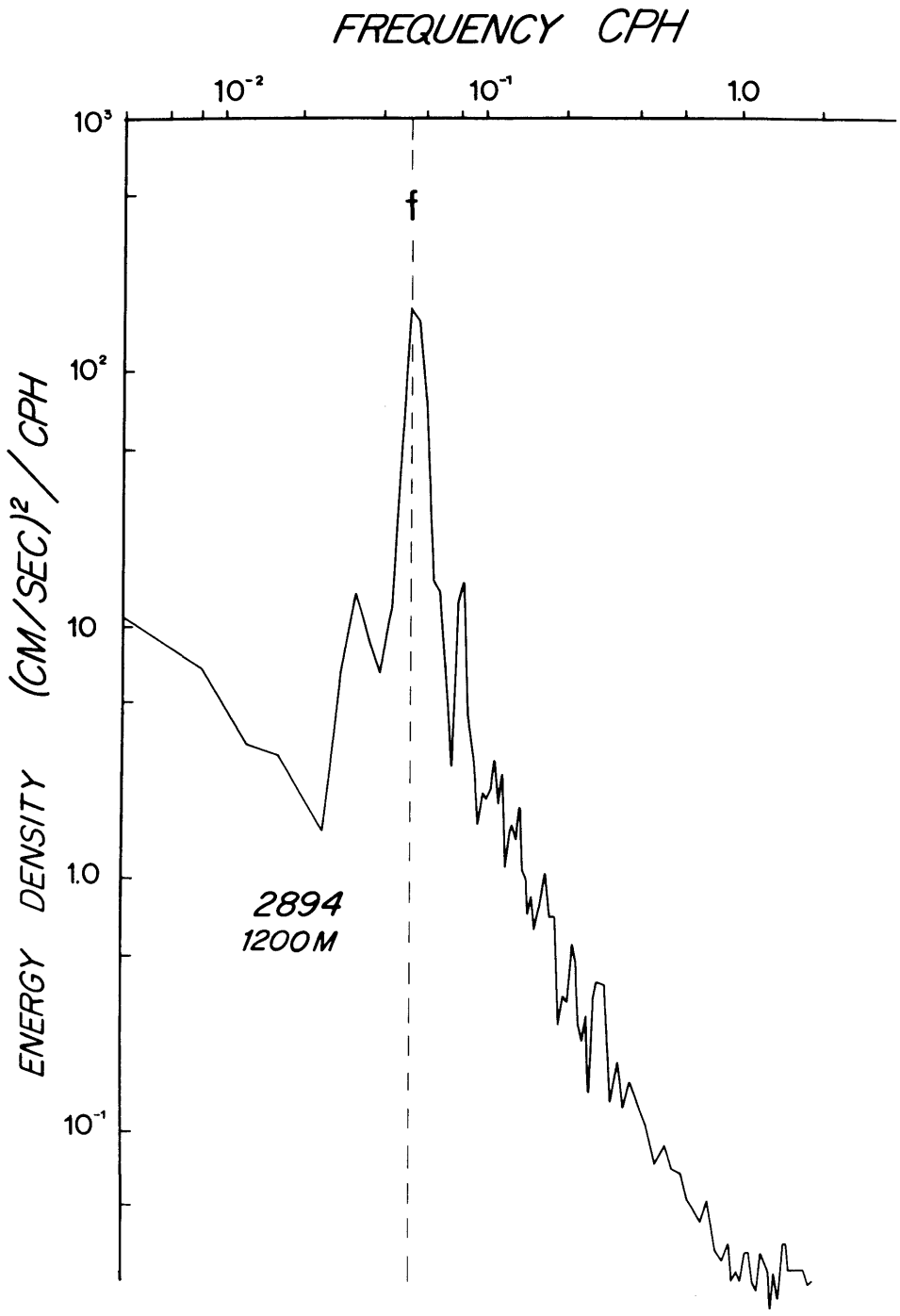


Figure 12 Power spectrum of currents at 1200 meters.

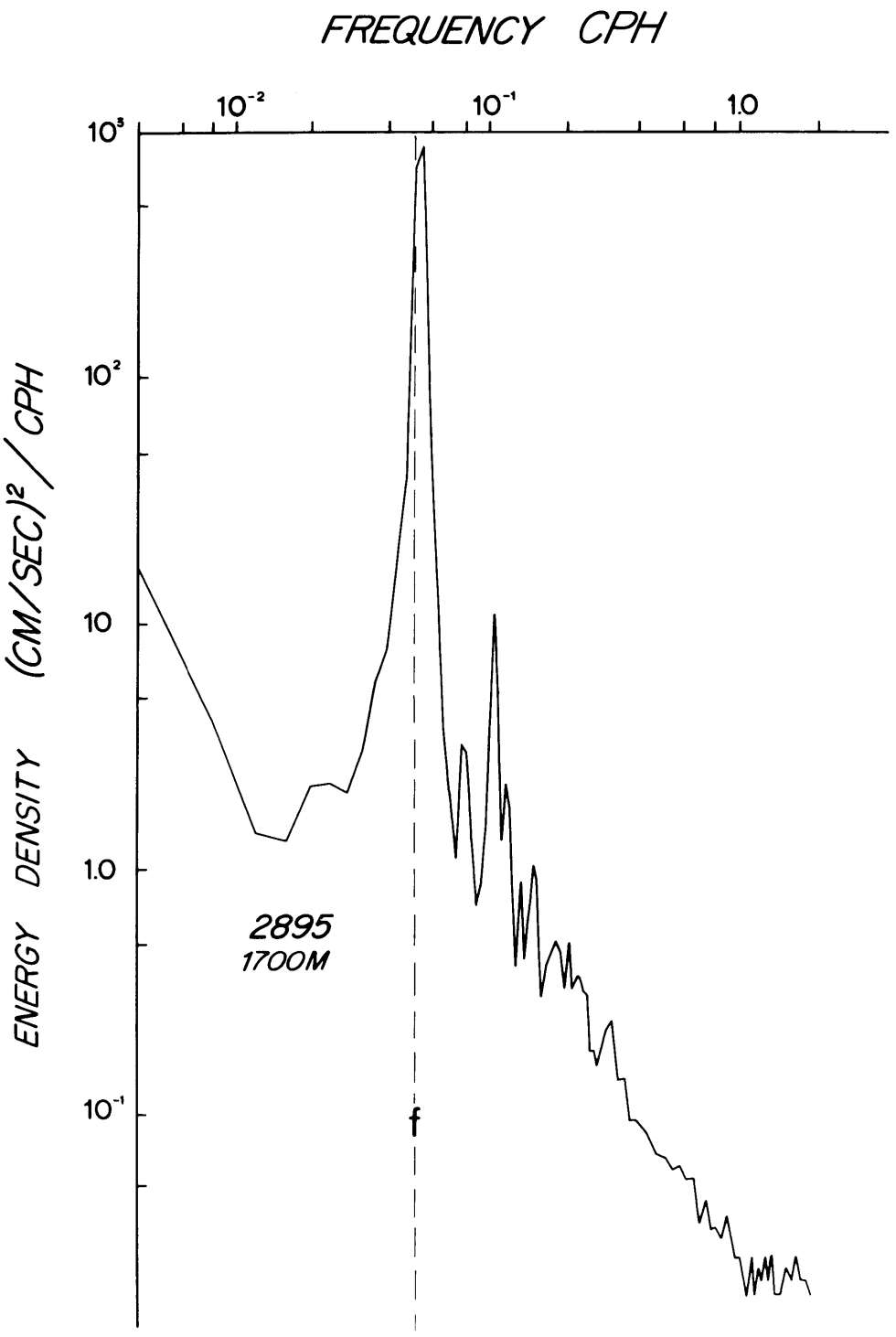


Figure 13 Power spectrum of currents at 1700 meters

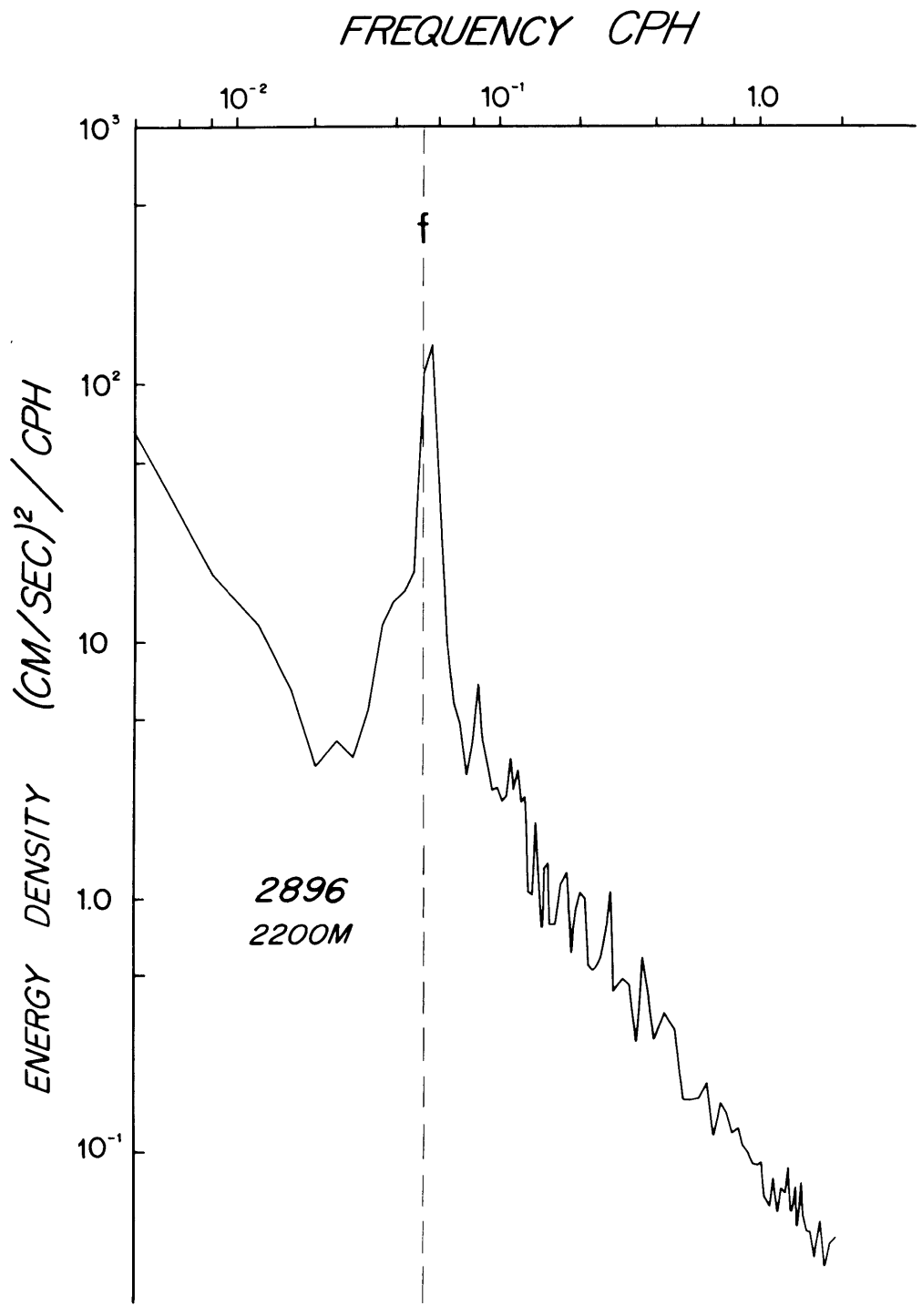


Figure 14 Power spectrum of currents at 2200 meters.

estimates would be distributed according to chi-squared with four degrees of freedom for each data section since there are two Fourier coefficients for each of the two scalar series. However, since the two series are nearly perfectly coherent near inertial frequency, only two degrees of freedom can be assumed in that frequency band. Hence the resultant spectrum is considered to be distributed according to chi-squared with 16 degrees of freedom except near inertial frequency where there are only 8 degrees of freedom. For the former case, the true spectral values are expected to be within a factor of 0.45 to 1.85 of the computed values at the 95% confidence levels and for the latter case, the corresponding factors are 0.30 and 2.38. Statistical stability of the spectral estimates has been sacrificed to some extent to give greater frequency resolution. Still it is clear from the plotted results that the width of the peak at inertial frequency is not resolved since it is defined by only two or three estimates.

It is of interest to note in passing that all spectra show the same characteristic shape at frequencies above inertial as do those measured at Site D and elsewhere. Harmonics can be seen at multiples of inertial frequency, presumably due to clipping caused by rotor stalls and leakage from the main peak.

A different view of the spectral content of the data is afforded by figure 15 where the same spectra have been recomputed with maximum frequency resolution and plotted on a log-linear scale in the vicinity of the inertial peak. This can only be done at the expense of statistical stability, which, according to the discussion just given, results in estimates distributed according to chi-squared with 2 degrees of freedom. Note that the spectrum of the 2200 meter measurements has only half the frequency resolution of the others since the series is only about half as long. The apparent structure shown near inertial frequency can be explained on the basis of statistical instability or by time varying properties of the signal, as well as by the signal having the indicated structure in a deterministic sense. One way of characterizing these spectra is through their value of Q, defined as the frequency width of the spectral peak divided by its central frequency. While values of Q are sometimes used as an indication of the extent to which damping is present in a highly tuned resonator, it is given here only as a guide to the sharpness of the spectral peak. The spectra of figure 15 show half-power bandwidths roughly equal to or double that imposed by the spectral analysis, which is 0.001 cycles per hour (1/1024 hrs.),

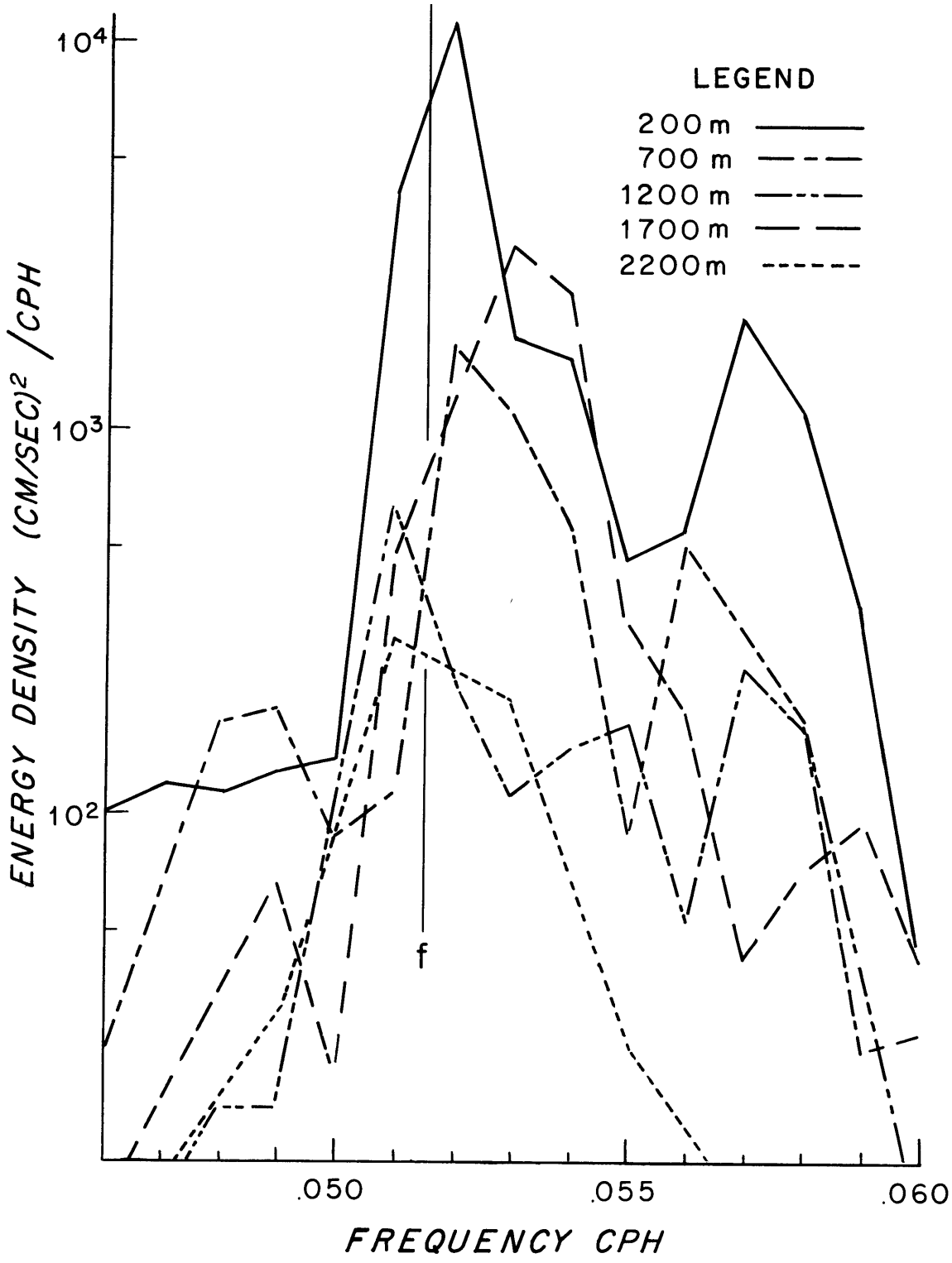


Figure 15 Energy spectra near inertial frequency at maximum frequency resolution for each of the data series.

indicating that the peaks are still not well resolved. The corresponding estimates for Q range from 25 to 50, which should be thought of as representing lower bounds.

The kinetic energy spectra do not indicate the extent to which the currents are circularly polarized, although it is clear from the progressive vector diagrams that the currents corresponding to inertial frequency have a strong rotary component in the clockwise direction. Documentation of the circular, clockwise character of the data is provided by the following scheme which is essentially due to Mooers (1970, Appendix III).

Given series u and v, corresponding to east and north components of current respectively, define the complex current U by $U = u + iv$. The n-th Fourier components U_n of U may be represented as

$$U_n = A_n e^{i\omega_n t} + A_{-n} e^{-i\omega_n t}$$

with complex coefficients A_n and A_{-n}. The current $e^{i\omega_n t}$ represents a current of unit magnitude rotating in a circular counterclockwise sense and in the representation for U_n, A_n defines its amplitude and phase. Similarly, A_{-n} defines the amplitude and phase of the circular, clockwise-rotating component of U_n. The coefficients A_n and A_{-n} are defined in terms of the

real Fourier coefficients of the u and v series as follows:

$$A_n = \tfrac{1}{2}[(a_{un} + b_{vn}) + i(a_{vn} - b_{un})]$$

$$A_{-n} = \tfrac{1}{2}[(a_{un} - b_{vn}) + i(a_{vn} + b_{un})]$$

where a_{un}, b_{un} are respectively the Fourier cosine and sine coefficients of series u for frequency ω_n, and a_{vn}, b_{vn}, are the corresponding coefficients of series v. The values a_{un}, etc., are recoverable given A_n, A_{-n}, which shows that the decomposition given for U_n is the most general possible. It is now reasonable to define the spectrum of U at frequency ω_n as

$$S_{UU}(\omega_n) = \overline{A_n A_n^*}$$

$$S_{UU}(-\omega_n) = \overline{A_{-n} A_{-n}^*}$$

where the overbar denotes ensemble averaging and * denotes complex conjugation. Thus at positive frequencies S_{UU} measures the clockwise energy. By applying the expressions for A_n and A_{-n}, and making use of the usual spectral relations

$$P_{uu}(\omega_n) = \overline{a_{un}^2 + b_{un}^2}$$

$$P_{vv}(\omega_n) = \overline{a_{vn}^2 + b_{vn}^2}$$

$$Q_{uv}(\omega_n) = \overline{a_{un}\, b_{vn}} - \overline{a_{vn}\, b_{un}}$$

where P_{uu}, P_{vv} are the autospectra of u and v respectively and Q_{uv} is the quadrature spectrum between them, one finds

$$S_{UU}(\omega_n) = \tfrac{1}{4}[P_{uu} + P_{vv} + 2Q_{uv}]$$

$$S_{UU}(-\omega_n) = \tfrac{1}{4}[P_{uu} + P_{vv} - 2Q_{uv}].$$

Note that the sum of these is the kinetic energy density at frequency ω_n. Table 1 shows these two quantities evaluated at inertial frequency for each data series. That the currents are almost totally circular, clockwise polarized is evident.

Table 1

Kinetic energy density at inertial frequency decomposed into counterclockwise and clockwise constituents.

Depth meters	$S_{UU}(f)$ $(cm/sec)^2/c.p.h.$	$S_{UU}(-f)$ $(cm/sec)^2/c.p.h.$
200	12.	2167.
700	4.	434.
1200	3.	164.
1700	3.	603.
2200	9.	106.

In terms of spectral analysis, it is possible to characterize to some extent the similarity between the various records, which is apparent in figure 4, for example, by computing coherence estimates between pairs of records. Here the coherence C between two scalar time series, say the east components of two current-vector series, is defined by

$$C = (P_{12}^2 + Q_{12}^2)^{\frac{1}{2}} (P_{11} P_{22})^{-\frac{1}{2}}$$

where P_{12} and Q_{12} are respectively the co- and quadrature spectra between series 1 and 2. Similarly P_{11} and P_{22} are the autospectra of series 1 and of series 2. (Note that some authors define C^2 as the coherence.) The associated phase θ is defined as $\theta = \tan^{-1} Q_{12}/P_{12}$. We recall that coherence at a particular frequency implies a consistent phase relationship between constituents of the two series at that frequency over the data series, and θ is a measure of that phase difference.

Table 2 shows the result of computing coherence at inertial frequency between corresponding components of various pairs of records. The records were divided into 9 sections of 128 hours each, for which the expected coherence for an incoherent, Gaussian process is .30 and for which coherence greater than 0.56 is significant at the 95% level according to Amos and Koopman (1963). An exception is made for the pair involving the deepest instrument since that instrument failed after February 20. In this case, there are only 5 data pieces and the corresponding expected and 95% significance levels are 0.41 and 0.73 respectively. Also computed is the coherence between the records from 200 and 1700 meter levels since they are the two most widely separated series for which there is an adequate

signal level.

Table 2

Coherence at inertial frequency between various pairs of current records.

Inst. Depths	East Components		North Components	
	C	θ	C	θ
200 - 700	0.7	119°	0.6	124°
700 - 1200	0.2	-166°	0.2	-145°
1200 - 1700	0.6	-22°	0.6	-29°
1700 - 2200	0.6	-84°	0.6	-85°
200 - 1700	0.6	-112°	0.5	-113°

All pairs show significant coherence except for the 700 - 1200 meter pair, even though both these series clearly contain signals of very nearly inertial frequency. This suggests that there is not a consistent phase relation between the two series. Examination of figure 4 shows in fact that the two series have nearly the same phase during the early part of the data series, but nearly opposite phase during the last part. It has already been noted that there was an apparent change

in the character of the records around mid-February. The phase estimates are more difficult to interpret, being angular averages which, as is clear from figure 4, are somewhat variable with time.

Variation of coherence with frequency is illustrated in figure 16 for the east components of the series at 200 and 1700 meters. It is fairly typical of coherence between the other pairs of series, decreasing to the expected value for an incoherent process at frequencies away from inertial.

The standard techniques which have been used here do not give any insight into the variations of amplitude and phase with time which are apparent in the data series shown in figure 4. One suspects that in view of the high signal strength in the records that other techniques are possible which would yield quantitative estimates of these variations. A technique for doing this, somewhat loosely called complex demodulation, has been devised and is now described.

Complex Demodulation

For inertial waves, one can define the complex current $U(t) = u + iv = Ae^{-ift}$. The hodograph of such a current describes a circle in the complex u, v plane,

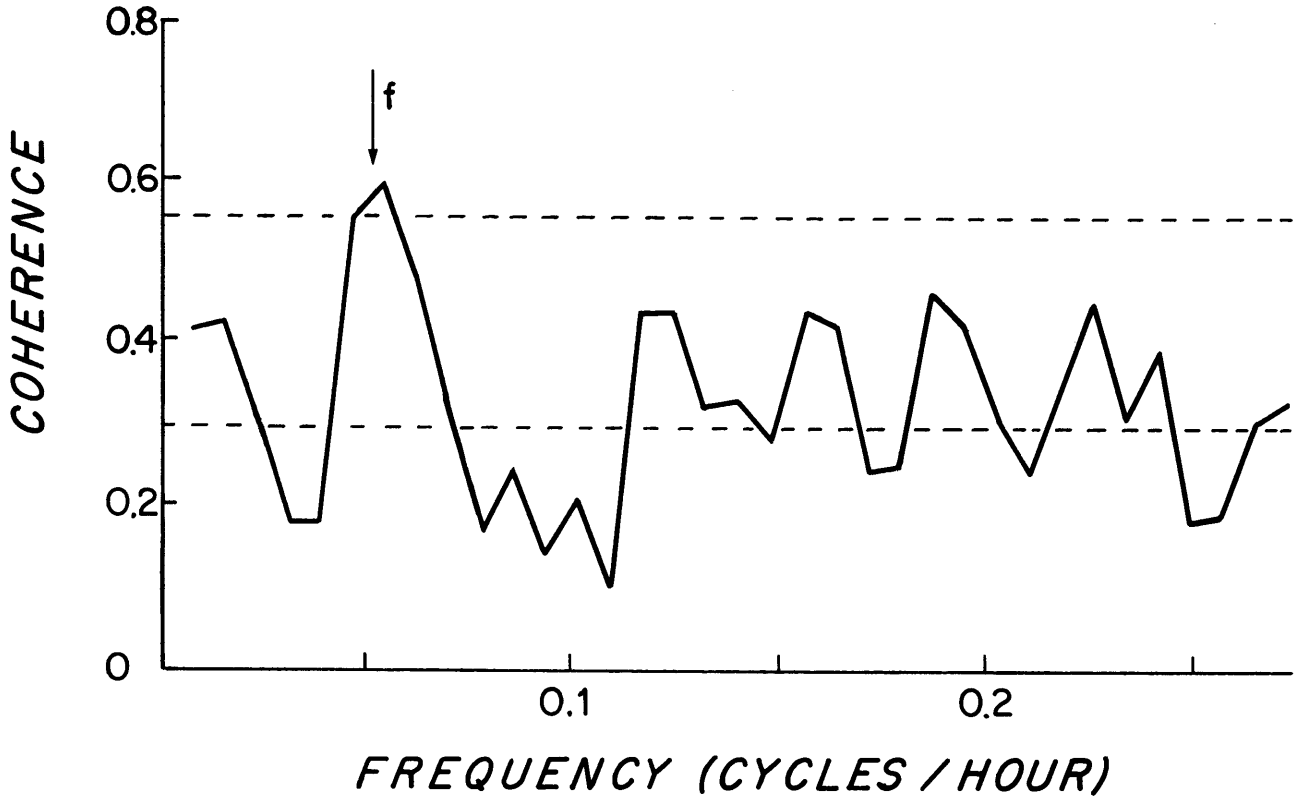


Figure 16 Coherence vs. frequency for the east components of data series at 200 and 1700 meters. The lower dashed line shows the expected value for incoherent processes and the upper the 95% confidence level.

rotating in the clockwise direction. More generally, we can also include a counter-clockwise rotating component and superimpose many such currents with different frequencies. Thus

$$U(t) = \int_{-\infty}^{\infty} d\omega\ A(\omega)\ e^{-i\omega t}. \qquad \text{II-1}$$

To be definite, it is imagined that the magnitude of A is sharply peaked near $\omega = f$ as is appropriate for a signal dominated by inertial oscillations.

Next, imagine an idealized inertial wave e^{-ift} and seek a complex coefficient D for it which makes it most closely resemble the given signal in a least squares sense over some interval of time 2T centered around some specified time τ. If 2T is held fixed throughout (two inertial cycles in the case at hand), then the resulting quantity $D(\tau)$ is called the complex demodulate of U or of u and v.[1] The defining criterion is then that

---

[1] This definition of complex demodulation is not analytically equivalent to that defined by Bingham, Godfrey and Tukey (1967) but has the same heuristic interpretation.

$$\int_{\tau-T}^{\tau+T} | D\, e^{-ift} - U(t) |^2 \, dt = \text{minimum} \qquad \text{II-2}$$

or, taking $\frac{\partial}{\partial D^*}$, where * denotes complex conjugation, we have at once

$$D = \frac{1}{2T} \int_{\tau-T}^{\tau+T} e^{ift}\, U(t)\, dt. \qquad \text{II-3}$$

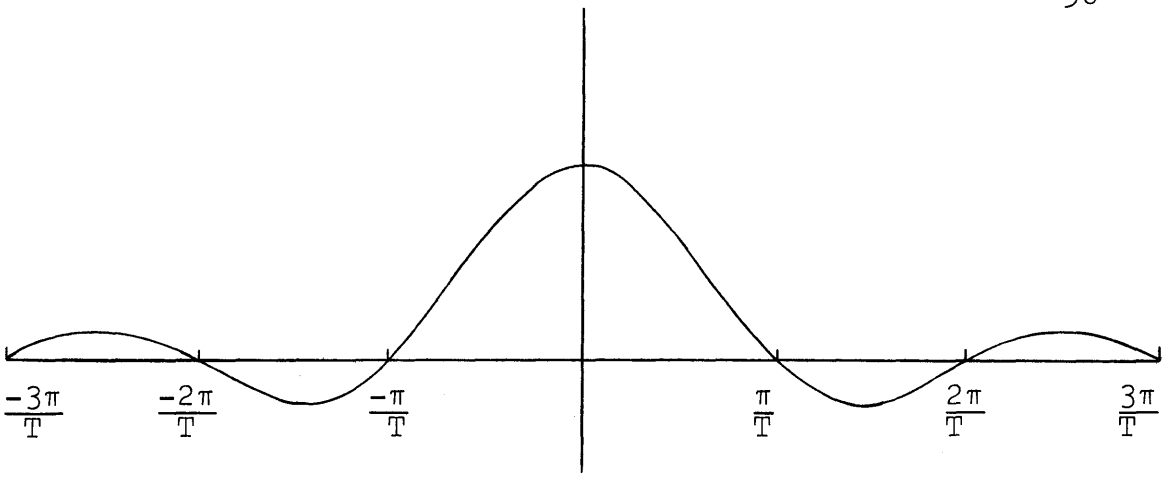
Substituting the specified expression for U and carrying out some easy integrations, we finally have

$$D(\tau) = \int_{-\infty}^{\infty} d\omega\, A(\omega)\, W(\omega-f)\, e^{-i(\omega-f)\tau}. \qquad \text{II-4}$$

Here $W(\omega)$ is the real amplitude window through which the demodulate D sees the spectral distribution A of the signal. It is given by

$$W(\omega) = \frac{\sin\, \omega T}{\omega T}. \qquad \text{II-5}$$

The shape of this window, which appears so often in spectral analysis, is shown in the accompanying sketch.



There is also a phase shift associated with the window; namely $(\omega-f)\tau$.

As an illustrative example, suppose the signal consists of a pure sine wave of frequency slightly different from f; say, $A(\omega) = A_o\delta(\omega-f-\varepsilon)$ so that $U(t) = A_o\, e^{-i(f+\varepsilon)}$. It then follows that

$$D(\tau) = A_o \int_{-\infty}^{\infty} d\omega\ \delta(\omega-f-\varepsilon)W(\omega-f)\ e^{-i(\omega-f)\tau}$$

$$= A_o W(\varepsilon)\ e^{-i\varepsilon\tau}. \qquad \text{II-6}$$

For ε sufficiently small, we have $W(\varepsilon) = 1$, but the phase continues to change linearly with time at a rate depending on the difference of the signal frequency from the demodulation frequency.

In practice, the demodulation frequency was chosen as the inertial frequency at the observing latitude, 38° 01'N, which corresponds to a period of 19.43 hours. The period 2T, over which the least-square fit by this signal was made, was chosen as two inertial periods and the complex demodulates $D(\tau)$ were computed for increments in τ of one inertial cycle. That is to say, a portion of data two inertial periods in length was chosen. This was fit by a curve of the form e^{-ift} to give a demodulate estimate $D(\tau_1)$. Then the next portion of data was chosen (in order of increasing time) of equal length and overlapping the preceding portion by one inertial period or one-half its length. This data was similarly fitted to give $D(\tau_2)$ and so on. Hence, each estimate of $D(\tau)$ is completely independent of all others except for the two which immediately precede and follow it, and with each of these the determining portions of data overlap by half their length. The mean was also determined for each piece at the same time the sine-wave fit was made. A linear trend was experimentally found as well but proved to have no significant effect on the other quantities.

As a numerical example, a signal was synthesized at 15 minute intervals consisting of white noise which was uniformly distributed between 0 and 80 cm./sec. plus a signal having the desired rotary characteristic with a magnitude or half-wave amplitude of 10 cm./sec. and a period of 19.0 hours. The signal was barely discernable in the resulting series. Results of demodulating this signal at 19.6 hours (3% lower frequency) in the manner described above is shown in figure 17 as a magnitude and phase. Exact values for magnitude and phase for the signal alone are shown by dashed lines. The 3% frequency difference appears as a uniform drift of phase with time. For the present case, demodulation clearly defines the signal frequency to within a small fraction of one percent. More generally, the precision to which the signal frequency can be determined depends on how long it remains constant and on the structure of the spectrum near its peak, as well as on the level of noise present. None of these factors can be known a priori for the data being considered here but this example indicates that if the spectrum is sharply peaked, demodulation can be expected to give a satisfactory estimate of the frequency of the peak even in the presence of substantial amounts of noise.

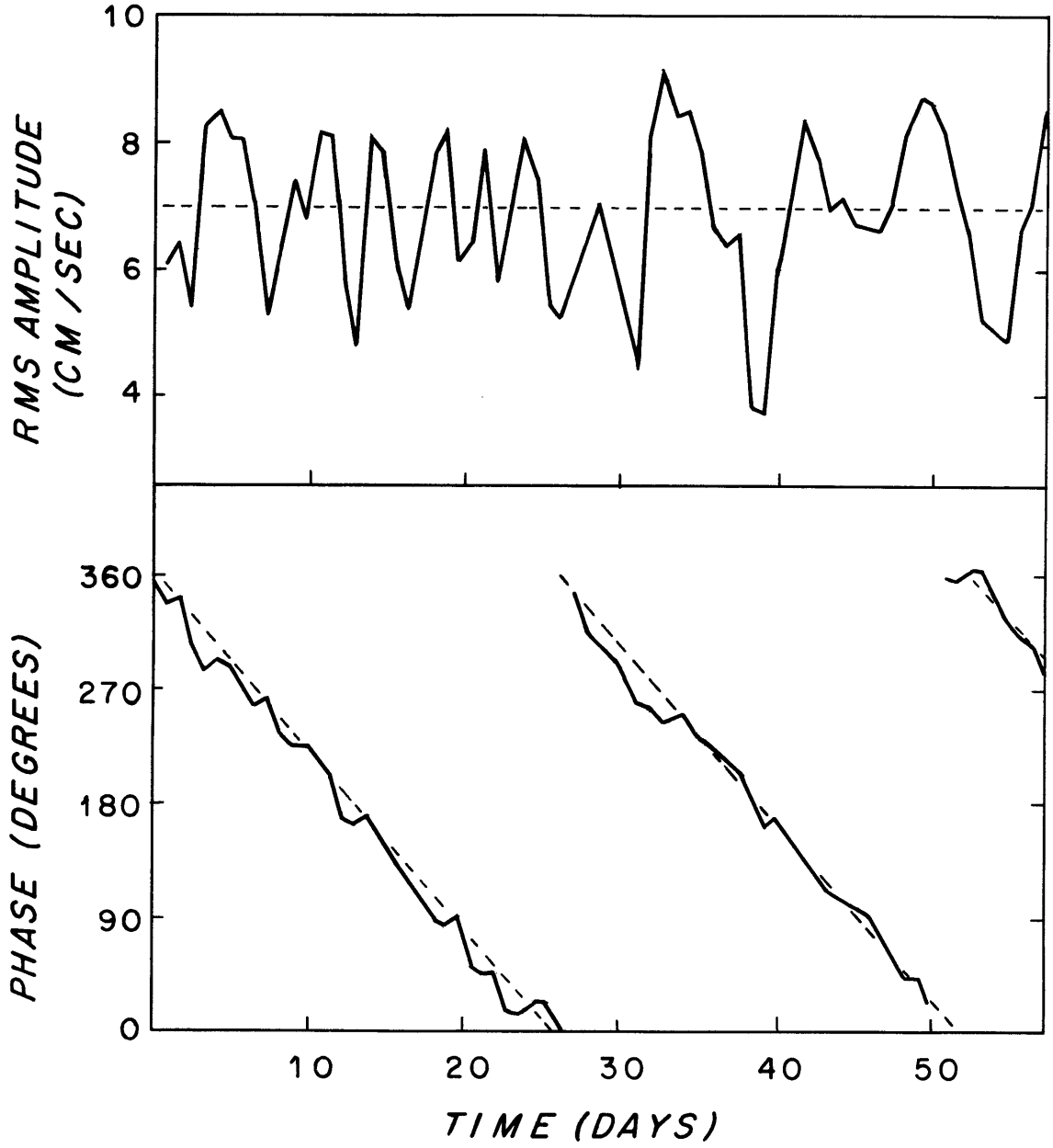


Figure 17 Complex demodulate of a synthetic signal plus noise as discussed in the text. The demodulation frequency was 3% lower than the signal frequency. Exact values of amplitude and phase for the signal alone are shown by dashed lines.

Results of the procedure when applied to the data are shown in figure 18 as a magnitude and phase. The right hand series of curves are the magnitude and the left hand series the phases with successive data series given in order of increasing depth. As noted in the preceding example, a slow change in phase is interpreted as a difference between the signal and demodulation frequencies. This is embodied in the inset at far right which shows slope of the phase curves for various departures of the signal above local inertial frequency as a percentage of that frequency.

It is clear that there is a systematic departure from local inertial period in the direction of increasing frequency. Particularly noteworthy is the first part of the data at the fourth (1700 m.) level, which was pointed out earlier as being unusually sinusoidal in appearance. The phase change there is remarkably uniform and corresponds to a frequency three percent above inertial. A similar trend is apparent in the other four curves during about the first three weeks of the data series. Also of interest during this period is the difference in phase between the various pairs of curves; the two upper curves have nearly the same phase at any given time and the three lower curves

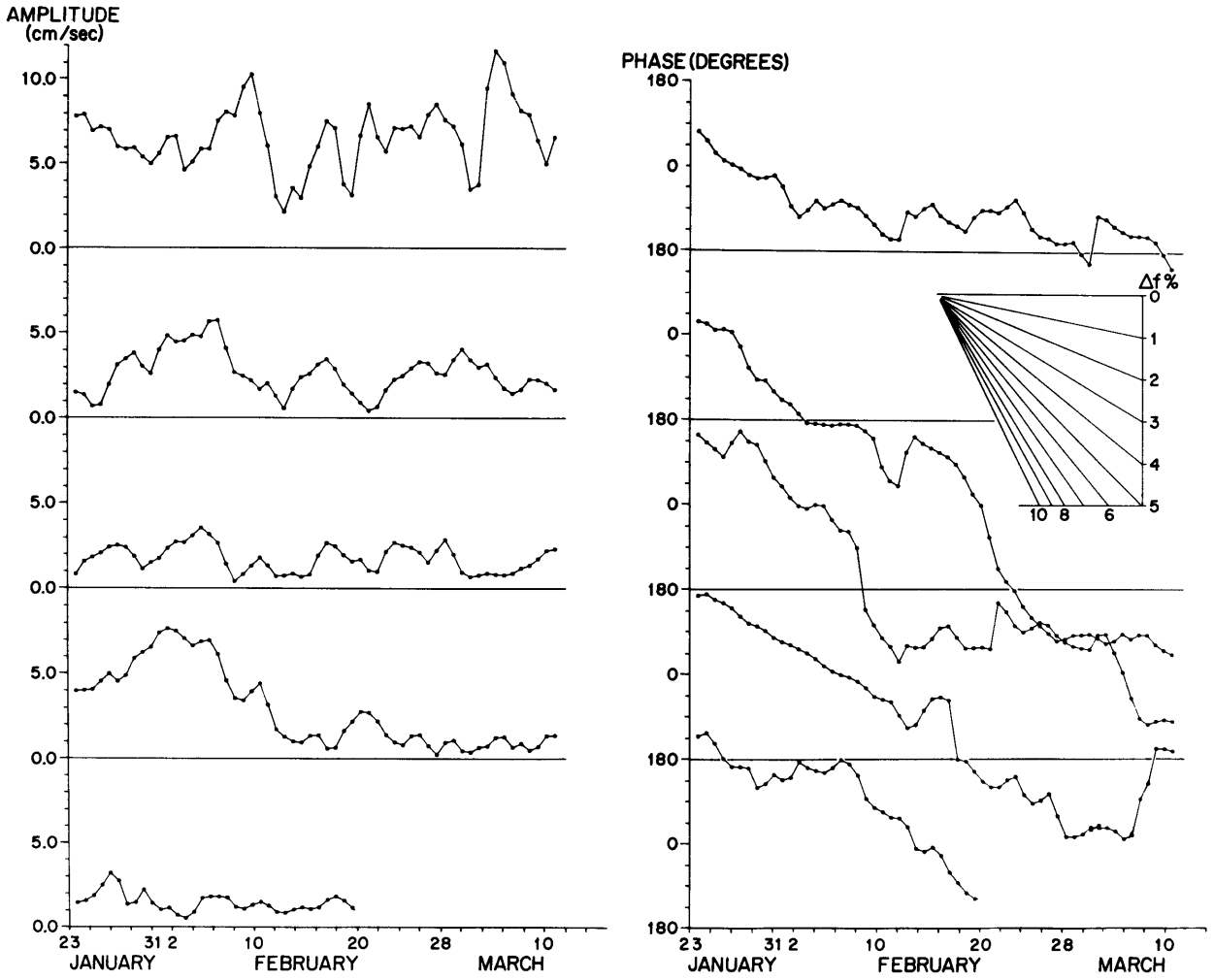


Figure 18 Complex demodulates of the five series of current measurements shown as amplitude and phase. The inset shows percentage increase of observed over local inertial frequency as a function of slope of the phase curves.

also have roughly the same phase, but these two phases differ from one another by about 180°. Those portions of data for which the phase estimates seem least stable correspond in general to intervals where amplitudes are quite small.

Thus the demodulation method gives more easily interpretable results than do the spectra in figure 15 for this particular set of data. A frequency shift is suggested in all of the spectra, but no quantitative estimate of it is possible even with spectra computed at maximum frequency resolution.

Two final points should be noted. Firstly, data from the bottommost instrument cannot be used after February 20 since directions are not available after that time. Secondly, the demodulation technique used here is so successful largely because of the very sharp single peak present in the spectra. The spectral window implied by the procedure is not a very good one, at least by the standards of conventional spectral analysis, and so cannot discriminate well against signals at other frequencies.

Some success has been achieved using the method at Site D where a strong tidal peak is present by adjusting the demodulation interval (2T) so that the

spectral window (W) has a zero at tidal frequency when demodulating an inertial signal. The results are not as clean as those shown here but suggest a shift towards high frequencies of the inertial energy.

Supporting data

A hydrographic station was made immediately after the mooring was set using a Bisset-Berman STD to a depth of 1500 meters. This has been combined with a conventional hydrographic station (AII-1273) made a few hours later at 40°N 6°E. The two are shown together in figure 19, with Station 1273 having been used below 1000 meters. Temperature points read from the STD trace at points between which the trace was nearly linear are shown by solid round dots and those from Station 1273 are denoted by solid squares. Correspondingly determined values for salinity are denoted by x's and +'s. Note the good agreement in the region between 1000 and 1500 meters where the two measurements overlap.

These data were used to compute the stability or Brunt-Väisälä frequency as a function of depth shown in figure 20. The plot is made on a displaced logarithmic scale in the vertical so that details may be seen in the surface layers. Open circles indicate

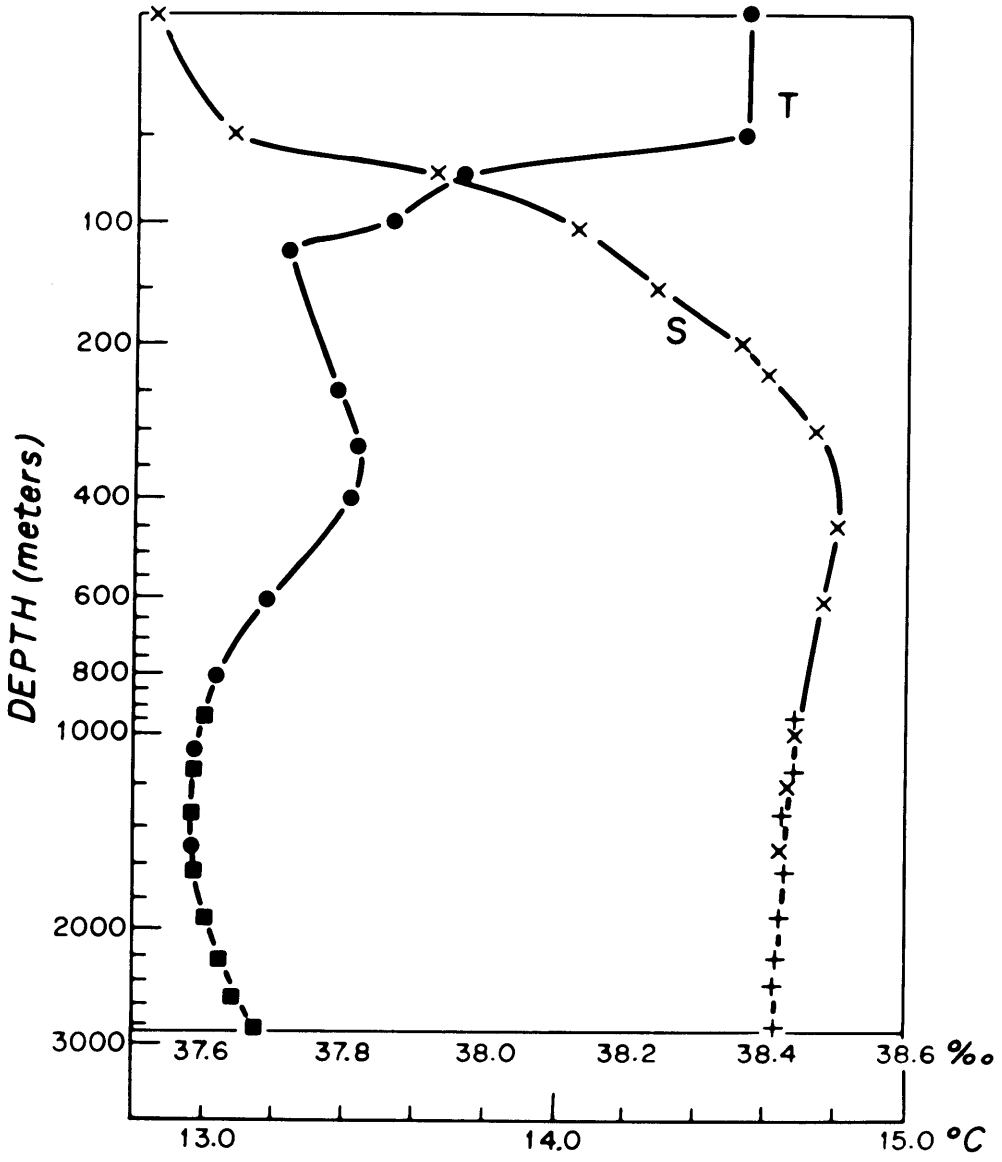


Figure 19 Temperature and salinity vs. depth. Circles and x's show temperature and salinity respectively from an STD lowering made at the observing site when the mooring was deployed. Squares and +'s are corresponding data from AII station 1273 at 40°N 6°E taken several hours later.

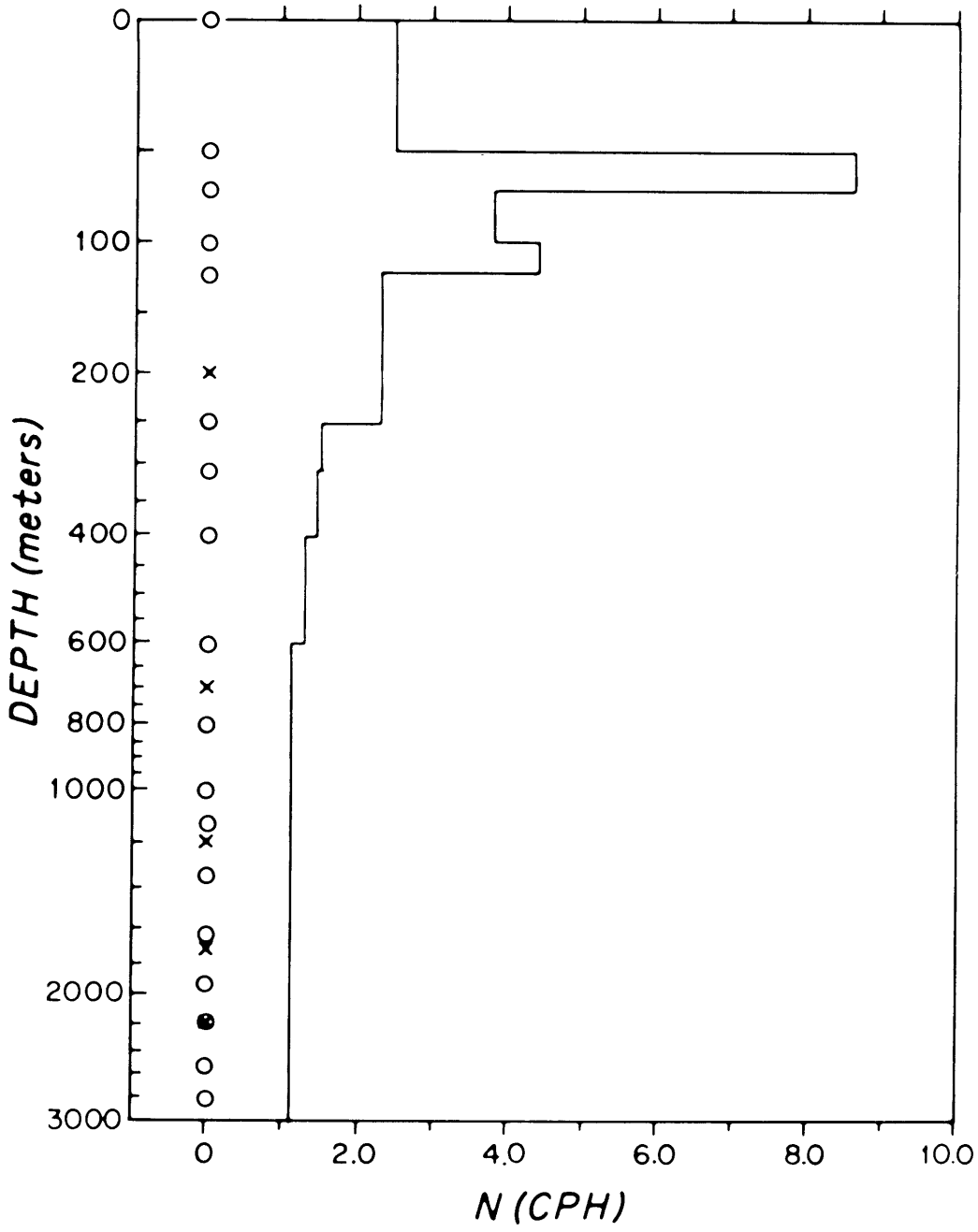


Figure 20 Brunt-Väisälä or stability frequency vs. depth.

depths at which temperature-salinity pairs were tabulated for the stability computation. They are useful primarily in the deep water where the constancy of the stability prevents the tabulated depths from being apparent; the uniformity of the deep stratification is not due to any lack of depthwise resolution in the observational data. Depths corresponding to current meter levels are marked by an x. Stability was computed from the equation of Hesselberg and Sverdrup using Ekman's equation of state for seawater (Fofonoff, 1962). Since it depends on gradients, the stability is determined as a piecewise constant function between tabulated depths. The stability frequency plays an important role in the dynamical arguments which follow, and it is unfortunate that additional determination of it could not have been made. This was due to scheduling of ship and personnel, whose primary commitment lay in exploring the hydrographic properties of the Mediterranean water much further north, around latitude 42°N. As a result of this activity, it is known that there were significant changes in the stability of this northern region both in space and time, believed to be associated with wintertime formation of deep water in the Mediterranean basin. These changes were

confined to the northern part of the basin however and historical data (W.H.O.I. archives) show no significant variation of stability within the observing region, changes being evident only in the near-surface levels over the months during which the current measurements were made. It is therefore reasonable to accept the computed stability to be a fair representation over the area of interest.

Figure 21 shows wind measurements as speed and direction throughout the observing period. These were obtained as geostrophic winds computed from the 12 hourly pressure data at selected grid points available through the Environmental Science Service Administration and interpolated to the observing site.[1] The grid points involved in this scheme were rather widely separated, being at 35°N 05°E, 40°N 00°E, 45°N 05°E, and 40°N 10°E. It can be argued both ways about the adequacy of this grid, depending upon whether one believes deep inertial oscillations to be generated by the wind, if they are at all, through either local or large scale forcing.

---

[1] The author is grateful to Christopher Welch for making available his computer programs for carrying out these computations.

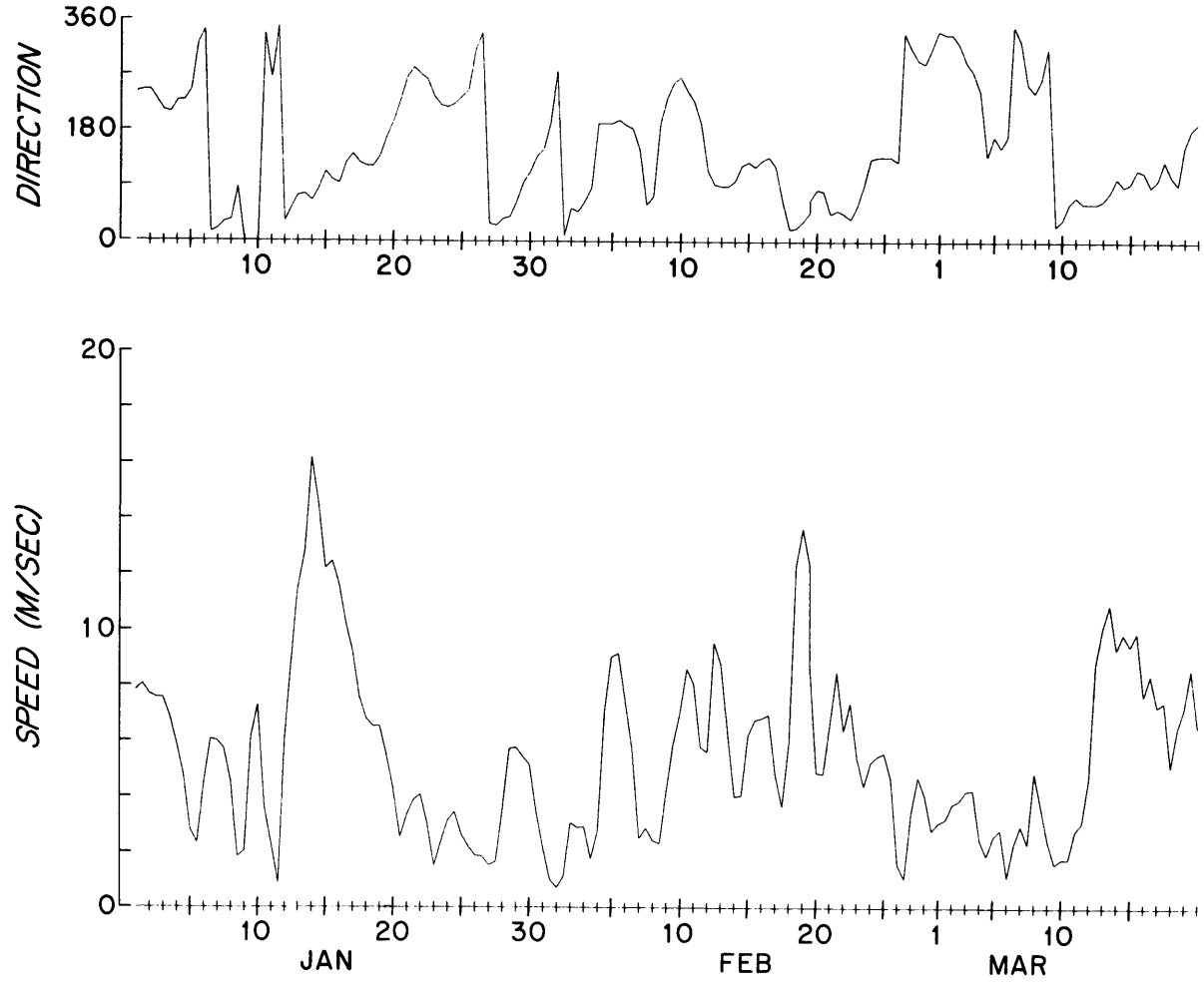


Figure 21 Geostrophic wind speed and direction at 12 hour intervals at the observing site.

Two possibly important features of the wind data are pointed out, namely the storms which took place around January 14 several days before the mooring was deployed and the stormy period in mid-February. It is possible that the latter is related to the change in the mean current or to the change in the character of the inertial oscillations which were observed during the same period. The former might similarly have been responsible for the large inertial signal observed throughout the first three weeks of observations.

Chapter III A ray theory interpretation

Techniques for tracing the flow of energy through a slowly varying medium have evolved into a fairly standard formalism as outlined, for example, by Whitham (1960) and the approach used here follows quite closely that of Eckart (1960), except that emphasis here is on local rather than global features of the solutions. Our attitude is similar to that of Blanford (1966) who examined, however, only horizontal paths of propagation. One feature inherent in moored current meter data is sparse sampling in the vertical. Yet it is sufficiently dense to require that account be kept of depths at which inertial-period energy may be found. Hence, our attention is fixed on vertical as well as horizontal components of wave propagation.

Basic equations

We begin by writing the equations of motion for a rotating, stratified, incompressible fluid in spherical coordinates where the Boussinesq approximation has been made:

$$
\begin{aligned}
u_t - fv &= - p_\lambda/(a \cos \phi) \\
v_t + fu &= - p_\phi/a \\
w_t &= - p_z - N^2\zeta \\
w &= \zeta_t \\
w_z + [u_\lambda &+ (v \cos \phi)_\phi]/(a \cos \phi) = 0
\end{aligned}
\qquad \text{III-1}
$$

where

$f = 2 \Omega \sin \phi$ is the coriolis frequency,

Ω is the earth's rotation rate,

ϕ, λ, z are latitude, longitude and elevation (measured upwards) respectively,

u, v, w are respectively east-west, north-south, and up-down components of velocity,

p is pressure variation about hydrostatic divided by the mean density,

ζ is vertical particle displacement from equilibrium,

a is the radius of the earth, and

N is the Brunt-Väisälä frequency, defined by $N^2 = -g\rho_z/\rho$

with $\rho = \rho(z)$ the in situ density and g the acceleration of gravity. The horizontal component of earth's rotation is neglected here, an approximation which is discussed later in this chapter and more fully in Appendix I. These are essentially the equations used by Munk and Phillips, for example, except that we will retain the term w_t in the third equation. It is possible to use

them in this form and it is essential to do so if one is interested in solutions valid over a wide range of latitude. But for our purposes, where the range of latitudes is limited, significant simplification is possible.

Define local Cartesian coordinates x, y with respect to some reference point ϕ_o, λ_o by

$$x = a(\lambda - \lambda_o) \cos \phi_o; \quad y = a(\phi - \phi_o).$$

Then making the approximations (all in the continuity equation)

$$\cos \phi \simeq \cos \phi_o$$

$$\sin \phi \simeq \sin \phi_o$$

and $v \tan \phi_o \ll v_y$

the equations become

$$\begin{aligned} u_t - fv + p_x &= 0 \\ v_t + fu + p_y &= 0 \\ w_t + p_z + N^2\zeta &= 0 \\ \zeta_t - w &= 0 \\ u_x + v_y + w_z &= 0. \end{aligned} \qquad \text{III-2}$$

Finally, so that f may have a simple dependence on y, we may make a Taylor expansion of f about ϕ_o which for small values of y leads easily to

$$f \simeq f(y) = f_o + \beta y \qquad \text{III-3}$$

where $f_o = 2\Omega \sin \theta_o$, $\beta = 2\Omega \cos \theta_o/a$. These are substantially the same equations as used by Blanford (1966) and constitute what may be called the non-equatorial beta-plane approximation.

Another way of viewing the approximation is that the chief neglect is of the convergence of the meridians towards the poles. At the latitudes of interest ($\sim 38°$) the meridians converge only by about 1% per degree of latitude, again indicating that the approximation is satisfactory. More important is that the latitudinal dependence of Coriolis force is retained since this variation determines behavior of the solutions having near-inertial frequency, as will be seen.

The phase function

We seek solutions of the form

$$(u, v, w, p, \zeta) = (U, V, W, P, Z)e^{i\Phi} \qquad \text{III-4}$$

where U, V, W, P, Z, and the phase function Φ are all, in general, functions of x, y, z, t. Note that if f and N are constant then U, ..., Z may be taken as constants so that Φ has the simple form

$$\Phi = kx + \ell y + mz + \omega t.$$

Substitution into the original equations then gives the familiar dispersion relation for inertio-gravity waves

$$(k^2 + \ell^2)(N^2 - \omega^2) = m^2(\omega^2 - f^2). \qquad \text{III-5}$$

Of interest here is the more general case $f = f_o + \beta y$ and $N = N(z)$. Nevertheless, to the extent that f and N are not rapidly varying, we suppose that U, ..., Z vary only slowly in space or time compared to Φ. Thus we neglect derivatives of U, ..., Z with respect to those of Φ; e.g.,

$$u_x = [U_x + iU\Phi_x]\, e^{i\Phi} \simeq iU\Phi_x e^{i\Phi}, \text{ etc.} \qquad \text{III-6}$$

This approximation, known as the WKB approximation, is the standard one in ray theory. Quite recently, attention has been drawn to the fact that in the case of inertial period motions there is necessarily a region, the size of which depends on the parameters involved, where the approximation breaks down. Approximation III-6 is essentially a short wavelength assumption, while, referring to the dispersion relation III-5, we see that as f approaches ω, corresponding to a wave group travelling northward, it follows that the horizontal scales become unbounded. Or, in terms of the phase function, Φ_x and Φ_y vanish, invalidating III-6. The extent of the region where this difficulty appears clearly depends on something like the ratio $(k^2 + \ell^2)/m^2$ which cannot be estimated at this time. Since there is no hope of delimiting the region in which ray theory is valid without some knowledge

of the spatial scales involved, the issue is not pursued further. Instead, the theory is assumed valid over a sufficiently large region for present purposes. In the next chapter, a quite different approach is followed, not depending on the approximation III-6.

Now substitution into the equations III-2 yields

$$\begin{aligned} iU\Phi_t - fV + iP\Phi_x &= 0 \\ iV\Phi_t + fU + iP\Phi_y &= 0 \\ iW\Phi_t + iP\Phi_z + N^2 Z &= 0 \\ U\Phi_x + V\Phi_y + W\Phi_z &= 0 \\ iZ_t - W &= 0 \end{aligned} \qquad \text{III-7}$$

In keeping with the foregoing discussion, we hold that U, ..., Z change slowly and treat the above equations as a linear system for those variables. Hence for solutions to be non-trivial, we require that the following determinant vanish:

$$\begin{vmatrix} i\Phi_t & -f & 0 & \Phi_x & 0 \\ f & i\Phi_t & 0 & \Phi_y & 0 \\ 0 & 0 & i\Phi_t & \Phi_z & N^2 \\ \Phi_x & \Phi_y & \Phi_z & 0 & 0 \\ 0 & 0 & -1 & 0 & i\Phi_t \end{vmatrix} = 0$$

This is entirely analogous to the derivation of the dispersion relation and reflects the hypothesis that the waves are locally comparable to plane waves corresponding to the local values of f and N.

Expanding the determinant we have[1]

$$(\Phi_x^2 + \Phi_y^2)(N^2 - \Phi_t^2) - \Phi_z^2(\Phi_t^2 - f^2) = 0. \qquad \text{III-8}$$

This is of course comparable to the dispersion relation except that N and f are no longer constant and the equation is treated as a partial differential equation for Φ called by Eckart the Hamilton-Jacobi equation. Although nonlinear, the equation is only first order and hence soluble. Fortunately, we can spot separable solutions of the form

$$\Phi = kx + \omega t + Q(y) + R(z) \qquad \text{III-9}$$

and the indicated dependence in x and t could have been assumed at the outset.

If the horizontal component of rotation is retained in the original equations, separable solutions are not possible unless, for example, N is constant. This is not an interesting case in terms of interpreting our data, but can be used to explore quantitatively the consequences

---

[1] A spurious factor of Φ_t has been dropped in III-8. In a more exact treatment, this factor is associated with Rossby waves.

of neglecting horizontal rotation. Carrying out the relevant calculations in Appendix I, we find the consequences to be negligible and we are amply justified in our approximation by the enormous simplification which results.

Upon substituting III-9 into III-8, we find the following equations for Q and R;

$$f_o^2 (k^2 + Q'^2) - s^2(\omega^2 - f^2) = 0$$

$$\text{and} \quad f_o^2 R'^2 - s^2(N^2 - \omega^2) = 0 \qquad \text{III-10}$$

where s is a separation constant of dimensions 1/length. The first of these can be integrated analytically since f has such a simple dependence on y ($f = f_o + \beta y$) but the second must be done numerically since N(z) is given only in tabulated form. For the moment this quadrature is simply indicated and the phase function Φ is taken as known;

$$Q = Q(y;\ \omega,\ k,\ s) = \pm \int_{y_1}^{y} [s^2(\omega^2 - f^2)\ f_o^{-2} - k^2]^{\frac{1}{2}}\, dy$$

$$R = R(z;\ \omega,\ s) = \pm \int_{z_1}^{z} [s^2(N^2 - \omega^2)\ f_o^{-2}]^{\frac{1}{2}}\, dz \qquad \text{III-11}$$

where y_1, z_1 are essentially arbitrary constants which we will eventually take to be the origin of a ray path.

Ray paths

Knowing the phase function, construction of the ray paths is straightforward, proceeding in the manner described by Eckart (1960). The rays will have the property of being everywhere parallel to the group velocity and so have the interpretation of being the lines along which energy propagates. By proceeding from first principles it is possible to arrive at simple analytical expressions for the rays.

Consider the sum of two wave-like constituents of the motion having slightly different values for their governing parameters; thus, for example,

$$u = U\{\exp i[k'x+\omega't+Q(y;\omega',k',s')+R(z;\omega',s')] + \exp i[k''x+\omega''t+Q(y;\omega'',k'',s'')+R(z;\omega'',s'')]\}$$

where we have assumed that the amplitude U is not strongly dependent on the parameters ω, k, s, and where $k' = k + \delta k$, $k'' = k - \delta k$, etc., for some suitably small values of δk, $\delta\omega$, and δs.

We may then write by Taylor's theorem

$$Q(y;\omega',k',s')=Q(y;\omega,k,s)+\frac{\partial Q}{\partial \omega}\delta\omega+\frac{\partial Q}{\partial k}\delta k+\frac{\partial Q}{\partial s}\delta s$$

and similarly for R, neglecting higher order terms. Substituting these into the expression for u we find

$$u=2U\cos\left[\left(\frac{\partial Q}{\partial k}+x\right)\delta k+\left(\frac{\partial Q}{\partial \omega}+\frac{\partial R}{\partial \omega}+t\right)\delta\omega+\left(\frac{\partial Q}{\partial s}+\frac{\partial R}{\partial s}\right)\delta s\right]$$

$$.\exp i[kx+\omega t+Q(y,\omega,k,s)+R(z,\omega,s)]. \qquad \text{III-12}$$

Thus the result resembles a wave having properties of the mean frequency and wavenumbers, but modulated by a carrier which is a slowly varying function of space and time. This is entirely analogous to the usual derivation of group velocity, except that the phase function is somewhat more complicated here, having other than linear dependence on the y and z variables. Energy is effectively trapped within its envelope and hence moving with the envelope. From the final expression III-12 for u, the envelope is seen to move according to:

$$\begin{aligned} \frac{\partial Q}{\partial k} &= x_1 - x \\ \frac{\partial Q}{\partial s}+\frac{\partial R}{\partial s} &= \ell_1 \\ \frac{\partial Q}{\partial \omega}+\frac{\partial R}{\partial \omega} &= t_1 - t. \end{aligned} \qquad \text{III-13}$$

With Q(y) and R(z) known, the first two of these determine a surface in x, y, z space in which the energy must travel and the third the travel time. Here x_1, ℓ_1 and t_1 are constants which are chosen so that the energy passes through a given point at a given time.

Carrying out the indicated differentiation of Q and R, one may write more explicitly

$$x - x_1 = \pm r f_o \int_{y_1}^{y} [\omega^2 - f^2 - r^2 f_o{}^2]^{-\frac{1}{2}} \, dy$$

$$\ell_1 = \pm l/f_o \int_{y_1}^{y} (\omega^2 - f^2)[\omega^2 - f^2 - r^2 f_o{}^2]^{-\frac{1}{2}} \, dy$$

III-14

$$\pm l/f_o \int_{z_1}^{z} [N^2 - \omega^2]^{+\frac{1}{2}} \, dz$$

$$t - t_1 = \mp s\omega/f_o \int_{y_1}^{y} [\omega^2 - f^2 - r^2 f_o{}^2]^{-\frac{1}{2}} \, dy$$

$$\pm s\omega/f_o \int_{z_1}^{z} [N^2 - \omega^2]^{-\frac{1}{2}} \, dz$$

with $r = k/s$. We see from these that any ray, corresponding to a specified value of r and s, will pass through the point x_1, y_1, z_1 at time t_1 if $\ell_1 = 0$

which we now assume. The two integrals in y can be carried out analytically:

$$\int[\omega^2 - f^2 - r^2 f_o{}^2]^{-\frac{1}{2}}\, dy = \frac{1}{\beta} \sin^{-1}\,[f\,(\omega^2 - r^2 f_o{}^2)^{-\frac{1}{2}}]$$

$$\text{and } \int(\omega^2 - f^2)[\omega^2 - f^2 - r^2 f_o{}^2]^{-\frac{1}{2}}\, dy \qquad \text{III-15}$$

$$= \tfrac{1}{2}(\omega^2 + r^2 f_o{}^2)/\beta \sin^{-1}[f\,(\omega^2 - r^2 f_o{}^2)^{-\frac{1}{2}}]$$

$$+ \tfrac{1}{2} f/\beta\, [\omega^2 - r^2 f_o{}^2 - f^2]^{\frac{1}{2}}$$

Geometry of the rays is determined entirely by the first two of the equations III-14, which depend only on the single parameter r. Thus for each value of r, there are in general eight curves which pass through the ray source x_1, y_1, z_1 corresponding to the various choices of sign. Four of these increase in z as x and y increase away from the origin and so are rejected since the ray origin is taken to be at the sea surface. The remaining four curves are symmetrical about the plane $x = x_1$, reducing to a pair of lines lying in the plane $x = x_1$ when $r = 0$.

Each ray has a northernmost limit which is characterised by vanishing of the radical in the expression III-15, corresponding to a latitude above which waves

of the prescribed frequency cannot propagate. This extremum is given by

$$y_{ext} = [\pm(\omega^2 - r^2 f_o^{\,2})^{\frac{1}{2}} - f_o]/\beta. \qquad \text{III-16}$$

The negative sign yields extreme or turning latitudes having very large negative values for y. These correspond to southward-bound rays which would reach turning latitudes in the southern hemisphere if it were not for the Algerian coastline from which they are reflected northwards in the present case. For the moment, these rays are ignored and we concentrate on the northward-bound rays which can arrive at the observing site without undergoing reflections.

Since the two northbound rays are symmetrical, it suffices to plot only one of them. This is done for a single frequency $\omega = f_o$ and various values of r in figure 22. The solid lines emanating from the chosen origin are the rays which may of course be shifted east or west without change of shape corresponding to a different choice of origin. Note that r acts as a steering parameter determining the ray direction. Solid lines intersecting the rays are lines of constant depth as indicated. Thus energy input at the chosen point can be expected to spread out along this surface, with different values of ω corresponding to different surfaces and

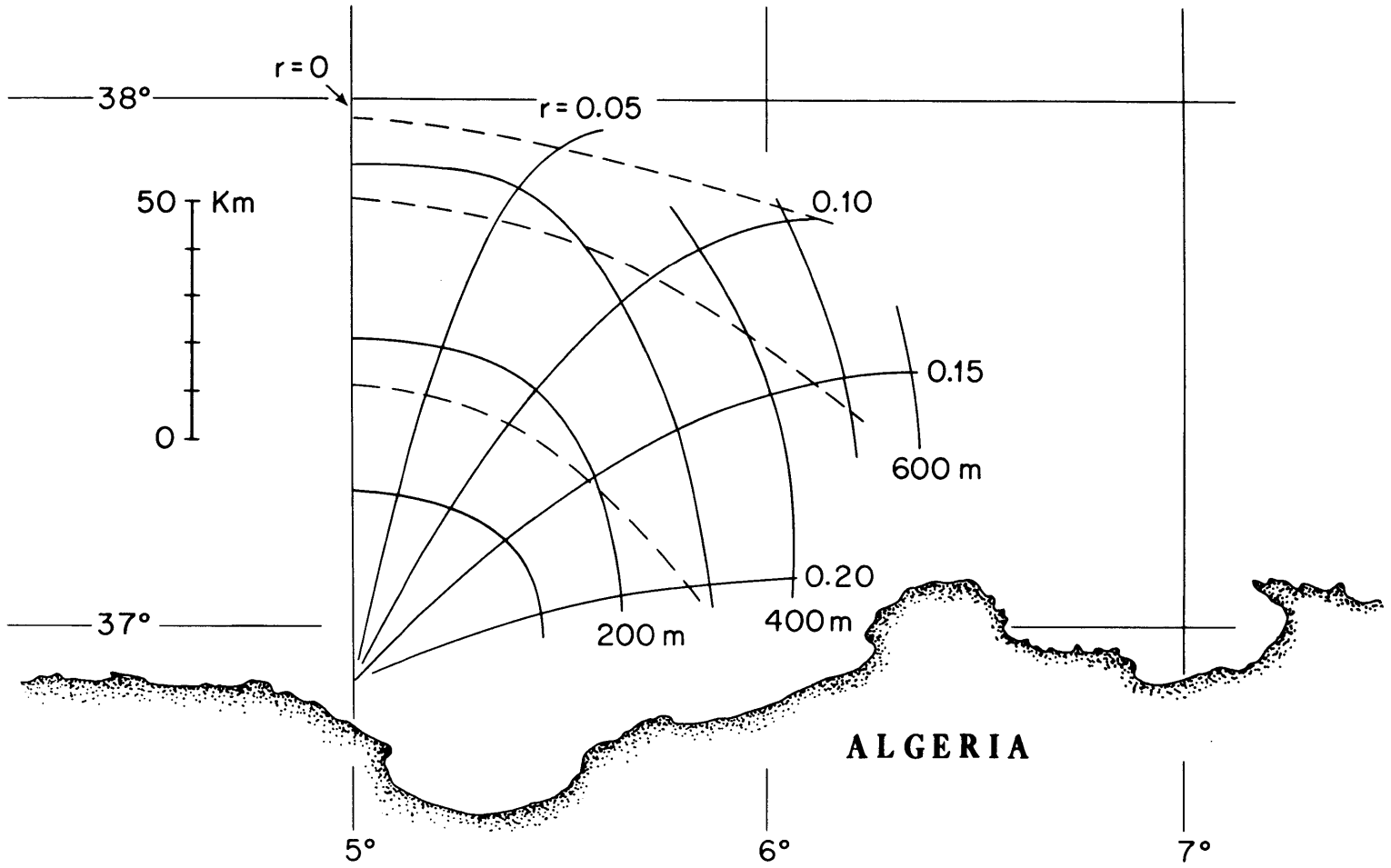


Figure 22 Ray paths corresponding to inertial frequency at 38°N are shown here emanating from a single point at the ocean surface. Intersecting solid lines indicate depth in meters and dashed lines indicate travel time. See text for a more complete description.

values of r determining direction within each surface.

Also shown in figure 22 are dashed lines intersecting the rays. These are determined from the third of the equations III-14 and are proportional to travel time from the origin. Note the crowding of these lines near their northernmost limit, especially for r very small. Such crowding corresponds to a bunching up of the energy in the corresponding region; hence the case $r \simeq 0$ is of particular interest. Although a ray point moves increasingly slowly as it moves northward, the travel time to its turning latitude is not infinite, even for the case $r = 0$ when the group velocity vanishes at the northern limit. Rather, the energy traverses the path in a finite time and is eventually reflected southward again.

Ambiguity in the travel time is apparent in the governing equation, for it depends not only on the parameter r which defines a ray for a given frequency, but also upon the separation constant s. In fact, travel times are proportional to s, which we do not know how to estimate. Hence a deep inertial oscillation which arrives from the ocean surface without having undergone reflections can be traced back to a fairly well defined region of the surface (depending upon how accurately its frequency can be determined) but we cannot know how long ago it originated there. This is a severe handicap for the ray theory, which prevents

establishing a direct relationship between deep inertial currents and meteorological processes.

The special geography of the Mediterranean is potentially quite important at this point, for the Algerian coastline places a limit on how far to the south the inertial energy can be generated. Thus there is a maximum depth to which energy arriving at the observing site directly from the surface (without reflection) can reach. Below this depth there is a shadow with respect to direct arrivals from the surface cast by the coast, below which energy can arrive only by having undergone one or more reflections. Of the rays with near-inertial frequency originating at the surface, those which do not travel northwards will intersect the coast and be reflected back into the hypothetical shadow zone, perhaps having been attenuated. This possibility is now explored.

That energy flow into the region of interest is possible through reflections of rays from the coast can be seen geometrically. Neglecting the east-west component of wavenumber k in the dispersion relation III-5, the expression can be rearranged into the form

$$m/\ell = \pm[(N^2-\omega^2)/(\omega^2-f^2)]^{\frac{1}{2}} = \tan\theta$$

where θ is the angle of the wavenumber vector with respect to horizontal. From the observed frequency and the value of f corresponding to the latitude of the coast, we have $\omega/f = 1.05$. Then if N = 1.0 cycle per hour, the corresponding value for θ is 89°; i.e. the wavenumber vector is about one degree from vertical. Thus for the particular frequencies chosen, the dispersion diagram in the ℓ,m plane is "X" shaped (or double cone-shaped in three dimensions) with a sharp vertex. It is apparent that as ω increases towards f, the vertex becomes increasingly sharp and θ approaches 90°. Hence since the group velocity is the gradient in wavenumber space of the curves corresponding to constant frequency, it is directed perpendicularly to the constant-ω curve and with a component towards the m axis.

In figure 23(a) a line OB having the same angle ϕ as that of the coast, estimated to be about 5°, is drawn through the origin in ℓ,m space. (The angles drawn are exaggerated for illustrative purposes, but their qualitative interrelationship is correct.) Also shown are the loci satisfying the dispersion relation for frequency ω. The short arrows at the extremities show the direction of the group velocity appropriate to each branch of the dispersion curve. A perpendicular to OB is constructed through the point K_i. In order that incident and reflected waves cancel

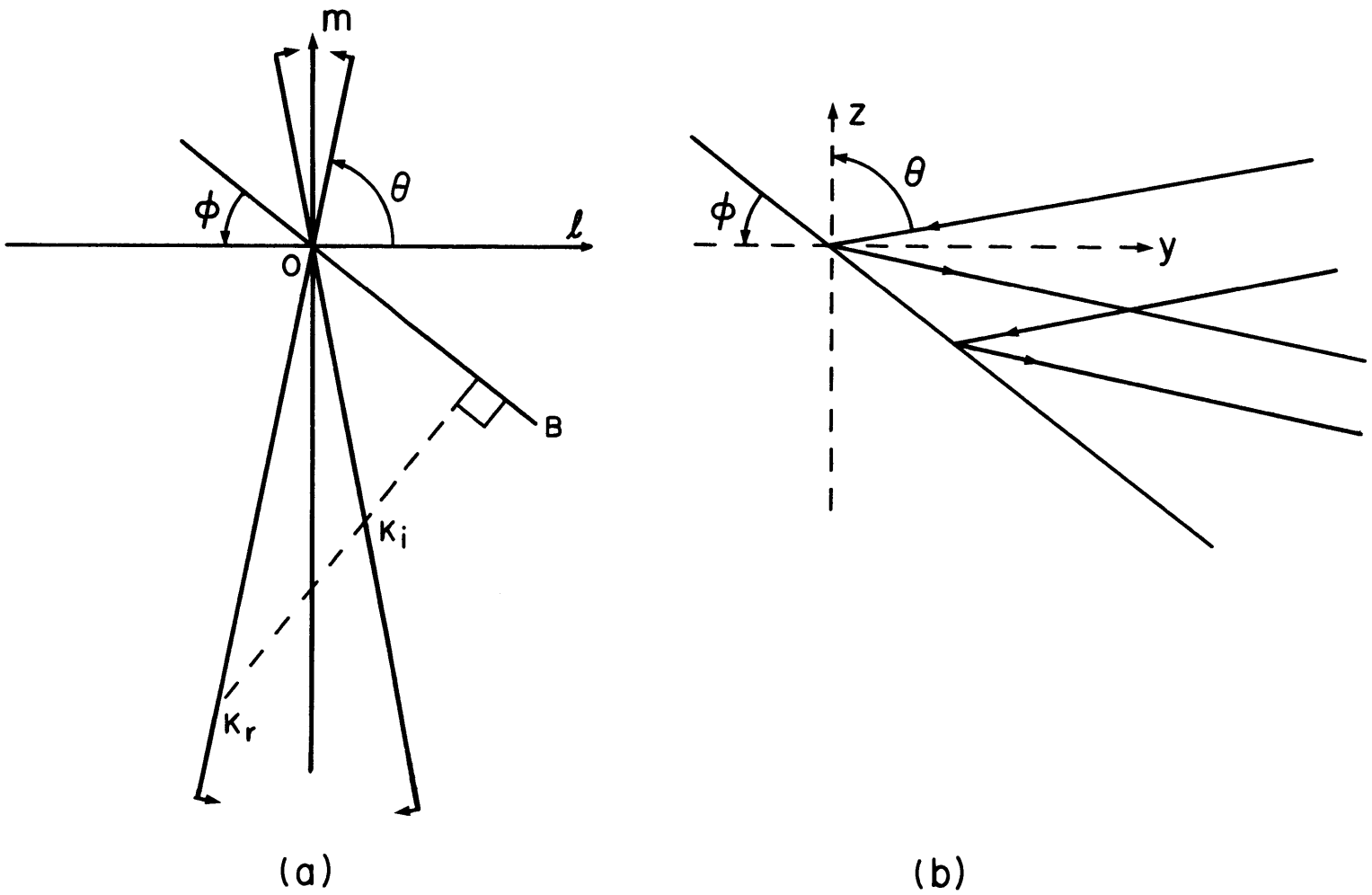


Figure 23 Reflection properties of waves of frequency 1.05f at a slope of angle ϕ in wavenumber space (a) and in geographic space (b). Incident and reflected rays make equal angles with the horizontal in the case shown here as explained in the text.

on the reflecting boundary, they must have the same frequency and their vector wavenumbers must have the same projection onto the line OB. Hence if OK_i is the incident vector, then OK_r must be the reflected, account being taken of the associated group velocity directions. Rays directed southward from the surface and reflected at the coast are thus directed downward after reflection. Incident and reflected rays form equal angles with respect to the horizontal rather than with respect to the normal of the plane reflecting surface. This situation holds unless the normal to the coast is more nearly vertical than the wavenumber vector, in which case, the reflected energy is directed upwards. In the present case, this does not happen unless the frequency exceeds about 0.1 cycles/hour.

In appraising the relative importance of energy arriving by direct arrival from the surface and by indirect arrival after having undergone one or more reflections, it is necessary to consider dissipation, dispersion and possible absorption during the reflecting process. The first two of these are increasingly effective as the distance increases which a ray must travel before its critical latitude is reached. Dissipation, say by viscosity, will be more effective through the increased travel time and will be particularly effective for motions with high wavenumbers and hence large shears. In this respect, it is significant that the typical reflection case considered in figure 23a results in a reflected wave

with wavenumber higher than that incident. The increase in magnitude of the wavenumber vector is given by $-\cos(\phi-\theta)/\cos(\phi+\theta)$ which, for $\theta = 89°$ and $\phi = 5°$, amounts to about 1.5. For reflection from the deep bottom where the slope is about 0.2° a similar elongation takes place, reflection being about the vertical. Hence for downward propagating rays, the first reflection is always such that the wavenumber vector is lengthened, although not by a very large amount. For unstratified fluids, a similar effect has been examined in detail by O.M. Phillips (1963).

A related phenomenon is shown in figure 23(b) where it is seen that the incoming parallel rays reflected from the coast have the spacing between them reduced, corresponding to an increase in the local energy density. The increase in energy density is given by the same factor as before, being about 1.5. A striking example of this mechanism in the non-rotating case in the laboratory has been reported by Sandstrom (1969).

Dispersion through spreading occurs in two ways, firstly because energy constituents traveling along a ray may have different travel times and secondly, if the generating region is localized, there will be roughly radial spreading of energy away from the source. Both effects will contribute to lower the energy level at the observing site due to energy arrival from a particular source of a particular time and can preferentially discriminate against reflected arrivals. However,

if energy introduced near inertial frequency persists sufficiently long for it to travel without substantial attenuation between boudnaries defined by the coast, critical latitude, and ocean top and bottom, dispersion will not play a significant role in lowering energy levels at great depths. Energy would in fact be dispersed throughout the water volume, having undergone repeated reflections from the bounding surfaces. It is this possibility which raises doubt about the reality of a shadow zone and even about the appropriateness of the ray approach. No definitive theoretical argument either way appears within reach.

The final possibility mentioned above for rays reflected from the coast is that they will be attenuated there in the sense that the reflected energy is less than the incident. The ratio of transmitted to incident energy can be conveniently described as the transmission coefficient of the surface. Recently, Longuet-Higgins (1969) has evaluated the reflection properties of various kinds of non-planar boundaries, showing that the transmission coefficient is an extremely complicated function of the geometry of the reflecting surface and that even small irregularities in the surface can produce large changes in the transmission coefficient. Although Longuet-Higgins' results are derived for the case of no rotation, his technique is applicable to the present case and similar conclusions hold. But applica-

tion of the theory to a particular irregular bottom would be difficult at best, and in any case, our knowledge of the Mediterranean bottom is not sufficiently detailed to carry out such a program.

Thus the conclusions to be drawn about energy propagation along rays purely from theory are a rather mixed lot. The possible existence of a shadow has been pointed out, depending on dissipation rates for inertial oscillations and on the detailed shape of the Algerian slope from which rays must reflect in order to reach deep water at the observing site. In a recent paper Larsen (1969) has pointed out that the existence of a pure shadow zone in which there is no energy at all is not tenable from the point of view of energy flux even though such a shadow is implied by ray theory. This is because in order to synthesize the shadow exactly by a normal mode expansion one must include modes propagating in from infinity towards the assumed source region, thereby violating the radiation condition. Nevertheless, Larsen's solution, found for a non-rotating, uniformly stratified channel of constant depth (except for a thin barrier) and synthesized from the first 300 normal modes, does not differ qualitatively from that obtained by the much simpler ray approach. In particular, the laboratory experiments of Sandstrom (1969) mentioned earlier do not permit one to distinguish between the two theories.

We next turn to an examination of the data in the light of what has been said about ray theory.

Application of ray theory

There are two complications in interpreting the data on the basis of ray theory which have so far been glossed over. These correspond to inadequate knowledge of ω and r. It is to be expected that the rays will be quite frequency dependent since a small change in frequency corresponds to a fairly large change in turning latitude; at Mediterranean latitudes, a 2% change in frequency corresponds roughly to a 1 degree change in turning latitude. For the special case r = 0, corresponding to rays traveling due north, figure 24 shows rays of various frequencies originating near the Algernian coast as computed from the measured stratification shown earlier in figure 20. Recall that these mark the limit below which one does not expect to find energy at inertial frequency, at least for the case r = 0, which has arrived directly from the ocean surface. They are labelled according to the turning latitude for a ray of given frequency and also according to the percent by which this frequency is greater than inertial. For this particular case (r = 0) we find that energy of the observed frequency of 1.03 inertial would not penetrate to the 1700 meter level where it was in fact

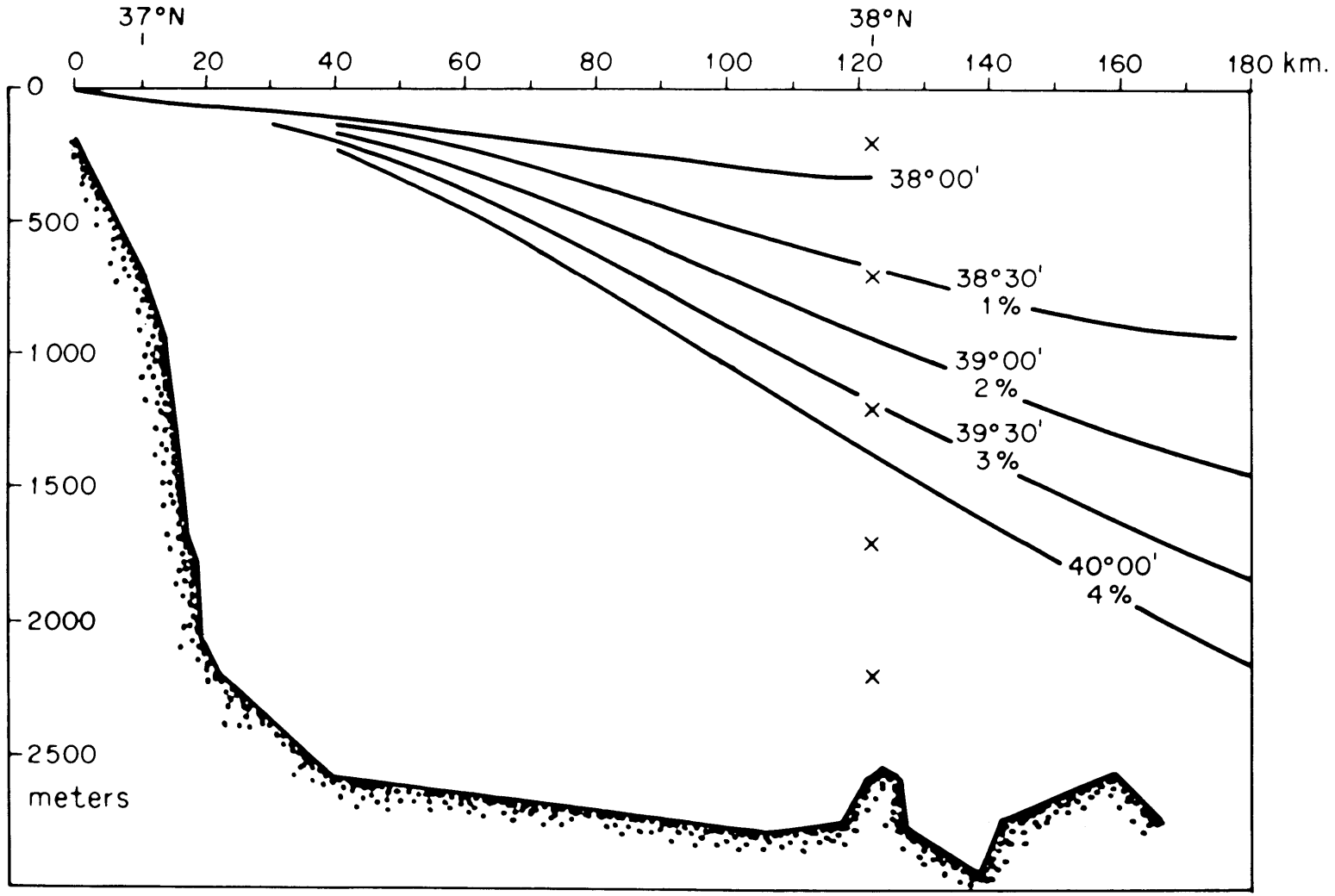


Figure 24 Trajectories of north-bound rays (r = 0) originating near the Algerian coast are shown for various frequencies corresponding to inertial frequency at the indicated latitude. The frequencies are also shown as approximate percentage increases over inertial frequency at 38°N.

observed. The case $r \neq 0$ is therefore considered next.

Unless $r = 0$, a ray having frequency exactly corresponding to inertial frequency of the observing latitude cannot reach the observing site. This can be seen either from figure 22 or equation III-16. Hence the case of interest involves taking $\omega > f_o$ and $r \neq 0$. Suppose one then plots the ray for a specified frequency ($> f_o$) which has its turning point at the observing site as shown in figure 25. We see at once that these rays penetrate more deeply than do those for $r = 0$. The value of r chosen is in fact the largest possible for which a ray of the specified frequency will reach the observing latitude. The ray thus defined also reaches the greatest depth at the observing site. From the figure it can be seen that a frequency shift of 2% or more permits energy to propagate to all depths where measurements were made. Waves of higher frequency can also pass through the site, so that 2% is the minimum frequency increase required for direct sorm arrivals at the deep instruments, but any higher frequency will do. Again it is argued that those rays closest to inertial frequency are the ones with which the largest amplitudes are associated by virtue of their slow propagation rate near the turning latitude. Consequently, what one expects to see as a result of direct arrival from the surface is a band of frequencies

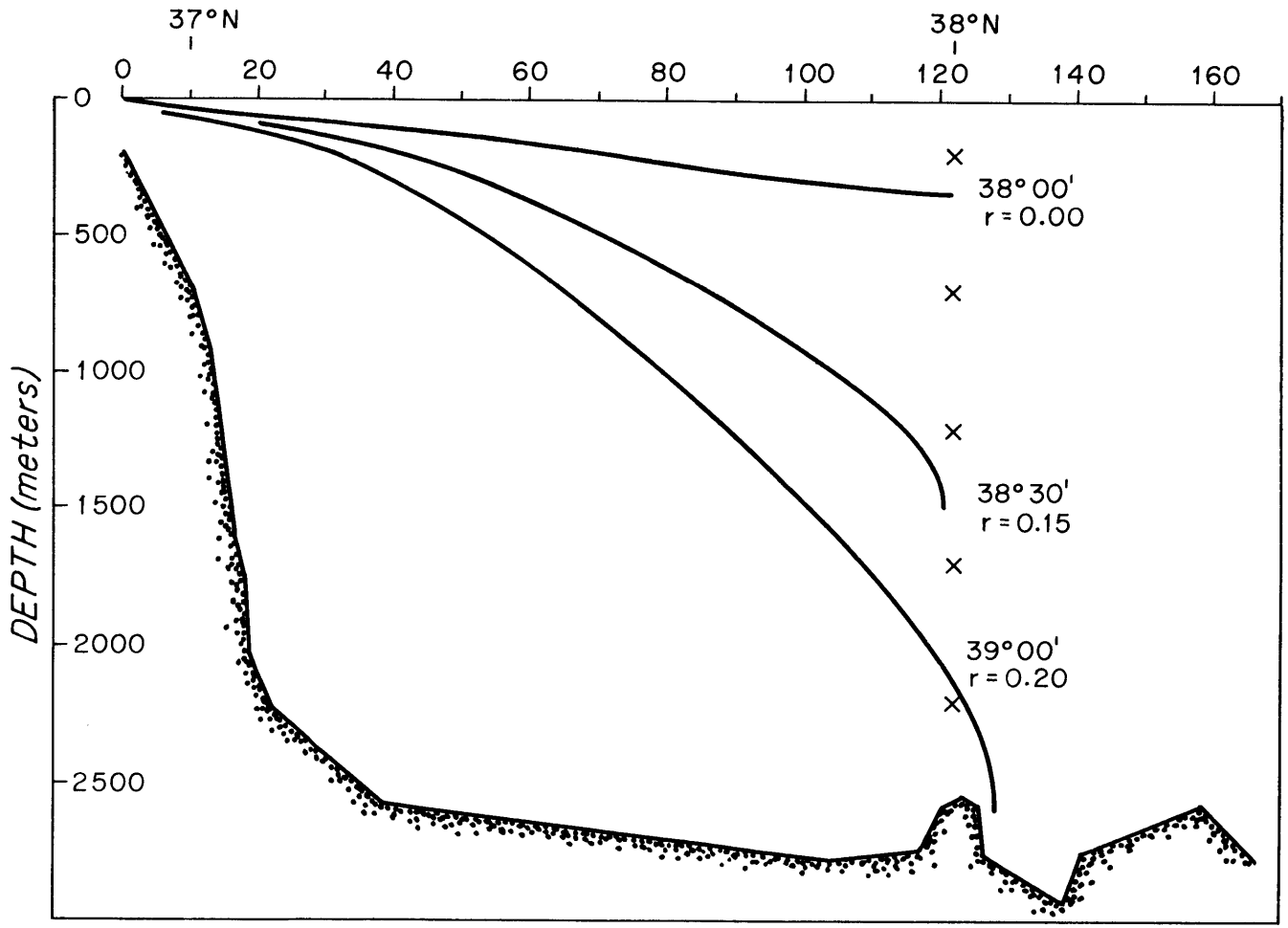


Figure 25 Similar to Fig. 24, except that the rays plotted are those having turning latitudes at 38°N. The rays have east-west components according to values of r (see Fig. 22) but are shown here projected into a north-south plane.

of 1.02 f_o and higher, but weighted towards the 1.02 f limit.

In a gross sense, this is what the data shows; there is a small frequency shift near 200 meters depth of about 1%, at least on a long-term basis, and a larger shift of about 3% at greater depths. The percentage shift above inertial frequency is slightly larger in both cases than might be expected if one were observing a band of frequencies centered around f_o at the upper instrument and 1.02 f_o at the lower ones. Also, the very low amplitudes characteristic of the deepest instrument might be considered as due to the hypothesized shadow zone. But there are also some disturbing discrepancies between observation and ray theory. There seems no evidence for a slowly increasing frequency with depth which might be expected from theory; the data at 700 meters shows as much of a frequency shift as the deepest instrument and even at 200 meters the early part of the record suggests a comparable shift. As pointed out previously, frequencies this high are not excluded by the theory, but if the excitation were broad-band in frequency, which seems most reasonable, the observed signal would consist of a band of frequencies, the mean of which would change slowly towards higher frequency as the observing depth increased.

Ray theory thus gives some insight into how inertial energy may propagate in the ocean and it partially explains the observed increase in frequency with depth. In the hope

of understanding additional aspects of the data, such as the variation of phase with depth, normal modes are next investigated.

Chapter IV Normal mode analysis

Solutions to equations III-1 or III-2 have so far been forced into a particular form so that the flow of energy could be traced. The form of the solutions was seen to correspond to a short-wavelength approximation and, consequently, the existence of boundaries did not affect the solutions except to block the flow of energy into certain regions. Solutions investigated in this chapter have quite a different nature, depending in an essential way on the shape of the basin in which they exist.

Equations III-1 have separable solutions of the form

$$u = e^{i(s\lambda - \omega t)} u_2(\phi) u_3(z)$$

etc.

with a corresponding separation for equations III-2. This fact combined with the simple boundaries of the Mediterranean region where the observations were taken, make it particularly simple to explore effects of these boundaries. With reference to figures 1 and 24, reasonable approximations to the irregular boundaries are seen to be a vertical, east-west wall along $\phi = 37°$ and a flat (z = constant) sea floor 2800 meters below

the surface. Under these assumptions, the boundaries fit naturally into the separation scheme outlined above to make the problem completely separable.

A particularly elegant and complete separation of the equations of motion in spherical geometry (III-1) has been reported by Munk and Phillips. Rather than go through a complete derivation here of the corresponding separation for the beta-plane approximation used in Chapter III, that given by Munk and Phillips is used. That both approaches yield basically the same result is shown in Appendix II inasmuch as both yield the same Airy function dependence in the north-south direction in the vicinity of the critical latitude. Thus a unifying link between investigators using spherical and beta-plane geometries is provided by the appendix.

Vertical structure

For reference purposes, the Munk-Phillips analysis is briefly summarized. With omission of the term w_t in equation III-1, solutions in the following separated form are sought

$$\begin{Bmatrix} u\cos\phi \\ v\cos\phi \\ p \end{Bmatrix} = \Omega a \mathrm{Re}\, Z(z) \exp i(s\lambda - \omega t) \begin{Bmatrix} U(\phi) \\ iV(\phi) \\ \Omega a P(\phi) \end{Bmatrix} \qquad \text{IV-1}$$

$$\begin{Bmatrix} w \\ \\ z \end{Bmatrix} = \Omega a \mathrm{Re}\ W(z)\ \exp\ i(s\lambda - \omega t)\ P(\phi) \begin{Bmatrix} i \\ \\ -1/\omega \end{Bmatrix}$$

where the variables U, V, W, P, Z define variation of the indicated variables in either the vertical or latitudinal directions. An equation for W is then found to be

$$W_{zz} + (\gamma N/2a\Omega)^2\ W = 0 \qquad \text{IV-2}$$

where γ is a dimensionless separation constant. Boundary conditions on W at the free surface and bottom are respectively

$$W_z - g(\gamma/2a\Omega)\ W = 0 \qquad \text{IV-3}$$

and

$$W = 0.$$

The analysis here departs from that of Munk and Phillips in that instead of making a WKB or short-wavelength approximation in solving the equation for W, it is solved numerically with values of N(z) as given in figure 20. This reflects the primary concern of this chapter with lower modes. Solutions to IV-2 and IV-3 are not possible for arbitrary values of γ, but only

for discrete values $\gamma = \gamma_n$, n = 1, 2, ___, each corresponding to a different solution $W_n(z)$ and thus identifying the n-th mode. This much is known from classical Sturm-Liouville theory. Once a particular W_n is known which describes the vertical dependence of w on z for a particular mode, then the corresponding vertical dependence Z_n of u, v, and p can be found from

$$Z_n = - \frac{4a}{\sigma\gamma^2} \frac{dW_n}{dz}. \qquad \text{IV-4}$$

As a practical matter, N(z) is known only as a piecewise constant function. Hence, in an interval where N is constant, IV-2 has sine and cosine solutions, the coefficients of which can be related to those of the preceding layer by requiring that W and Z be continuous across the common interface of the two layers. This corresponds to continuity of vertical displacement and pressure respectively across the interface. With two coefficients in the top layer related through IV-4 but otherwise arbitrary, IV-2 can be integrated in this fashion from top to bottom. This procedure is repeated for various values of γ until a value is found for which the bottom boundary condition is satisfied. Then IV-4 can be solved for Z, again giving trigonometric solutions in each layer.

The results of this calculation are shown in figure 26, in which vertical structure of horizontal currents are plotted for the first five modes; that is $Z_n(z)$, $n = 1,\ldots, 5$. Accompanying each of these curves are five horizontal line segments at depths corresponding to the five observing depths. Hence the length of each line segment within a given mode represents the maximum horizontal velocity reached relative to that at a different depth. Comparison between modes is not possible since each may be multiplied by an arbitrary scaling factor. In the figure, the curves have been normalized to have the same maximum amplitude, not the same total energy.

Table 3

Vertical separation constants γ_n corresponding to the first few vertical modes.

mode	γ
0	5.
1	539.
2	957.
3	1314.
4	1728.
5	2170.

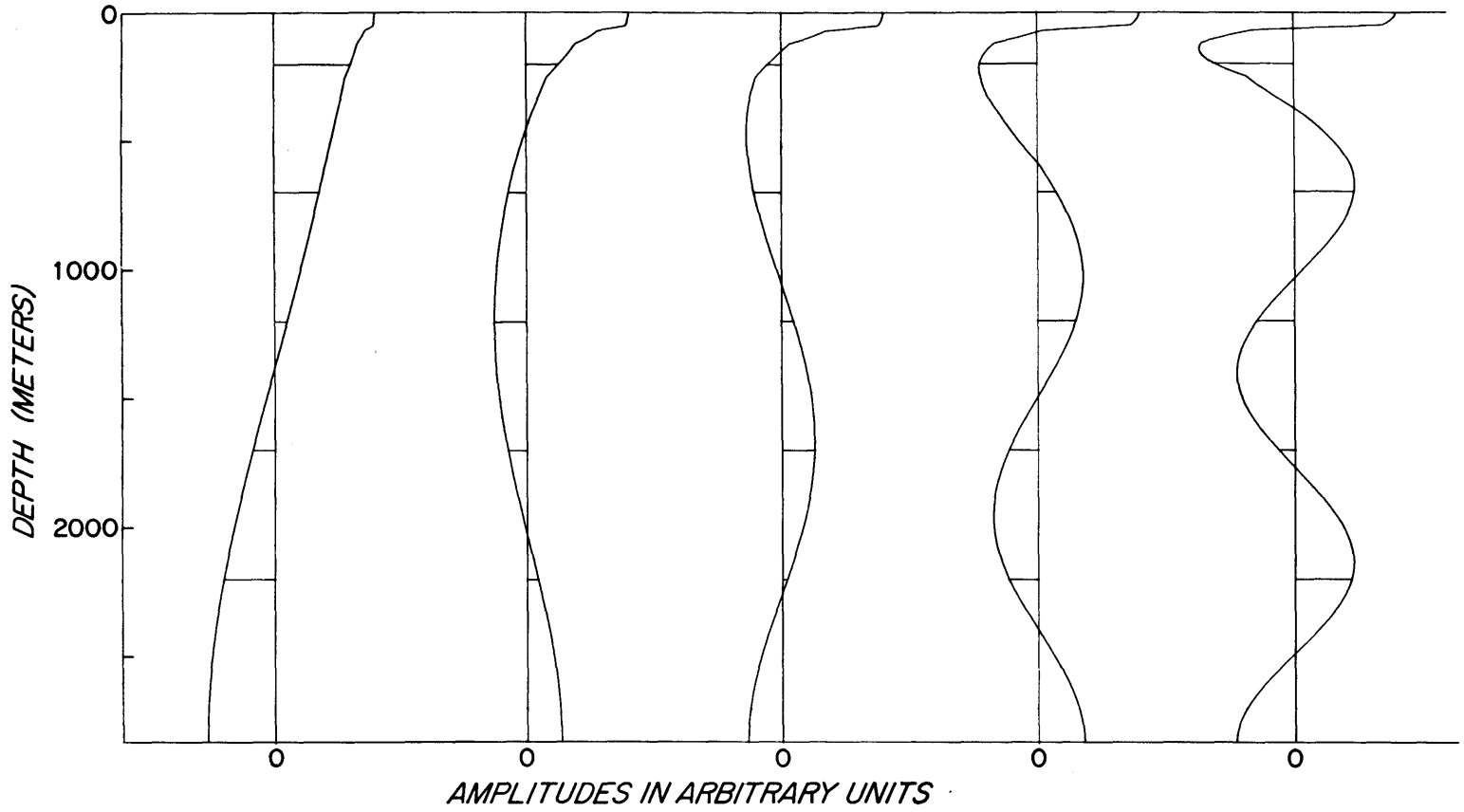


Figure 26 Structure of the first five vertical modes at inertial frequency at the observing site.

Values found for the vertical separation constant γ for these modes plus the barotropic mode (n = 0) are shown in Table 3. The dimensionless quantity γ is a measure of the vertical wavenumber m which for the case of constant N is given exactly by $m = \gamma N/2a\Omega$. With N = 1.0 c.p.h., we note that the barotropic mode yields $m = 130\ km^{-1}$. The vertical wavelength is thus much greater than the water depth, corresponding to the fact that the horizontal velocities for this mode are essentially constant over the water column. Such a large value is admissible and in fact required by the free surface. However, referring to the dispersion relation III-5, one finds that for $\omega = 1.03f$, the corresponding horizontal wavelength is on the order of 10^4 kilometers. It therefore seems doubtful that the barotropic mode plays a significant role in the present situation.

For data sufficiently densely sampled in the vertical, it is possible to make a formal decomposition of the observations into modes by using the fact that the modes are orthogonal; that is, after being suitably scaled, they have the property

$$\int_{-h}^{0} z_n(z)\, Z_m(z)\, dz = \begin{cases} 1 \text{ if } n = m \\ 0 \text{ otherwise} \end{cases}$$

where h is the ocean depth. But in the present case, there is not a sufficient number of instrument levels to carry out this procedure. High order modes (high compared with the fifth say) cannot be distinguished from lower modes. Nevertheless, comparing predicted amplitudes and phases at the five observation depths for the third mode with those given by either the Cartesian components (figure 4) or the complex demodulates (figure 18) shows a very suggestive correlation. Particularly noticeable is the phase reversal between 700 and 1200 meters during the first half of the data series. That the frequency at each of the bottom four depths appears nearly the same, at least on average during the first half of the series, also suggests a single process in effect at those depths.

The observations at 200 meters do not fit particularly well into this simple scheme since amplitudes there are somewhat higher than expected on the basis of the third mode alone. One possibility is that many high order modes are superimposed on a basic third

mode structure. Since these tend to vary with depth as $N^{\frac{1}{2}}$, the 200 meter depth, where N is about double that at the other depths, would tend to have amplitudes about 40% higher from these modes than would the other depths.

From a completely different point of view, an argument for the dominance of a single vertical mode whether or not it is the third can be made from the observed relationship between phases of inertial oscillations at the several observing depths. As previously noted, the difference in phase of oscillations between any pair of depths tends to be either 0° or 180°, at least during the first portion of data when amplitudes are large. But suppose two modes were present so that the oscillations at any depth were the sum of two vectors. Amplitudes of the two vectors would be different functions of depth, each varying with depth in a manner characteristic of its mode and in general reversing phase several times within the water column. At any particular instant, the sum of the two vectors at one depth would thus not in general lie in the same plane with that at another. Hence the difference in phase between the two depths, which can be thought of as the difference in the resultant directions at some instant of time, will not in general be

either 0° or 180°. This is a compelling argument considering the many pairs of depths involved. It is now restated more analytically.

Suppose two modes are present with depth dependence $a_1(z)$ and $a_2(z)$, not necessarily the first and second modes, and have the same frequency ω. We then may write for the complex current $U = u + iv$ at each of two distinct depths z_1 and z_2

$$U(z_j) = U_j = e^{i\omega t}\left\{a_{1j}e^{i\phi_1} + a_{2j}e^{1\phi_2}\right\} \quad j = 1,2$$

where $a_{ij} = a_i(z_j)$

and ϕ_1 and ϕ_2 are phases of modes with depth dependence a_1 and a_2 respectively. Rewriting this as amplitude and phase, we have in obvious notation

$$U_j = a_j e^{i(\omega t + \theta_j)} \qquad j = 1,2$$

with $\quad a_j^2 = a_{1j}^2 + a_{2j}^2$

and $\tan\theta_j = (a_{1j}\sin\phi_1 + a_{2j}\sin\phi_2)/(a_{1j}\cos\phi_1 + a_{2j}\cos\phi_2)$.

We now ask under what circumstances the phases θ_1 and

θ_2 at the two depths could differ by 0 or 180°, that is $\tan \theta_1 = \pm \tan \theta_2$. Clearly if one mode dominates, say $a_1 >> a_2$, this will happen. It also happens if $\phi_1 - \phi_2 = n\pi$ for integer n, so that the modes themselves are either exactly in or out of phase.

It is possible to analyze the observations directly in terms of normal modes. The procedure selected for doing this is based on analysis of the complex demodulates. Resolution of the data is much better in time than in depth, and it is appropriate to analyze first in the time variable. Since the time variability is known to be on the order of several cycles and the signal frequency is typically near 1.03f, demodulates were recomputed for 10 inertial periods and a demodulation frequency of 1.03f. The longer time interval gives more stable amplitude estimates and better frequency resolution. Interpreting the demodulates as the current vector corresponding to the demodulation frequency at some particular time, given for example by east and north components, there then remains the problem of approximating these components as a linear superposition of the normal modes shown in figure 26. The same mode will in general have a different amplitude in each of the two Cartesian components and so

has a phase and magnitude of its own. Phases for each mode are thus to be interpreted as the orientation of the plane in which lie current vectors describing the particular mode at the time when the demodulates describe the direction of current. Because of the way in which the normal mode values are normalized, the magnitude of each mode can be interpreted as the maximum speed attained by that mode within the water column.

Finally, the particular modes used in the approximation and the number of them must be chosen. In principle, one could pick any five modes and construct a linear combination of them which would pass exactly through the currents (as measured by their demodulates) at each of the observing depths. However the resulting equations do not appear sufficiently well conditioned to permit this. For when it was tried with the modes 0 through 4 or 1 through 5, the modes were found to have unreasonably large magnitudes (~ 90 cm/sec) but the same phase, indicating the tendency to cancel one another at the observing depths. This difficulty was removed by requiring a least-squares fit by only 4 modes. In that case, the modes do not give an exact representation of the demodulates and have a residue corresponding to the difference between

the observed current and that synthesized by the normal modes.

Tables 4a and 4b show the results of analyzing the demodulates for modes 0 through 3 and 1 through 4 respectively to find amplitudes a_i and phases θ_i for each of 4 modes. Since sound theoretical arguments have been given for believing that there is no barotropic mode (mode 0) in the Mediterranean, it is noteworthy that such a low amplitude is given for it by the analysis. The three modes which the two tables have in common are very much the same, giving some confidence in the stability of the procedure used. In neither case do the residues referred to above exceed 1.5 cm./sec. Lack of a phase drift with time for the third mode indicates that the demodulation frequency chosen is the correct one for that mode. What appears to be a consistent rate of phase change in modes 1 and 2 suggests a possibly higher frequency for these modes. While it is not possible to adequately assess the reality of these small frequency shifts, we will see later on that a similar effect follows theoretically; that is, each mode will be found to have its own characteristic frequency. Note that the modal decomposition could not be continued beyond mid-February

Table 4a

Normal mode fit to complex demodulates of the data series, given as amplitudes a_i (cm/sec) and phases θ_i (degrees measured counterclockwise with respect to east) for the i-th mode for modes 0-3.

Time at center of demodulation interval	a_0	θ_0	a_1	θ_1	a_2	θ_2	a_3	θ_3
1/27	0.6	-141.	5.7	156.	6.4	149.	10.0	-122.
1/31	0.1	-133.	4.4	167.	6.1	154.	16.1	-113.
2/04	0.4	149.	5.3	-150.	6.4	177.	22.8	-110.
2/08	0.8	172.	7.1	-141.	9.6	-156.	20.5	-109.
2/12	0.3	-158.	4.4	-140.	6.3	-134.	9.7	-106.
2/16	0.5	-44.	2.5	-93.	8.0	-48.	6.5	-62.

Table 4b

The same as Table 4a except for modes 1 - 4.

Time at center of demodulation interval	a_1	θ_1	a_2	θ_2	a_3	θ_3	a_4	θ_4
1/27	5.9	155.	7.8	111.	7.5	-125.	3.2	59.
1/31	4.9	163.	8.8	138.	14.7	-121.	2.4	111.
2/04	5.9	-158.	8.4	173.	22.8	-117.	1.7	159.
2/08	7.3	-146.	7.1	-159.	19.2	-111.	1.5	46.
2/12	4.2	-144.	2.9	-152	7.3	-105	2.6	63.
2/16	2.4	-89.	4.7	-38.	4.9	-57.	2.2	115.

due to failure of direction sensors in the bottommost instrument.

With a single point in the horizontal, nothing can be said about horizontal structure of the currents from an observational standpoint. Nevertheless, the long east-west coastline exerts a dominant effect which can be determined theoretically, thereby providing some insight into what scales of motion might be possible. The following section explores this possibility.

Horizontal structure

In a manner similar to the derivation of the vertical dependence, Munk and Phillips derive the following equation which describes the latitudinal structure:

$$\frac{d^2V}{d\mu^2} + \delta^2 V = \left[\frac{\gamma^2\sigma \cos^2\phi \sin\phi}{s^2 - \frac{1}{4}\gamma^2\sigma^2 \cos^2\phi}\right]\left[\frac{1}{2}\sigma \frac{dV}{d\mu} - s \sin\phi\, V\right] \qquad \text{IV-5}$$

where μ is a north-south Mercator coordinate

$$\mu = \int_0^{\phi} \sec\phi\, d\phi, \quad \delta^2 = \gamma^2\cos^2\phi(\tfrac{1}{4}\sigma^2 - \sin^2\phi) - (2s/\sigma)\cos^2\phi - s^2,$$

and σ is the non-dimensional frequency $\sigma = \omega/\Omega$. Again a WKB solution is possible since the variable coefficients

of the equation are generally slowly varying. But it is found that near the latitude where the wave frequency approximates the local inertial frequency, the approximation breaks down. Careful balancing of terms in IV-5 then leads approximately to the Airy equation

$$\frac{d^2V}{d\eta^2} - \eta V = 0 \qquad \text{IV-6}$$

where $\eta = \frac{\phi - \phi_0}{L} + (\alpha L)^2 - \frac{\sigma - 2\sin \phi_0}{2L \cos \phi_0}$

$$\sigma = \omega/\Omega$$

$$L = (\gamma^2 \sin 2\phi_0)^{-1/3}$$

$\alpha = s/\cos \phi_0$ (or $\alpha = ka$ with k the east-west wavenumber) and ϕ_0 is a reference latitude, taken here as that of the observing site. Solutions thus are given by the Airy functions and so

$$V(\phi) = A\ Ai(\eta) + B\ Bi(\eta).$$

But Bi increases exponentially towards the north while Ai decreases exponentially. Hence, since at any northern

boundary it must be that V = 0, the Ai and Bi terms cancel there which requires that A >> B if the boundary is sufficiently far northward. Consequently, the Bi term can be safely neglected here. Thus the following boundary conditions are appropriate for IV-5:

$$V \to 0 \text{ for } \phi >> \phi_0$$

$$V = 0 \text{ at } \phi = \phi_1 \qquad \text{IV-7}$$

when ϕ_1 is the southern boundary.

Existence of the Balearic islands somewhat clouds the simple situation presented above, particularly since observations suggest a frequency corresponding to a latitude of about 40°. The fact is that to treat normal modes in detail for a basin of general shape is a formidable problem and beyond the scope of this thesis. But the intent here is only to gain some insight into variation of amplitude with latitude and not to make a detailed comparison with observations, so that the great simplification which results would seem to justify the liberties taken with the northern boundary condition.

At the southern boundary, $V(\eta) = 0$ and so η must take on the value of one of the zeros of the Airy function

Ai there, say $\eta = \eta_m$. With each value of η thus specified for the southern boundary latitude (37°) and frequency fixed at 1.03 f, the second of equation IV-6 determines a relationship between γ and α or between γ and k, the east-west wavenumber. Then with permissible values of γ known from the vertical equation IV-2, corresponding discrete values for k can be found. The situation is summarized in figure 27. Curved lines show the relationship between γ and k corresponding to the first five zeros of Ai with η_m defining the m-th horizontal mode. Broken horizontal lines, corresponding to the first few values of γ, that is, to the first few vertical modes, intersect the curved lines, thus giving permissible values for k. It is seen that there are n possible horizontal modes corresponding to the n-th vertical mode. For the case n = 3, the three possible latitudinal dependences are shown in figure 28, corresponding to the observed frequency, 1.03 times inertial frequency of the observing latitude. Since each possibility shows appreciable amplitude at the observing site, the hypothesis of a dominant third vertical mode is tenable.

Horizontal structure is completely determined by vertical and horizontal mode numbers and the frequency;

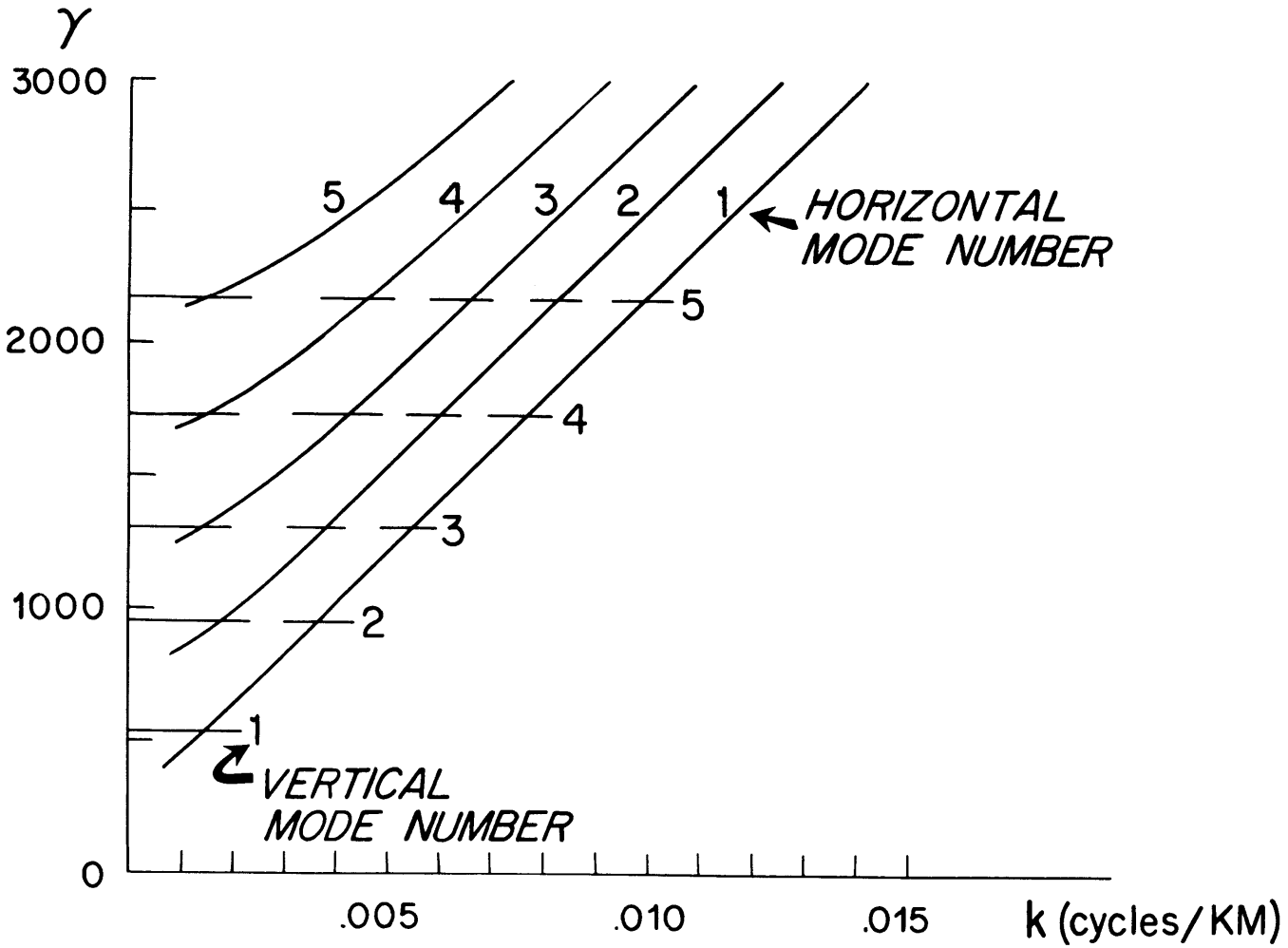


Figure 27 Curved lines show relationship between east-west wavenumber k and vertical eigenvalue γ for each of the first five north-south modes. Broken horizontal lines are permissible values of γ for the first five vertical modes. Intersections of the two families of curves constitute discrete permissible values for k and γ.

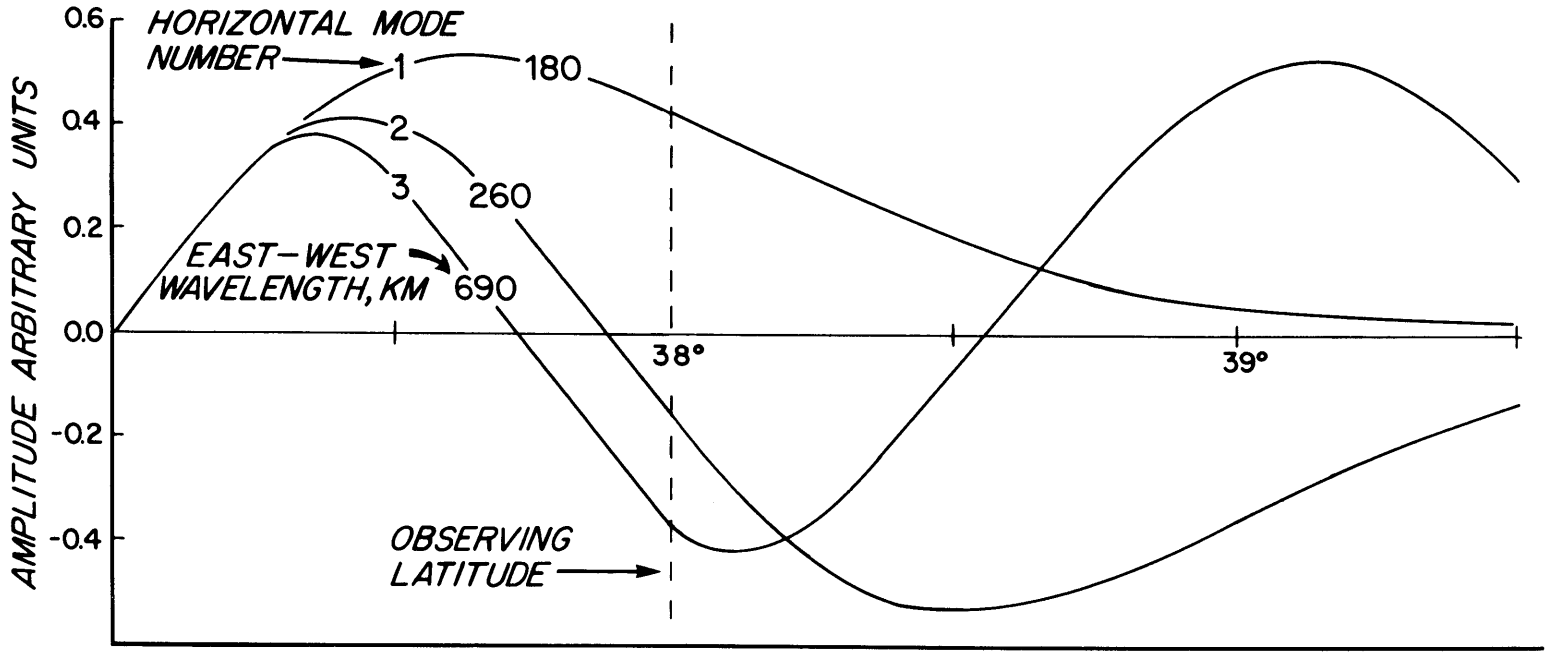


Figure 28 The three possible north-south modes corresponding to the third vertical mode are shown together with their corresponding east-west wavelengths.

it remains to see whether the possibilities available for the third vertical mode and observed frequency are consistent with geometry of the observing region. With reference again to figure 28, the three possible wavelengths are 180, 260, and 690 km. The only significance attached to these numbers is that they are reasonable in view of the size of the Western Mediterranean basin.

Selection of frequency and mode

What has been done thus far is to derive possible horizontal scales of motion, both in the east-west and north-south directions, from observed values of frequency and vertical mode number. In a way, this procedure is rather involuted. A basin such as the Mediterranean has well defined resonant modes which are calculable in principle and it is these that are of interest in this chapter. But in a detailed calculation, the irregular basin boundaries would need to be considered; the problem is then non-separable and one would have to solve the full three-dimensional problem numerically with frequency as an eigenvalue, requiring an enormous and probably prohibitive amount of computation.

Precise frequency and mode calculations thus appear out of reach. What is done here instead is to assume a separable geometry roughly resembling the Mediterranean basin and to compute eigenvalues for that case. The main point of interest is to find the spacing of the frequency eigenvalues. Particularly we ask whether the frequency band corresponding to the range of inertial frequencies is well represented and, if so, whether it is particularly rich in third vertical modes. What we have in mind here is that the surface layers of the ocean have a frequency response to the wind which is very sharply peaked near the local inertial frequency. If this response is the energy source for deep inertial oscillations, then the limited latitudinal width of the Mediterranean would preferentially select those modes with eigenfrequencies lying within the corresponding frequency band.

Accordingly, the eigenfrequencies were computed for a basin of 600 km. in the east-west direction, bounded in the south at 37° latitude and open towards the north, and with a depth of 2800 m. Stratification was taken to be as shown in figure 20. Completely separable solutions are then possible having as eigenfunctions in each direction, sine waves in the x (east-

west) direction, Airy functions in the y (north-south) direction and the special functions shown in figure 26 in the z (up-down) direction. All possible frequencies for modes numbers one through five in all three directions have been computed. For present purposes, the mode number is defined for horizontal currents as the number of internal zeroes (not counting those at boundaries) for the vertical eigensolutions and as the number of internal zeroes plus one for eigensolutions in each of the two horizontal directions. Results of these calculations are shown in Table 5, tabulated in order of increasing period. Each digit of the three-digit number which accompanies each period represents the corresponding mode numbers in x, y and z directions respectively. By way of reference, we note the inertial period at a few typical Mediterranean latitudes:

40°	18.62 hours
39°	19.02
38°	19.44
37°	19.89

If the basic assumption is correct that the detailed geometry of the Mediterranean produces spacing

Table 5

Periods in hours for the first five internal modes in east-west, north-south, and up-down directions

551	11•859	242	17•772	144	18•680
541	12•024	433	17•805	525	18•683
531	12•211	322	17•834	435	18•686
521	12•430	152	17•836	155	18•687
511	12•707	513	17•865	122	18•717
451	13•343	544	17•868	223	18•774
441	13•553	343	17•974	234	18•779
431	13•790	454	17•990	245	18•780
421	14•070	121	18•036	212	18•790
411	14•426	253	18•050	313	18•807
351	14•781	232	18•051	324	18•833
341	15•040	534	18•057	335	18•845
331	15•333	423	18•061	145	18•849
552	15•625	142	18•091	414	18•868
321	15•679	555	18•163	134	18•887
542	15•821	444	18•164	425	18•887
251	16•015	333	18•203	515	18•928
532	16•041	354	18•222	235	18•959
311	16•123	153	18•223	123	18•962
522	16•297	312	18•224	224	19•015
241	16•318	243	18•261	135	19•029
452	16•386	524	18•275	325	19•049
442	16•602	545	18•316	213	19•123
512	16•622	455	18•356	314	19•125
231	16•664	434	18•359	124	19•126
432	16•844	222	18•376	415	19•138
151	16•859	132	18•380	112	19•147
553	16•925	413	18•383	225	19•166
352	17•032	254	18•392	125	19•237
221	17•074	344	18•401	315	19•304
543	17•111	143	18•438	214	19•312
422	17•128	323	18•470	113	19•317
141	17•196	535	18•486	215	19•425
342	17•265	154	18•496	114	19•426
533	17•319	233	18•498	115	19•498
453	17•389	355	18•509		
412	17•487	445	18•512		
252	17•526	514	18•549		
332	17•528	244	18•575		
523	17•560	424	18•585		
131	17•580	334	18•602		
443	17•586	255	18•620		
211	17•602	111	18•627		
554	17•699	345	18•668		
353	17•769	133	18•680		

of the frequency eigenvalues comparable to those computed, it follows that the observed dominant frequency and mode have no special significance as eigensolutions. One can argue that the spatial distribution of forcing might preferentially excite certain modes but it is difficult to see how this can be extracted from weather observations without more detailed calculations of the modal structure. As previously noted, another possibility is that the observed distribution of phase and amplitude with depth is a superposition of many higher modes which happen to be in phase. Distinguishing between these alternatives must await still more extensive measurements.

Chapter V Discussion and conclusions

Inertial oscillations have been found throughout the water column at a location in the Mediterranean, including the deep water. Their general properties, apart from any interpretation given to them, differ appreciably from those discussed in the introduction. We point in particular to the long persistence (3 weeks or more), large vertical coherence scale (virtually the entire water column) and high Q of the signal (about 25 to 50 versus about 10 for the Site D data) for the present data series. The observed oscillations are not of large amplitude, as compared with Site D, for example, although they are sometimes larger than the mean current.

The first 3 weeks of data at 1700 meters show an unequivocal frequency shift of very nearly 3% above local inertial frequency, at least in the sense that the measured frequency represents the mean of a narrow frequency band. Less clear, although still convincing, is the evidence for a similar shift in frequency at the 700, 1200 and 2200 meter levels. The topmost instrument, at 200 meters depth, shows what may be a comparable shift during the first several days, but later appears to have frequency within about 1% of f.

The technique which has led to these results has proved very useful for the data under discussion here owing to the very high ratio of inertial signal to noise (everything other than inertial signal). Such stable estimates of frequency do not arise from a corresponding analysis of the Site D data, although it is not clear whether this is an inherent difference between the two locations or due to limitations of our technique in the presence of strong signals at other frequencies at Site D, such as tides.

We have sought to account for the above facts in the light of both ray and normal mode theory, a duality which pervades much of wave mechanics. It should be pointed out that these two approaches are not mutually exclusive. There is no reason why the data cannot show some features from each theory; both are linear and one can imagine the two superimposed. Although not an inherent part of the theory, our attitude in the case of the ray analysis is that the motion is traceable to some localized or identifiable forcing region such as at the surface, and that it may be transient. For normal mode theory, forcing is not considered explicitly and the motions are treated as free oscillations, the structure of which is determined by the geometry of the

Mediterranean Basin.

A discussion of the ray paths along which inertial energy propagates, taking into account the full three-dimensional properties of these paths, reveals two noteworthy features. First, the arrival time of energy from discrete sources cannot be calculated without knowledge of a certain parameter (essentially the vertical wavenumber) which is not available. Although the spatial paths along which energy travels are determined, travel time along these paths is not. Secondly, it is found that a coast, such as the Algerian coast, can cast a shadow with respect to that part of the inertial energy which originates at the ocean surface and which arrives at the observing site without having undergone reflection. Existence of a shadow was found to depend upon details of how energy is dissipated and how it is reflected from the coast. The interest in such a hypothetical shadow arises from the fact that its shape is independent of the unknown travel time of the oscillations. Its detection would give strong support to the hypothesis that deep inertial oscillations are generated at the surface.

Precise shape of any such shadow would be critically frequency dependent. Rays having lower frequencies do not reach the observing latitude at all, being constrained to propagate southward of it. But rays of higher frequencies can propagate not only through the observing site, but into the shadow region as well to an extent determined by their frequency. A ray of frequency 2% or more higher than inertial and originating at the surface could in fact reach all depths at the mooring location (see figure 25). Although the frequency increase over inertial of 3% observed at the deep locations is sufficient to permit energy to have penetrated directly from the surface, we do not find the gradual increase of frequency with depth which would follow from broad-band excitation at the surface and neglect of energy reflected from the coast.

With respect to transient generation of inertial motion, consider in more detail the flow of energy destined to go through the observing site at a depth of, say, 1700 meters. The higher frequency components would arrive first since they have the higher group velocity, with other frequencies nearer to inertial arriving later. Thus what one would expect from such a storm is that there would be a signal with frequency

tending slowly towards inertial. It has already been noted that there is a hint of this effect during the beginning of the 200 meter record, but it is very clearly not present in that at 1700 meters.

If we persist in interpreting our data by ray theory and surface generation, there seems little alternative to the random superposition model described by Munk and Phillips. This involves energy of appropriate frequencies traveling along their respective ray paths, possibly including reflections, but having very long residence times near the northernmost extremes of their travel, typically on the order of weeks or longer. At any given time at the observing site there would be an assortment of frequencies with energy associated with various meteorological events and with travel times well "randomized" by the slow, varying travel times of the various constituents. Thus at any given depth we have a variety of frequencies near inertial but not directly relatable to any particular storm. There could however be a trend towards higher frequencies with increasing depth, and at 1700 meters this change would be at least 2%, consistent with that observed.

Persistence and bandwidth estimates are also interesting in this context. For the complex current U(t) (=u(t) + iv(t) with u and v east and north components of current), one can write

$$U(t) = \int_{-\infty}^{\infty} A(\omega)e^{-i\omega t}\, d\omega$$

much as was done in the discussion of complex demodulation in Chapter II. Since U and A are Fourier transform pairs, there are a number of analytically specified, realistic choices for A which yield appropriate expressions for U. If A is chosen to have a magnitude with a peak near $\omega = f$, then U will be a slowly modulated signal with frequency near f. Considering various choices of transform pairs, the general statement can be made that the persistence of the signal (as measured between times when U(t) has dropped to half its maximum value) is roughly the reciprocal of the bandwidth (as measured between the frequencies where A has dropped to half its maximum value).

Without knowing the horizontal scales involved, it is not possible to say whether persistence is controlled by the bandwidth of the process or by advection

of energy through the observing site. Qualitatively however, advection can be expected to lower the persistence time so that corresponding estimates of bandwidth will tend to be larger than would be found if advection were not important. Bearing this in mind, the observed persistence of about 20 days yields an upper limit for the bandwidth of 0.05 cycles per day as was also found from the spectral estimates.

A comparable theoretical argument was given by Munk and Phillips for the open ocean case. They worked out the extent to which each inertial constituent was peaked with latitude. By assuming energy distributed among those constituents corresponding to reasonable values of horizontal and vertical wavenumbers, a bandwidth corresponding to persistence of about 100 days was found. This is too long to fit observations, persistence in the open ocean being on the order of a few days at most. Either advection of energy or transient forcing can be invoked to account for this discrepancy.

In earlier observations, it is possible to find persistence on the order of 20 days only in those made in the Baltic, especially those by Gustavson and Kullenberg (1933). Presumably the connection here is that both data are from relatively small enclosed

regions so that, whether advected or not, energy is trapped within the basin.

Ray theory, which is the basis for much of the above discussion, is rigorously applicable as a short-wavelength approximation. But since we do not know what wavelengths predominate in inertial oscillations, the observations were also compared with normal mode theory. The modal theory summarized by Munk and Phillips has been adapted to the present geometry by approximating the Mediterranean with a basin of uniform depth bounded in the south by a vertical wall as is suggested by figure 24. Given the known stratification near the observing site (figure 20), the vertical structure of horizontal currents satisfies a classical Sturm-Liouville problem, giving rise to a discrete family of possible vertical dependencies, the first few of which are shown in figure 26. Comparison with depth dependence actually observed either in the basic series (figure 4) or in the complex demodulates (figure 18) shows a structure during the first 3 weeks of observations which strikingly resembles the third vertical mode. This conclusion was supported by direct fitting of the observations by normal modes. It is of

course not possible to analyze fully the vertical structure with only five point vertical sampling. What appears here to be a single vertical mode could in fact be one or more higher modes, in a manner similar to but more complicated than the usual aliasing of high-frequency oscillations which is familiar from spectral analysis.

In addition to discrete vertical modes established by boundary conditions at the ocean surface and bottom, modes in the horizontal are established by the southern wall and the condition that all inertial oscillations decay sufficiently far northward. (If this last condition is replaced by a northern wall at, say, the latitude of the Riviera, the solutions remain essentially unchanged.) As might be expected from the slow change in Coriolis frequency with latitude (about 2% per degree in the Mediterranean), horizontal modes, unlike those in the vertical, are highly frequency dependent. With this caveat, we see in figure 28 the three possible horizontal modes corresponding to the apparent third vertical mode and observed frequency of 1.03 times inertial. We find no inconsistency with the assumption of a third vertical mode since any of these three horizontal modes gives appreciable

amplitude at the observing latitude. Furthermore, the east-west scales associated with each mode are quite reasonable in view of the dimensions of the Mediterranean basin.

In conclusion, it is reiterated that the application of ray theory in the Mediterranean to inertial oscillations points to their not being relatable to particular, local events at the ocean surface; measurements of frequency do not show the characteristic variation of frequency with time which such a generating mechanism would produce. Normal mode analysis yields more positive results in this case. The apparent dominance of a third vertical mode throughout much of the data is an important conclusion, representing a much simpler vertical structure than has been heretofore supposed.

Appendix I

The effect of neglecting the horizontal component of earth rotation on rays having near-inertial frequency

The paths followed by rays of inertial frequency are to a certain extent dependent upon whether or not the horizontal component of the earth's rotation is included in the basic equations. In order to measure this extent, use is made of the fact that the Hamilton-Jacobi equation, which leads to the ray paths, is separable when the stability N is constant both with and without the additional horizontal rotation terms. Both cases are worked out here and the difference between them gives a qualitative measure of the difference to be expected for the more general case when N is not constant.

A related ray analysis for inertial oscillations which retains the horizontal component of rotation and uses spherical geometry has been carried out by Hughes (1964) for the case of constant N. His analysis was carried far enough to derive expressions for the components of group velocity, but the final quadrature to give the ray paths explicitly was not done nor was any account given of the effect of the horizontal rotation components. Hughes' approach, which is

more exact than that given here, is not followed due to the extensive algebra involved.

The equations of motion may be written in the following form

$$\begin{aligned} u_t - fv + hw &= -p_x \\ v_t + fu &= -p_y \\ w_t - hu &= -p_z - N^2\zeta \\ u_x + v_y + w_z &= 0 \\ w &= \zeta_t \end{aligned} \qquad \text{AI-1}$$

where $h = h_o + \alpha y$ $\qquad f = f_o + \beta y$

$h_o = 2\Omega \cos\theta_o$ $\qquad f_o = 2\Omega \sin\theta_o$

$\alpha = -2\Omega \sin\theta_o / R_e$ $\qquad \beta = 2\Omega \cos\theta_o / R_e$

and all other variables are as defined in Chapter III. Here h is the horizontal component of the earth's rotation. Since its effect can be removed in the final results by setting $h \equiv 0$, both cases of interest can be obtained by working with the single system of equations above.

The argument of Chapter III can be repeated for these equations to yield the corresponding Hamilton-Jacobi equation for the phase function Φ

$$(\Phi_x^2+\Phi_y^2)(N^2-\Phi_t^2) + (f\Phi_z+h\Phi_y)^2 - \Phi_t^2\Phi_z^2 = 0. \qquad \text{AI-2}$$

For the case $N = N(z)$ and $h = 0$ it has previously been shown that this equation has separable solutions. For the case $h = h_o + \alpha y$ now being considered, separation is possible only if N is independent of depth. Solutions can then be found in the form

$$\Phi = kx + mz - \omega t + Q(y) \qquad \text{AI-3}$$

where, k, m, and ω are constant and Q satisfies the equation

$$Q' = [-fhm \pm \{h^2a^2 - f^2m^2\delta^2 + a^2\delta^2\}^{\frac{1}{2}}]/(h^2 + \delta^2) \qquad \text{AI-4}$$

with $a^2 = m^2\omega^2 - k^2 (N^2 - \omega^2)$

$\delta^2 = N^2 - \omega^2$.

Since f and h are know functions of y, the integration for Q is readily carried out for any given values of k, m and ω.

Hence $$Q + Q(y; k, m, \omega) = \int_{y_1}^{y} Q' \, dy \qquad \text{AI-5}$$

where y_1 is an arbitrary value for y which will, for convenience, eventually be taken as the starting latitude for a ray point.

Following again the derivation of Chapter III, the

equations for the trajectory of a ray point are found, namely

$$\begin{aligned} x &= x_1 - Q_k \\ z &= z_1 - Q_m \\ t &= t_1 + Q_\omega . \end{aligned} \qquad \text{AI-6}$$

The first two of these equations determine the spatial path of a ray point and the third its travel time. Three more constants, x_1, z_1, t_1, have been introduced. It is easy to see that the ray point will have coordinates x_1, y_1, z_1 at time t_1, hence one can assume x_1, z_1, and t_1 to be zero so that all rays will pass through the point $(0, y_1, 0)$ at time $t = 0$, which is taken as the origin for all rays.

Rewriting equations AI-6 more explicitily by using AI-5 and AI-4, one finds after carrying out the indicated differentiations

$$x = \pm\alpha\delta^2 \int_{y_1}^{y} \{(h^2+\delta^2)(\omega^2-\alpha^2\delta^2) - f^2\delta^2\}^{-\frac{1}{2}}\, dy$$

$$z = \int_{y_1}^{y} [fh \mp \{(h^2+\delta^2)\omega^2-f^2\delta^2\}\{(h^2+\delta^2)(\omega^2-\alpha^2\delta^2)-f^2\delta^2\}^{-\frac{1}{2}}]$$

$$\cdot[h^2+\delta^2]^{-1}\, dy$$

$$t = -2\omega m \int_{y_1}^{y} [h^2+\delta^2]^{-2}[fh\mp\{(h^2+\delta^2)(\omega^2-\alpha^2\delta^2)-f^2\delta^2\}^{\frac{1}{2}}]\, dy$$

AI-7

$$\pm\omega m \int_{y_1}^{y} [(h^2+\delta^2)(1+\alpha^2) + f^2-\omega^2+\alpha^2\delta^2]$$

$$\cdot[h^2+\delta^2]^{-1}[(h^2+\delta^2)(\omega^2-\alpha^2\delta^2) - f^2\delta^2]^{-\frac{1}{2}}\, dy$$

where $\alpha = k/m$ and a and δ are as previously defined.

A number of points can be made at this time. Ray paths are symmetric about the $x = 0$ plane corresponding to the choice of sign in the first of AI-7, but are not symmetric about $z = 0$ unless $h = 0$. Note that the negative sign must be chosen in order that the rays lie within the ocean. As was the case for $h = 0$ and N variable, the ray geometry depends, for a given frequency, only on a single parameter, defined in the present case as $\alpha = k/m$. Travel time however depends not only upon α but upon an additional parameter, in this case the vertical wavenumber m, to which it is proportional. Qualitatively, these results do not differ appreciably from those found in Chapter III.

The integrands in equations AI-7 are well-behaved functions of y and are easily computed numerically for any specified values of ω and α with the simple dependence on m implicitly assumed. Figure 29 shows the results of these

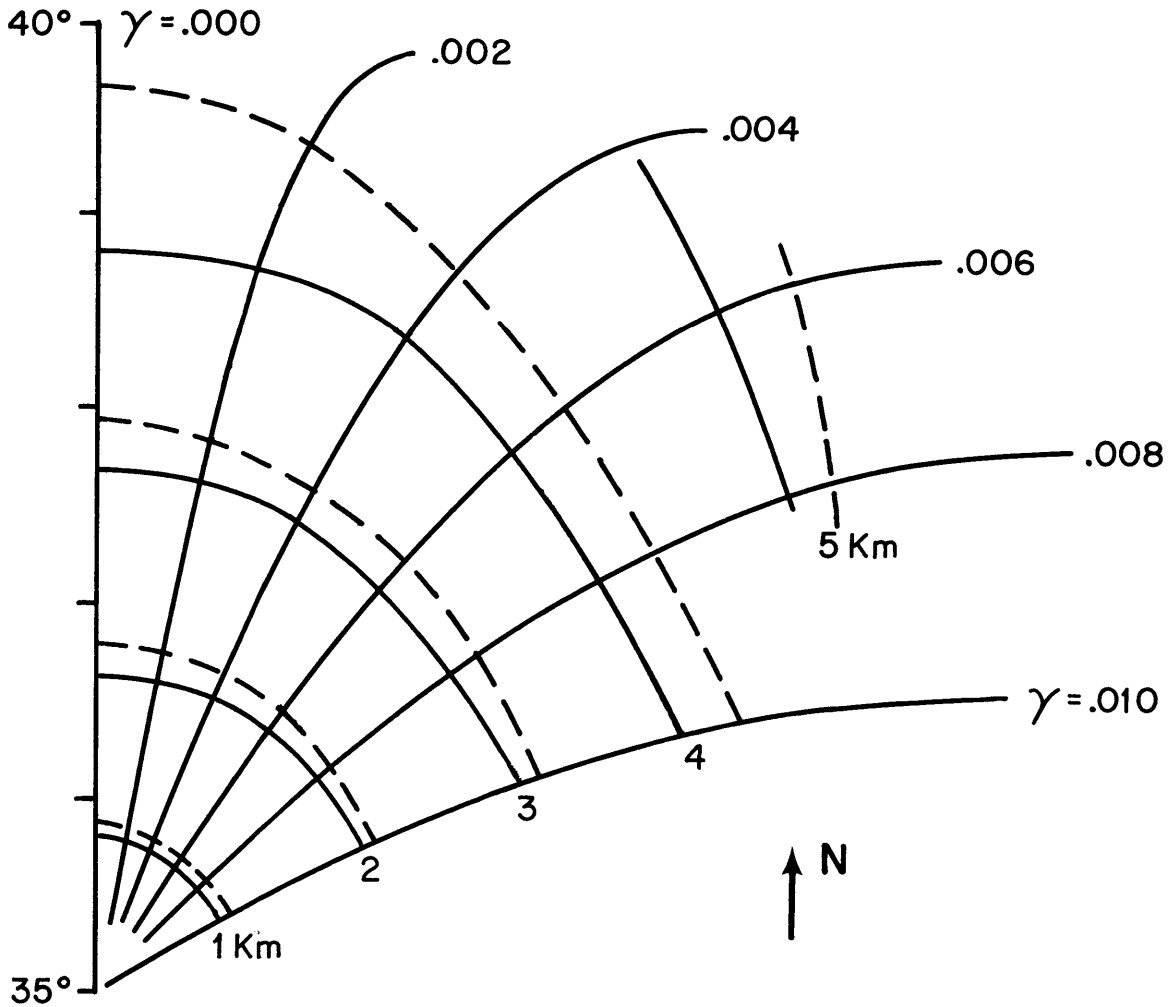


Figure 29 Paths of rays having inertial frequency at 40° latitude are shown emanating from a single point at the sea surface. The stability frequency is constant at 2 cycles per hour. Including the horizontal component of the earth's rotation shifts the intersecting, solid iso-depth lines to the dashed position, but horizontal paths of the rays remain the same.

calculations. The rays are plotted in a horizontal plane as radiating from a point source at latitude 35° and for frequency corresponding to inertial frequency at latitude 40°. Trajectories of the rays in the horizontal are independent of whether or not h = 0 to within plotting error, so that the same set of curves suffices for both cases. The same holds true for travel times which are not shown in the figure. There are two families of depth curves which intersect the rays, solid curves for the case h = 0 and dashed curves for $h = h_o + \alpha y$. Thus the essential feature of including the horizontal component of rotation is to decrease the depth to which the rays penetrate by 10 or 20 percent.

Appendix II

Airy-function structure of inertial oscillations derived from a local beta-plane approximation

The basic equations of motion admit separable solutions both in spherical geometry (Munk and Phillips, 1968) and in a locally-valid β-plane, Cartesian geometry (Blandford, 1966). These correspond to the two sets of equations III-1 and III-2 respectively both of which have been used in the present work. The Munk-Phillips solutions to the spherical equations yielded an Airy-function structure in the region where the wave frequency is close to the local inertial frequency. In view of the remarks made in Chapter III in defense of the simplified equations III-2, it seems reasonable that they should have comparable behavior under similar circumstances. This will turn out to be the case, although exact solutions (to the approximate equations) are found to be parabolic cylinder functions. Thus, although some of the results of this appendix have been anticipated, the fact that they can be derived from simplified equations reinforces the arguments used in defense of the simplifications. In addition, since both sets of equations III-1 and III-2 are in common use, the appendix provides a framework for intercomparing results derived by alternate methods.

Rather than separate the equations in their usual form, which requires some assumptions about the character of the solutions to be practicable, several of the variables are eliminated first. Elimination of ζ between the third and fourth of equations III-2 yields

$$\begin{aligned} u_t - fv + p_x &= 0 \\ v_t + fu + p_y &= 0 \\ w_{tt} + N^2 w + p_{zt} &= 0 \\ u_x + v_y + w_z &= 0 \end{aligned} \qquad \text{AII-1}$$

where in general $f = f(y)$ and $N = N(z)$.
Using the third of these to eliminate p in the first two

$$\begin{aligned} u_{ztt} - fv_{zt} - (N^2 + \partial^2/\partial t^2)w_x &= 0 \\ fu_{zt} + v_{ztt} - (N^2 + \partial^2/\partial t^2)w_y &= 0 \\ u_x + v_y + w_z &= 0 \end{aligned} \qquad \text{AII-2}$$

Finally u can be eliminated using the last of these with each of the first two, again without differentiating f with respect to y or N with respect to z, to give

$$\partial^2/\partial z\partial t\,[f\partial/\partial x + \partial^2/\partial y\partial t]v$$
$$+[\partial^2/\partial x^2\,(\partial^2/\partial t^2+N^2) + \partial^4/\partial z^2\partial t^2]w = 0$$

AII-3

$$\partial^2/\partial z\partial t\,[f\partial/\partial y - \partial^2/\partial x\partial t]v$$
$$+[\partial^2/\partial x\partial y\,(\partial^2/\partial t^2+N^2) + f\partial^3/\partial z^2\partial t]w = 0$$

It is not possible to eliminate either of the remaining dependent variables. At this point, solutions are sought in the form

$$v = \exp i(kx - \omega t)\; v_2(y)\; v_3(z)$$

AII-4

$$w = \exp i(kx - \omega t)\; w_2(y)\; w_3(z)$$

Substitution of these forms into AII-3 leads to

$$v_2 v_{3z}\;\omega(\omega^2-f^2) + w_3(fkw_2+\omega w_{2y})(N^2-\omega^2) = 0$$

AII-5

$$v_{3z}\;\omega(fkv_2-\omega v_{2y}) - w_2(k^2(N^2-\omega^2)w_3 + \omega^2 w_{3zz} = 0$$

Each of these equations is easily rewritten as a sum of two terms, one a function of y only and the other a function of z only so that each term must be a constant. Denoting by C_1 and C_2 the two constants which thus arise, one finds

$$v_{3z} + C_1(N^2-\omega^2)w_3 = 0$$

$$v_{3z} - C_2k^2(N^2-\omega^2)w_3 - C_2\omega^2 w_{3zz} = 0$$

AII-6

$$fkw_2 + \omega w_{2y} + C_1 v_2\ \omega(f^2-\omega^2) = 0$$

$$w_2 - C_2\omega(fkv_2 - \omega v_{2y}) = 0$$

thus giving four equations for the four unknown functions.

Between the first two of equations AII-6, v_3 is easily eliminated to give the vertical equation

$$w_{3zz} + (k^2+ C^2)(N^2 - \omega^2)/\omega^2 w_3 = 0 \qquad \text{AII-7}$$

where $C^2 = C_1/C_2$.

This together with boundary conditions at the ocean surface and bottom, define an eigenvalue problem for w_3 with C as an eigenvalue. The equation holds uniformly for all frequencies but the case of interest here is for $\omega \sim f_o$ so that $N^2>>\omega^2$. For the special case N constant, AII-7 has solutions of the form $w_3 \sim e^{imz}$, leading to

$$C^2 = m^2\omega^2/(N^2 - \omega^2) - k^2 \qquad \text{AII-8}$$

which will be of use later on. Typical values of the parameters involved are N^2 = 1.0 cph, $\omega = f_o$ = .05 cph, m = 1.0 cycle/km. and k = .01 cycle/km., from which it follows that C = 0.7 cycles/km.

Similarly w_2 can be eliminated from the last two of the equations AII-6;

$$v_{2yy} - \omega^{-2}[f^2k^2 + \omega\beta k - C^2(\omega^2 - f^2)]v_2 = 0 \qquad \text{AII-9}$$

If now, after having been differentiated, f is taken as constant, AII-9 has solutions $v_1 \sim e^{i\ell y}$ so that

$$(k^2+\ell^2)(N^2-\omega^2) - m^2(\omega^2-f^2) + \beta k(N^2-\omega^2)/\omega = 0. \qquad \text{AII-10}$$

This dispersion relation encompasses both the inertio-gravity and Rossby waves, reducing to the usual case III-5 for inertio-gravity waves when variation in f is neglected (β = 0), and to the case for barotropic Rossby waves when m = 0.

Of central interest here is equation AII-9 alone since it contains all the information concerning variation of horizontal velocity with latitude. With f taken as a simple linear function of y, the equation has the form

$$v_{2yy} + (py^2 + qy + r)v_2 = 0 \qquad \text{AII-11}$$

where $p = -\beta^2(C^2 + k^2)/\omega^2$

$q = -2f_o\beta(C^2 + k^2)/\omega^2$

$r = [\omega\beta k - f_o^2k^2 + C^2(\omega^2 - f_o^2)]/\omega^2.$

Since p is negative, this in turn can be written in the real cannonical form

$$v_{2\eta\eta} - (\tfrac{1}{4}\eta^2 + a)v_2 = 0 \qquad \text{AII-12}$$

where a and η are the non-dimensional quantities

$$a = -\tfrac{1}{2}(\beta k/\omega + C^2)(C^2 + k^2)^{-\frac{1}{2}}\,\omega/\beta$$

$$\eta = (y + f_o/\beta)\,[4\beta^2(C^2 + k^2)/\omega^2]^{1/4}.$$

It will be of value to note magnitudes of a and η in the present situation. Taking $\beta = 10^{-5}$ cph/km. and other parameters as previously estimated, one finds $a \sim -200$ and $\eta \sim 15$, with the value of y having little effect on the value of η for y on the order of hundreds of kilometers.

In the notation of J. C. P. Miller (1964), solutions to equation AII-12 are the parabolic cylinder functions $U(a,\eta)$ and $V(a,\eta)$. The $V(a,\eta)$ solution increases exponentially for large, positive values of y while U decreases

exponentially. Thus the second or V solution can be ignored unless there is a coastline only slightly northward from the observing latitude, y = 0.

From the defining equation, it can be seen that η, the non-dimensional latitude, is referred to a pseudo-equator defined by $\eta = 0$ or $y = -f_o/\beta \sim -5000$ km. The distance from the observing site to this equator is great compared with the distance to the southern boundary under the circumstances of interest here. Since the parabolic cylinder function must have a zero at that coast and since its zeros are quasi-uniformly spaced, the zeros of interest will be of high order, and these are not well tabulated. Thus an approximation is introduced to bring the solutions into a more tractable form. The approximation is applicable in the vicinity of the observing latitude, y = 0.

According to J. C. P. Miller, the following holds in the present case where a is large and negative and η positive

$$U(a,\eta) = 2^{-1/4 - 1/2\,a}\,\Gamma(\tfrac{1}{4} - \tfrac{1}{2}a)[t/(\zeta^2-1)]^{1/4}\,Ai(t) \qquad \text{AII-13}$$

where $\zeta = \eta(-a)^{-\frac{1}{2}}$ $\qquad (\zeta \leq 1)$

$t = (-4a)^{2/3}\,\tau$

$\tau = -(3\theta/2)^{2/3}$

$$\theta = \frac{1}{4}\{\cos^{-1}\zeta - \zeta(1-\zeta^2)^{\frac{1}{2}}\}$$

and Ai is an Airy function in the usual notation. But since for the parameter range of interest, ζ is very close to unity, one can introduce the small quantity ϕ by

$$\zeta = \cos\phi \qquad \phi << 1$$

so that $\phi^2 \sim 2(1-\zeta)$, by a Taylor series expansion of cos ϕ. Similarly expanding θ in terms of ϕ yields $\theta \sim \frac{1}{6}\phi^3$. Hence

$$\theta \sim \frac{1}{6}\,[2(1-\zeta)]^{3/2} \qquad \text{AII-14}$$

and so

$$t \sim -2(1-\zeta)(-a)^{2/3} \qquad \text{AII-15}$$

Thus, except for the very slowly varying coefficient

$$[t/(\zeta^2-1)]^{1/4} \sim [2(-a)^{2/3}/(1+\zeta)]^{1/4}$$

the essential behavior of the solutions are given by

$$v_2 \sim \mathrm{Ai}(t) \qquad \text{AII-16}$$

Finally expressing t in terms of the original parameters, after taking $\omega = f_o$, we have to a good approximation

$$a \sim -\frac{1}{2} C f_o/\beta \qquad\qquad 1 - \zeta \sim -y\beta/f_o$$

so that

$$t \sim y/L \qquad\qquad \text{AII-17}$$

where L is the length scale for the Airy argument t given by

$$L = (2C^2 \beta/\omega)^{-1/3} \qquad\qquad \text{AII-18}$$

This is the same scale as found by Munk and Phillips when their result is converted to the present notation.

Bibliography

Amos, D. E., and L. H. Koopmans (1963) Tables of the distribution of the coefficient of coherence for stationary bivariate Gaussian processes. Sandia Corporation, 327 pages. Available from: Office of Technical Services, Department of Commerce, Washington 25, D. C.

Bingham, C., M. D. Godfrey and J. W. Tukey (1967) Modern techniques of power spectrum estimation. IEEEE Trans. on Audio and Electroacoustics, Vol. AU-2, No. 2, p. 56-66.

Birchfield, G. E. (1969) Response of a circular model Great Lake to a suddenly imposed wind stress. Jour. of Geophysical Res., Vol. 74, No. 23, pp. 5547-5554.

Blandford, R. (1966) Mixed gravity-Rossby waves in the ocean. Deep-Sea Res., Vol. 13, No. 5, pp. 941-961.

Cahn, A. (1945) An investigation of the free oscillations of a simple current system. Jour of Meteorology, Vol. 2, No. 2, pp. 113-119.

Crépon, M. (1969) Hydrodynamique marine en regime impulsionel. Cahiers Oceanographique, Vol. 21, No. 9, pp. 863-877.

Csanaday, G. T. (1968) Motions in a model Great Lake due to a suddenly imposed wind. Jour. of Geophysical Res., Vol. 73, No. 20, pp. 6435-6447.

Eckart, C. (1960) Hydrodynamics of Oceans and Atmospheres, Pergamon Press, New York, 290 pages.

Fofonoff, N. P. (1962) Physical properties of sea-water. In: The Sea, Vol. 1, pp. 3-30, M. N. Hill, ed., Interscience Publishers, New York, 864 pages.

Fofonoff, N. P., and Y. Ercan (1967) Response characteristics of a Savonius rotor current meter. W.H.O.I. Ref. 67-33 (unpublished manuscript).

Bibliography (cont.)

Gonella, J., M. Crépon , and F. Madelain (1969) Observations de courant, de vent et de temperature a la Bouée Laboratoire (Position A), Sept-Oct., 1966. Cahiers Océanographiques, Vol. 21, No. 9, pp. 845-854.

Gustavson, T., and B. Kullenberg (1933) Trägheitsströmungen in der Ostsee. Goteborgs K. Vet. Vitt.-Samh. Handl., Femte Foljden, Vol. B3, No. 6, 7 pages.

Hendershott, M. C. (1964) Inertial oscillations of tidal period. Doctoral dissertation, Department of Physics, Harvard University. 135 pages.

Hughes, B. A. (1964) Ph.D. dissertation, University of Cambridge.

Kullenberg, B., and J. Hela (1942) Om tröghetssvangningar i Ostersjön, Svenska Hydrograf. Biol. Komm. Skrifter Ny Ser. Hydrograf. No. 16, 14 pages.

Larsen, L. H. (1969) Internal waves incident upon a knife edge barrier. Deep-Sea Res., Vol. 16, No. 5, pp. 411-419.

Longuet-Higgins, M. S. (1969) On the reflexion of wave characteristics from rough surfaces. Jour. of Fluid Mechanics, Vol. 37, part 2, pp. 231-250.

Malone, F. D. (1968) An analysis of current measurements in Lake Michigan. Jour. Geophysical Res., Vol. 73, No. 22, pp. 7065-7081.

Miller, J. C. P. (1964) Parabolic cylinder functions. In: Handbook of Mathematical Functions, pp. 685-720, Abramowitz and Stegun, Ed., U. S. Government Printing Office, Washington, D. C. 1045 pages.

Mooers, C. N. K. (1970) The interaction of an internal tide with the frontal zone in a coastal upwelling region. Ph.D. Thesis, Oregon State University, 480 pages.

Bibliography (cont.)

Munk, W., and N. A. Phillips (1968) Coherence and band structure of inertial motion in the sea. Rev. of Geophysics, Vol. 6, No. 4, pp. 447-472.

Nan-niti, T., H. Akamatsu, and T. Yasuoka (1966) A deep current measurement in the Japan Sea. Oceanographic Magazine, Vol. 18, No. 1, pp. 63-71.

Phillips, O. M. (1963) Energy transfer in rotating fluids by reflection of inertial waves. Physics of Fluids, Vol. 6, No. 4, pp. 513-520.

Pollard, R. T. (1970) On the generation by winds of inertial waves in the ocean. To appear in Deep-Sea Research.

Pollard, R. T., and R. C. Millard, Jr. (1970) Comparison between observed and simulated wind-generated inertial oscillations. To appear in Deep-Sea Research.

Sandstrom, H. (1969) Effect of topography on propagation of waves in stratified fluids. Deep-Sea Res., Vol. 16, No. 5, pp. 405-410.

Verber, J. L. (1966) Inertial currents in the Great Lakes. Great Lakes Res. Division, University of Michigan, Pub. No. 15, pp. 375-379.

Webster, F. (1968) Observations of inertial-period motions in the deep sea. Rev. of Geophysics, Vol. 6, No. 4, pp. 473-490.

Webster, F. (1967) A scheme for sampling deep-sea currents from moored buoys. Trans. 1967 Buoy Tech. Symp., Marine Technology Society, Washington, D. C., pp. 419-431.

Webster, F., and N. P. Fofonoff (1965) A compilation of moored current meter observations, Volume I. (unpublished manuscript) W.H.O.I. Ref. 65-44.

Webster, F., and N. P. Fofonoff (1966) A compilation of moored current meter observations, Volume II. (unpublished manuscript) W.H.O.I. Ref. 66-60.

Bibliography (cont.)

Webster, F., and N. P. Fofonoff (1967) A compilation of moored current meter observations, Volume III. (unpublished manuscript) W.H.O.I. Ref. 67-66.

Whitham, G. B. (1960) A note on group velocity. Jour. of Fluid Mech., Vol. 9, pp. 347-352.

Biographical Note

NAME: Henry Perkins

BORN: March 20, 1938, Rahway, New Jersey

MARITAL STATUS: Married to the former Valerie Lockhart.

EDUCATION:

Institution	Dates of Attendance	Degree Earned	Date of Degree	Major Field
Mass. Inst. of Technology	9/56-6/60	B.S.	6/60	Mathematics
New York University	9/60-6/64	M.S.	6/64	Mathematics

EMPLOYMENT:

Institution	Dates of Employment	Duties
Watson Laboratories (IBM) New York City	10/61-11/62*	Mathematical Analysis & Computer programming
Woods Hole Ocean. Inst.	11/62-9/65*	Research Ass't. in Geophysics

* During periods of employment when also attending N.Y.U., I was a full-time employee and a part-time student. The M.S. thesis was written in absentia at Woods Hole.

PUBLICATIONS:

Voorhis, A. D., and H. T. Perkins (1966), The spatial spectrum of short-wave temperature fluctuations in the near-surface thermocline. Deep-Sea Res., Vol. 13, pp. 641-654.

SUPPORT FOR GRADUATE STUDIES:

In addition to support for the thesis itself, for which acknowledgement has been previously made, the author received support during three semesters of study during 1965-1967 under a grant administered by Massachusetts Institute of Technology from the Ford Foundation. A variety of support was also provided by the Woods Hole Oceanographic Institution, including a Summer Student Fellowship in 1966 and a Summer Graduate Fellowship in 1969. For all these assistances, grateful acknowledgment is made.